# Foundational Studies for Array-based Electrophoretic Exclusion of Proteins

by

Fanyi Zhu

A Dissertation Presented in Partial Fulfillment
of the Requirements for the Degree
Doctor of Philosophy

Approved April 2019 by the
Graduate Supervisory Committee:

Mark Hayes, Chair
Alexandra Ros
Daniel Buttry

ARIZONA STATE UNIVERSITY

May 2019

ABSTRACT

Disease prevention and personalized treatment will be impacted by the continued integration of protein biomarkers into medical practice. While there are already numerous biomarkers used clinically, the detection of protein biomarkers among complex matrices remains a challenging problem. One very important strategy for improvements in clinical application of biomarkers is separation/preconcentration, impacting the reliability, efficiency and early detection. Electrophoretic exclusion can be used to separate, purify, and concentrate biomarkers. This counterflow gradient technique exploits hydrodynamic flow and electrophoretic forces to exclude, enrich, and separate analytes. The development of this technique has evolved onto an array-based microfluidic platform which offers a greater range of geometries/configurations for optimization and expanded capabilities and applications. Toward this end of expanded capabilities, fundamental studies of subtle changes to the entrance flow and electric field configurations are investigated. Three closely related microfluidic interfaces are modeled, fabricated and tested. A charged fluorescent dye is used as a sensitive and accurate probe to test the concentration variation at these interfaces. Models and experiments focus on visualizing the concentration profile in areas of high temporal dynamics, and show strong qualitative agreement, which suggests the theoretical assessment capabilities can be used to faithfully design novel and more efficient interfaces. Microfluidic electrophoretic separation technique can be combined with electron microscopy as a protein concentration/purification step aiding in sample preparation. The integrated system with grids embedded into the microdevice reduces the amount of time required for sample preparation to less than five minutes. Spatially separated and preconcentrated proteins are transferred directly from an upstream reservoir

onto grids. Dilute concentration as low as 0.005 mg/mL can be manipulated to achieve meaningful results. Selective concentration of one protein from a mixture of two proteins is also demonstrated. Electrophoretic exclusion is also used for biomarker applications. Experiments using a single biomarker are conducted to assess the ability of the microdevice for enrichment in central reservoirs. A mixture of two protein biomarkers are performed to evaluate the proficiency of the device for separations capability. Moreover, a battery is able to power the microdevice, which facilitates the future application as a portable device.

To Mom and Dad, for all your patience, support, and encouragement.

爸爸，妈妈，我爱你们！

ACKNOWLEDGMENTS

I first must thank my advisor, Dr. Mark Hayes. I still remember the first day I met with Mark. At that time, I just came to ASU and did not even know the building very well. I was interested in Mark's work and scheduled a short meeting with him. However, I was lost when I was wandering around on the second floor. Fortunately, the place I got lost was very close to Mark's office and he stopped me when I almost went to the wrong way. That is also what I feel like during these years-Mark is like a lighthouse, leaves me much freedom but also guides me when I feel lost. I really appreciate the time and help from Mark!

I would also like to thank you to my committee members, Dr. Daniel Buttry and Dr. Alexandra Ros for your time commitment and discussions over the years. I would also like to recognize the influential people when I was an undergraduate: Drs. Xiangmin Zhang, Mingxia Gao, Weifeng Shen, and Liang Li – thank you for showing me what is research and the encouragement to go to grad school.

I felt so lucky that I joined this group and met a lot of good friends. Dr. Kenyon, you were the first person I met in this group. I was so impressed that you were super nice, taught me all the techniques and tips, and trained me on every aspect you knew. Many thanks to Dr. Jones for sharing your experience of oral presentations with me. Dr. Woolley, it was so nice to work with you on both course projects and research projects. Even though you do not talk too much, I know you are such a nice and helpful friend! Thank you to Dr. Keebaugh for providing useful tips when I run COMSOL simulations. My special thanks to Dr. Ding. You are more than a good friend to me, sometimes, I even feel like you are my elder sister. You helped me so much not only in research, but also in

my life. You introduced many friends, plenty of delicious restaurants, and interesting TV shows to me, which saved me from loneliness! I am more than happy to witness your important moments-your wedding and final defense. Wish to see you and your little baby in Boston soon! Ryan, thanks for taking care of everything when I first came into group. Miss your guinea pigs, hedgehogs, and little Susan. Dr. Crowther and Dr. Hilton, we attended a lot of courses and taught a lot of labs together. Thank you two so much for always being there for help when I have any questions. I really enjoy communicating with you two when we have discussions that cover all kinds of topics. Yameng, thanks for coming into our lab! I really appreciate the time when we have lunch together!

On a more personal level, I must acknowledge my parents and my siblings. Thanks so much for all your love, patience, tolerance and understanding. Secondly, thank you to my friends all around the world, Drs. Yueqi Li, Yue Deng, Jinghui Luo, Mian Yang, Zhen Gong, Wenbo Chang, Chenwen, Runli, Yanyang, Yueming, Jing, Ling, Yingjing, Liyi… (so many good friends, just name a few), thank you all for your encouragement and support when I feel I cannot go through.

In addition, thank you to Mr. Ailun Guo for demonstrating the value of insistent on dreams and keeping on the things you really love.

TABLE OF CONTENTS

Page

LIST OF TABLES

LIST OF FIGURES

# CHAPTER 1

# INTRODUCTION

## 1.1 Electrophoresis

### 1.1.1 History of electrophoresis

The late eighteenth century witnessed the proposal of the laws of electrolysis by Faraday. Johann Wilhelm Hittorf, Walther Nernst, and Friedrich Kohlrausch combined electrolysis concepts with some early electrochemistry knowledge, and designed experiments to study the properties and behaviors of small ions moving through aqueous solutions under the influence of an electric field. Kohlrausch also came up with general mathematical descriptions of the electrochemistry in aqueous solutions, especially for charged particles with varying concentrations moving through solutions [1]. In 1937, Swedish scientist Arne Tiselius successfully applied electrophoretic techniques for the separation of colloidal mixtures [2]. Tiselius was awarded the Nobel Prize in Chemistry in 1948, "for his research on electrophoresis and adsorption analysis, especially for his discoveries concerning the complex nature of the serum proteins" [3].

However, electrophoresis was not widely known or accessible until the development of new electrophoresis approaches in late 1940s. These new electrophoresis approaches appeared to address some of the drawbacks from the Tiselius apparatus and attempted to separate compounds with similar electrophoretic properties. Instead of moving charged molecules freely through solutions, these new approaches used anticonvective media, such as solid or gel matrices to help separate compounds into discrete and stable bands (zones). In 1950 Tiselius named one of these methods zone electrophoresis [4]. Although it is one of the most widely used separation techniques, slab

gel electrophoresis still suffers from long analysis times, low efficiencies, and difficulties in detection and automation.

An alternative to the slab-format is to perform the electrophoretic separation in narrow-bore tubes or capillaries. Since narrow capillaries are themselves anticonvective, gel media are not essential to perform that function. This allows the performance of free-solution (or open tube) electrophoresis, as well as the use of the traditional gel media in the capillary. The earliest example of the use of capillaries for electrophoretic separations with high electric fields was from Hjerten in 1967, where he demonstrated the separation of proteins with a 3 mm I.D. capillary [5]. In 1974, Virtenen [6] discussed several advantages of using smaller diameter columns in electrophoretic separations. However, due to the inability for producing stable capillary columns, these works were unable to achieve high efficiencies.

The commonly accepted modern capillary electrophoresis (CE) system was introduced by James W. Jorgenson and his graduate student Krynn Lukacs, at the University of North Carolina, Chapel Hill. As a result of their pioneering work in the 1980s [7-10], the CE system has been widely used in academia, and resulted in CE industrial commercial availability in the late 1980s. From their work, fundamental concepts of modern capillary electrophoresis, such as zone broadening, as well as theoretical ideas on CE separation mechanisms, were proposed and presented [9].

Today, capillary electrophoresis is gaining popularity as a powerful analytical tool for various applications in terms of high separation efficiency, simplicity, low sample and solvent volume consumption, and short analysis time, and it has demonstrated tremendous capabilities for a wide range of applications [11].

### 1.1.2 Electrophoresis mechanism

Electrophoresis is defined as the motion of ions under the influence of an electric field in a condensed liquid phase. The ion undergoes force induced by the electric field and a frictional drag force. The force induced by the electrical field ($F_E = qE$) is proportional to its effective charge, $q$, and the electric field, $E$. The frictional force ($F_f = fv_{ep}$) is proportional to the velocity of the ion, $v_{ep}$, and the friction coefficient, $f$. The ion reaches a steady state velocity when the force induced by the electric field equals the frictional force:

$$qE = fv_{ep} \quad (1)$$

Rearranging equation (1) yields:

$$v_{ep} = \frac{q}{f}E = \mu_{ep} \times E \quad (2)$$

Here $\mu_{ep}$ is the electrophoretic mobility of the ion, which is a constant of proportionality between the velocity of the ion, $v_{ep}$, and the electric field, $E$. The electrophoretic mobility is proportional to the effective charge of the ion, $q$, and inversely proportional to the friction coefficient, $f$. The friction coefficient of the moving ion is related to the hydrodynamic radius, $r$, of the ion, and the viscosity, $\eta$, of the surrounding medium:

$$f = 6\pi\eta r \quad (3)$$

So

$$\mu_{ep} = \frac{q}{f} = \frac{q}{6\pi\eta r} \quad (4)$$

This indicates that for a given charge state a larger hydrodynamic radius is correlated to a lower electrophoretic mobility.

## 1.2 Equilibrium gradient focusing

Capillary electrophoresis can be used for a wide range of charged samples, but it is still restricted by a low concentration limit of detection and limited reproducibility. As a result, it becomes a major challenge for the increasing demand of complex sample analysis. To improve the efficiency of capillary electrophoresis, researchers have focused on many other electrophoretic techniques, for instance, isotachophoresis (ITP), field amplified sample stacking (FASS), sweeping, and equilibrium gradient focusing [12-18].

The equilibrium gradient principle was first summarized by Giddings in 1971 with the proposal of a separation scheme that largely overcomes the sensitivity limitation of traditional separation methods while retaining the high-resolution benefit associated with these techniques [19]. In conventional CE, the concentrated bands/zones continuously migrate through the separation channel, which might contribute to the band-broadening. In contrast, equilibrium gradient focusing sets a condition similar to Hooke's Law, where the deviation from the equilibrium point would result in a restoring force, pushing the analytes to be concentrated in narrow bands.

Equilibrium gradient focusing strategies generally utilize an electric field to drive charged analytes to a position of net zero force [20, 21]. These methods can be classified into two categories. In the first category, a constant external field is applied along the separation channel and a gradient in some properties, such as density or pH can be created. Isoelectric focusing (IEF) is an example of the first category, where a pH gradient is established through the application of an electric field and ampholytic analytes reach their unique isoelectric points [22]. The other strategy, also known as counter-flow gradient focusing, employs a force that is the opposite of a gradient force to establish the equilibrium condition [23]. Earlier research was from O'Farrell's counteracting

chromatographic electrophoresis (CACE) approach, where a separation column was packed with two different materials of different porosities to induce a gradient hydrodynamic velocity, opposing a constant electrophoretic velocity [24]. Later counter-flow gradient focusing techniques employed a gradient electrophoretic velocity induced by establishing conductivity [25-27], electric field [28-30], or temperature [31, 32] gradients within the system to counterbalance a hydrodynamic flow. More recent work also uses varying hydrodynamic velocity field to oppose the constant electric field for separation as gradient elution moving boundary electrophoresis (GEMBE) [33-39]. Simultaneous separation and preconcentration can be achieved through equilibrium gradient focusing techniques. Compared with IEF, counter-flow gradient focusing has a wider application of analytes with charges as it does not require ampholytic materials.

**1.3 Electrophoretic exclusion**

Inspired by the techniques mentioned above, Hayes research group, who is also working on the development of electrophoretic separation for biological sample applications, came up with another new technique, electrophoretic exclusion.

The principle of electrophoretic exclusion is illustrated with a simplified module with two reservoirs connected by one channel (Figure 1). The device is filled with solution containing two different analytes (black and green dots). The black analyte has a higher mobility than that of the green one (Figure 1 A). Once the solution is injected into the device from the left side, due to the pressure difference, hydrodynamic flow velocity is induced. This flow carries analytes moving from left to right. Potentials are applied to the electrodes to create an electric field, which induces electrophoretic velocity. By employing proper potentials, the direction of electrophoretic velocity can be opposite to

the hydrodynamic flow velocity. When the electrophoretic velocity of an analyte is larger than the hydrodynamic flow velocity, this analyte can be excluded at the entrance to the channel. Electrophoretic velocity depends on the mobility and the electric field. With a properly selected electric field, the black analyte, with a larger mobility, has a higher electrophoretic velocity to counterbalance the hydrodynamic flow velocity, thus being excluded at the entrance to the channel; while for the green analyte, its electrophoretic velocity is smaller than the hydrodynamic flow velocity, so it can flow through the channel. In this way, species with different mobilities can be separated (Figure 2 B). As the separation takes place at the entrance to the channel, the isolated analytes also experience accumulation simultaneously, which facilitates preconcentration.

A) B)

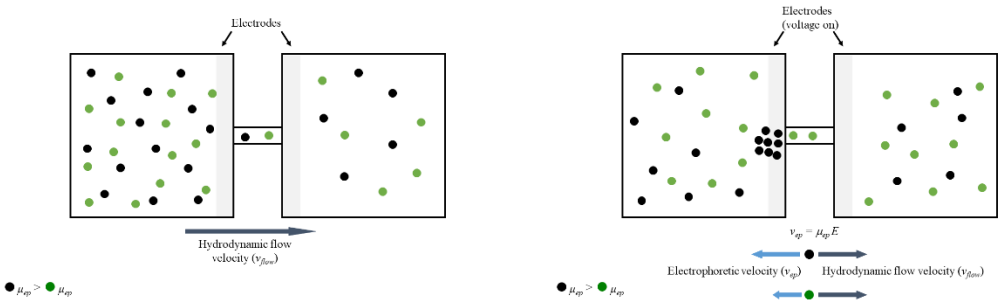


Figure 1.1 A simplified module with two reservoirs connected by one channel to illustrate the principle of electrophoretic exclusion. A) The solution contains analytes is loaded from the left side of the device to induce a hydrodynamic flow velocity. Two analytes are of different electrophoretic mobilities (black>green). B) A properly selected electric field across the channel induces electrophoretic velocity for these two charges particles. When the electrophoretic velocity is larger than the hydrodynamic velocity, sample can be excluded at the entrance of the channel. The electrophoretic velocity depends on the electrophoretic mobility and the applied electric field. With a carefully selected electric field, the analyte with a higher mobility can be excluded, while the analyte with a smaller mobility can still flow through the channel. Separation can be performed with this strategy.

This technique was first demonstrated as a bench-top device by Polson et al. [40]. Later, theoretical study on the conditions to achieve electrophoretic exclusion was investigated by the collaboration of Hayes group and KP Chen's group [41]. Meighan et al. showed the exclusion with an in-house built instrument [42] using an acidic buffer to minimize the electroosmotic flow (EOF) for simple interpretation and stable flow. The principle of exclusion was confirmed by using a mixture of fluorescent methyl green and neutral red dyes. A similar apparatus was used for the separation of proteins [43]. The capillary was modified via polyimide coating to eliminate the EOF. Myoglobin was concentrated over 1000-fold within a short period of time. Moreover, multiple proteins were able to separate, including a mixture of two positively charged species, and another mixture of species with opposite charges. Theoretical work from Kenyon et al. presented that electrophoretic exclusion can separate species with very similar mobilities (~$10^{-13}$ $m^2$/Vs), indicating that this technique may be able to generate better experimental results than those reported for CE [44].

Compared to other gradient focusing techniques, electrophoretic exclusion establishes a punctuated gradient instead of a smooth varying or incrementally stepped gradient within a channel to create a distinct interfacial zone at the channel entrance, which could allow separation of species with very similar mobilities at the interface. Moreover, since the exclusion takes place outside the channel, unlike those of chromatography, this technique is independent of the length of the channel, which makes this technique adaptable for use in microfluidic devices. Furthermore, species are separated in the bulk solution based upon their native properties without the need for a binding step or other pretreatment, and it can be easily coupled with various techniques

for detection, such as spectroscopy, mass spectrometry, and electron microscopy. The device is easy to fabricate, without using any membranes, which could avoid many issues, such as the retention of small molecules, and non-uniformities of the fields. Moreover, by applying small pressures, analytes can be easily separated with low absolute magnitude voltage, which could minimize bubble formation from electrolysis. In addition, due to the high surface to volume ratio of the micro-channels, the heat dissipation is of high efficiency.

### 1.4 Microfluidics

Emerging in the early 1990s, microfluidics refers to a set of technologies for the manipulation of small fluid volumes (μL, nL, pL) within artificially fabricated microsystems [45]. These devices can be made from different materials, with polymers presently emerging as the most popular choice. Other than being optically clear, non-toxic and inexpensive, polymers can also be easily fabricated with a variety of techniques. In addition, there are many polymer surface modification methods available to improve the efficiency of these devices [46]. Microfluidics have been widely adopted in various fields of analytical chemistry and life science. Recent decades have witnessed the rapid development of microfluidic devices due to their advantages over bench-top devices, such as portability, flexibility in design, miniaturization of operating systems, reduced reagent consumption, decreased run time, minimized sample dilution, and accelerated mass and heat transfer [47].

Consequently, the realization of microfluidic platforms for the manipulation and analysis of protein biomarker samples has attracted significant interest, especially for point-of-care diagnosis in future clinical applications.

### 1.5 Protein biomarkers

Biomarkers have been initially defined as “cellular, biochemical or molecular alterations that are measurable in biological media such as human tissues, cells or fluids” [48]. The definition has been broadened to objective indicators that can be measured or evaluated to reflect the biological, pathologic or pharmacologic processes [49].

More attention has been attracted to the biomarkers from the beginning of this century, as biomarkers could allow prediction of individual diseases, differentiation of “good outcome” from “poor outcome”, decision of whom to treat and/or how aggressively to treat, assessment of a particular treatment, measurement of drug effect, and guidelines of dose selection [50].

Among all the research on biomarkers, 78% is focused on disease-related biomarkers and is one of the best strategies to combat diseases since they can provide early diagnosis and assist with administration of effective treatment (drugs, surgery, and vaccines) [51]. These efforts can potentially improve human life expectancy [52].

Several types of analytes can be considered as potential biomarkers, including physical symptoms, DNA or RNA, proteins, processes such as death cells or proliferation, and existence of small molecules in serum such as glucose [53].

Among these, protein biomarkers have been extensively studied, as they are the critical machinery of the functioning living organism, acting as hormones, hormone or drug receptors, enzyme and enzyme substrates or inhibitors, antigens and antibodies, structural elements and transporting molecules [54]. The protein domain is more likely to be affected by disease, response and recovery when compared to transcriptional profiling, DNA methylation, and metabolomics approaches [55]. Protein concentration are

relatively more detectable by current technologies, and guidelines and predications can be obtained through genomics as complementary information [56]. Accordingly, great focus has been placed on proteins in biomarker research. Protein biomarkers include peptides, globular proteins, fibrous proteins, and membrane proteins. Their differential expression/abundance (including absence), and structural or functional alterations (e.g. via post-translational modifications) can provide markers of certain biological states [57].

With rapid developments in clinical trial results and new technology developments, disease prevention and personalized therapy and treatment will be supported with the integration of protein biomarkers into medical practice.

One major focus of bioanalytical chemists and clinical researchers is the detection of protein biomarkers among complex matrices or biofluids, such as plasma, serum, urine, and cerebrospinal fluid (CSF). Identification and quantification of proteins remains as a significant analytical problem. The proteome of a cell or serum is defined by a combination of genome, environment, and history, which is quite complicated, dynamic, and adds many challenges to protein analysis and interpretation. Moreover, a human cell may express up to 20, 000 proteins with a high dynamic range spanning over ten orders of magnitude, while the target protein biomarker may be in the low abundance range [58].

Therefore, it is generally necessary to perform a preconcentration process prior to performing detection of protein biomarkers in order to improve the reliability and efficiency of the measurement. Separation science, thus, plays an important role for better protein biomarker analysis. Various methods have been presented for the isolation and preconcentration of proteins, including chromatographic (e.g. high-performance liquid

chromatography (HPLC) and gas chromatography (GC)) and electrophoretic methods (e.g. gel electrophoresis, capillary electrophoresis and equilibrium gradient focusing techniques).

### 1.6 Dissertation objectives

This dissertation is dedicated to describing an electrophoretic separation technique on a microfluidic device that is envisioned as a tool for protein biomarker isolation and preconcentration for future point-of-care diagnosis in clinical applications. Electrophoretic exclusion, the off-gel electrophoretic separation method presented here, was initially performed on a bench-top device. The performance of a capillary-based bench top apparatus has been examined and the resolution is estimated to be comparable to a conventional CE instrument. The bulk of the work presented in this document discusses the investigation of electrophoretic exclusion on a microdevice for developmental aspects and applications of this technique. These two aspects are closely related, and three main topics are derived from these two aspects, including: the influence of electrode placement on concentration, the possibility of manipulating diluted protein samples for electron microscopy detection and structural determination, as well as the separation and preliminary quantification of biomarkers. These works are expected to move steps towards point-of-care diagnosis in future clinical applications.

### 1.7 Dissertation summary

To first introduce the field of electrophoretic-related separation and preconcentration techniques on miniaturized devices, a review is included as Chapter 2. This chapter covers several gradient-based techniques according to a broad definition, including conductivity, field, and concentration, organized by the method of gradient

generation. Each technique is introduced and described, and recent seminal advances are explored. Articles that are reviewed in this chapter are focused on literature in the past few years. Chapters 3-4 present simulations and experiments with electrophoretic exclusion. Chapter 3 describes the advantages of an array-based microdevice of electrophoretic exclusion and presents general results using dye molecules obtained from this device with detection occurring in central reservoirs and/or channel areas. Chapter 4 investigates different electrode placement patterns by comparing the simulation results from commercial finite element mesh software to experiment results, demonstrating subtle changes at interfacial zone have significant and non-linear impact on distribution of concentration profiles. A 3D simulation is also developed and included in this chapter.

Chapter 5-6 covers applications on more practical samples and realistic scenarios with array-based microfluidic electrophoretic exclusion. Chapter 5 presents coupling of electrophoretic exclusion with transmission electron microscopy, especially focused on demonstrating electrophoretic exclusion as a method to improve electron microscopy sample preparation and loading process with diluted protein samples, which potentially benefits further structural determination as well as protein biomarker structural identification and validation. Chapter 6 demonstrates consistent separation and concentration behaviors of two protein biomarkers with current electrophoretic exclusion microdevice. A preliminary test without bulky high voltage power supply is also investigated, which opens up the possibility of electrophoretic exclusion microdevice for point-of-care diagnosis. An intermediate design is also proposed to achieve separation and preliminary quantification in an integrated system.

Chapter 7 summarizes the goals and results of the electrophoretic exclusion technique that were presented in Chapters 3-6. Conclusions and future directions are also discussed.

**1.9 References**


[1] Kohlrausch, F., *Annalen der Physik* 1897, *298*, 209-239.

[2] Tiselius, A., *Transactions of the Faraday Society* 1937, *33*, 524-531.

[3] NobelPrize.org, Nobel Media AB 2019, p. https://www.nobelprize.org/prizes/chemistry/1948/summary/.

[4] Tiselius, A., Flodin, P., *In Advances in Protein Chemistry* 1953, *8*, 461-486.

[5] Hjertén, S., *Chromatographic reviews* 1967, *9*, 122-219.

[6] Virtanen, R., *Acta Polytechnica Scandinavica-Chemical Technology Series* 1974, *123*, 1-67.

[7] Jorgenson, J. W., Lukacs, K. D., *Journal of Chromatography A* 1981, *218*, 209-216.

[8] Jorgenson, J. W., Lukacs, K. D., *Clinical chemistry* 1981, *27*, 1551-1553.

[9] Jorgenson, J. W., Lukacs, K. D., *Science* 1983, *222*, 266-274.

[10] Jorgenson, J. W., Lukacs, K. D., *Journal of High Resolution Chromatography* 1985, *8*, 407-411.

[11] Rajput, H. H., Deokate, U. A., Nawale, R. B., *World J. Pharm. Pharm. Sci* 2016, *5*, 450-465.

[12] Breadmore, M. C., *Electrophoresis* 2007, *28*, 254-281.

[13] Breadmore, M. C., Thabano, J. R., Dawod, M., Kazarian, A. A., Quirino, J. P., Guijt, R. M., *Electrophoresis* 2009, *30*, 230-248.

[14] Breadmore, M. C., Dawod, M., Quirino, J. P., *Electrophoresis* 2011, *32*, 127-148.

[15] Breadmore, M. C., *J Chromatogr A* 2012, *1221*, 42-55.

[16] Breadmore, M. C., Shallan, A. I., Rabanes, H. R., Gstoettenmayr, D., Abdul Keyon, A. S., Gaspar, A., Dawod, M., Quirino, J. P., *Electrophoresis* 2013, *34*, 29-54.

[17] Breadmore, M. C., Tubaon, R. M., Shallan, A. I., Phung, S. C., Abdul Keyon, A. S., Gstoettenmayr, D., Prapatpong, P., Alhusban, A. A., Ranjbar, L., See, H. H., Dawod, M.,

Quirino, J. P., *Electrophoresis* 2015, *36*, 36-61.

[18] Breadmore, M. C., Wuethrich, A., Li, F., Phung, S. C., Kalsoom, U., Cabot, J. M., Tehranirokh, M., Shallan, A. I., Abdul Keyon, A. S., See, H. H., Dawod, M., Quirino, J. P., *Electrophoresis* 2017, *38*, 33-59.

[19] Giddings, J. C., Dahlgren, K., *Separation Science* 1971, *6*, 345-356.

[20] Ista, L. K., Lopez, G. P., Ivory, C. F., Ortiz, M. J., Schifani, T. A., Schwappach, C. D., Sibbett, S. S., *Lab on a chip* 2003, *3*, 266-272.

[21] Wang, Q., Tolley, H. D., LeFebre, D. A., Lee, M. L., *Analytical and bioanalytical chemistry* 2002, *373*, 125-135.

[22] Righetti, P. G., Chillemi, F., *Journal of Chromatography A* 1978, *157*, 243-251.

[23] Shackman, J. G., Ross, D., *Electrophoresis* 2007, *28*, 556-571.

[24] O'FARRELL, P. H., *Science* 1985, *227*, 1586-1589.

[25] Greenlee, R. D., Ivory, C. F., *Biotechnology progress* 1998, *14*, 300-309.

[26] Ren, C. L., Li, D., *J Colloid Interface Sci* 2006, *294*, 482-491.

[27] Barz, D. P. J., *Microfluidics and Nanofluidics* 2008, *7*, 249-265.

[28] Humble, P. H., Kelly, R. T., Woolley, A. T., Tolley, H. D., Lee, M. L., *Analytical chemistry* 2004, *76*, 5641-5648.

[29] Sun, X., Farnsworth, P. B., Woolley, A. T., Tolley, H. D., Warnick, K. F., Lee, M. L., *Analytical chemistry* 2008, *80*, 451-460.

[30] Sun, X., Farnsworth, P. B., Tolley, H. D., Warnick, K. F., Woolley, A. T., Lee, M. L., *Journal of chromatography. A* 2009, *1216*, 159-164.

[31] Hoebel, S. J., Balss, K. M., Jones, B. J., Malliaris, C. D., Munson, M. S., Vreeland, W. N., Ross, D., *Analytical chemistry* 2006, *78*, 7186-7190.

[32] Shackman, J. G., Munson, M. S., Ross, D., *Analytical and bioanalytical chemistry* 2007, *387*, 155-158.

[33] Shackman, J. G., Munson, M. S., Ross, D., *Analytical chemistry* 2007, *79*, 565-571.

[34] Burke, J. M., Ivory, C. F., *Electrophoresis* 2008, *29*, 1013-1025.

[35] Strychalski, E. A., Henry, A. C., Ross, D., *Analytical chemistry* 2009, *81*, 10201-10207.

[36] Strychalski, E. A., Henry, A. C., Ross, D., *Analytical chemistry* 2011, *83*, 6316-6322.

[37] Smejkal, P., Bottenus, D., Breadmore, M. C., Guijt, R. M., Ivory, C. F., Foret, F., Macka, M., *Electrophoresis* 2013, *34*, 1493-1509.

[38] Ross, D., Munson, M. S., *Electrophoresis* 2014, *35*, 770-776.

[39] Sikorsky, A. A., Fourkas, J. T., Ross, D., *Analytical chemistry* 2014, *86*, 3625-3632.

[40] Polson, N. A., Savin, D. P., Hayes, M. A., *Journal of Microcolumn Separations* 2000, *12*, 98-106.

[41] Pacheco, J. R., Chen, K. P., Hayes, M. A., *Electrophoresis* 2007, *28*, 1027-1035.

[42] Meighan, M. M., Keebaugh, M. W., Quihuis, A. M., Kenyon, S. M., Hayes, M. A., *Electrophoresis* 2009, *30*, 3786-3792.

[43] Meighan, M. M., Vasquez, J., Dziubcynski, L., Hews, S., Hayes, M. A., *Analytical chemistry* 2011, *83*, 368-373.

[44] Kenyon, S. M., Keebaugh, M. W., Hayes, M. A., *Electrophoresis* 2014, *35*, 2551-2559.

[45] Halldorsson, S., Lucumi, E., Gomez-Sjoberg, R., Fleming, R. M. T., *Biosens Bioelectron* 2015, *63*, 218-231.

[46] Lim, C. T., Zhang, Y., *Biosens Bioelectron* 2007, *22*, 1197-1204.

[47] Tabeling, P., *Introduction to microfluidics*, Oxford University Press on Demand 2005.

[48] Humphries, S., *Journal of epidemiology and community health* 1991, *45*, 173.

[49] Naylor, S., 2003, 525-529.

[50] Vogenberg, F. R., Barash, C. I., Pursel, M., *Pharmacy and Therapeutics* 2010, *35*, 560.

[51] Diamandis, E. P., *Mol Cell Proteomics* 2004, *3*, 367-378.

[52] Sonker, M., Sahore, V., Woolley, A. T., *Anal Chim Acta* 2017, *986*, 1-11.

[53] Rusling, J. F., Kumar, C. V., Gutkind, J. S., Patel, V., *Analyst* 2010, *135*, 2496-2511.

[54] Wu, L., Qu, X., *Chem Soc Rev* 2015, *44*, 2963-2997.

[55] Rifai, N., Gillette, M. A., Carr, S. A., *Nat Biotechnol* 2006, *24*, 971-983.

[56] Hanash, S. M., Pitteri, S. J., Faca, V. M., *Nature* 2008, *452*, 571-579.

[57] Nahavandi, S., Tang, S. Y., Baratchi, S., Soffe, R., Nahavandi, S., Kalantar-zadeh, K., Mitchell, A., Khoshmanesh, K., *Small* 2014, *10*, 4810-4826.

[58] Chandramouli, K., Qian, P. Y., *Hum Genomics Proteomics* 2009, *2009*.

# CHAPTER 2

# EXPLORING GRADIENTS IN ELECTROPHORETIC SEPARATION AND PRECONCENTRATION ON MINIATURIZED DEVICES

## 2.1 Introduction

Superior capabilities of microfluidic devices, compared to bench-top equivalents, have earned them significant popularity. Advantages for the microdevices include miniaturized operation systems, reduced reagents consumption, minimal waste, and reduced time per operation. Examples of these features include separation and preconcentration methods, including gravitational force [1], electrophoretic force [2-6], magnetic force [7, 8], acoustic waves [9-11], and optofluidics [12-14].

Electrophoretic-based separation and preconcentration schemes were initially drawn from capillary electrophoretic methods. Electrophoresis has exerted a powerful influence and has led to a variety of derivations and branches, including field-amplified sample stacking [15-24], isotachophoresis [19, 25-33], free flow electrophoresis [34-38], and gradient focusing [39-46]. Among them, gradient techniques are of special interest. In addition to creating separations, they can function in sample preparation and/or preconcentration roles to increase sensitivity of microdevices [41, 42, 46].

This chapter focuses on strategies that include gradients which improve performance. The term gradient, as used here, has a broad definition and includes conductivity, concentration or velocity profile. Articles are sourced from recent years and the review does not attempt to be comprehensive or exhaustive, but instead, provides a new perspective of recent developments. Several subjects are excluded for clarity and

space, including dielectrophoresis, field-flow electrophoresis, and droplet-based microfluidics—while these are all recognized to use gradients.

### 2.2 Conductivity gradient

One strategy to create a gradient is to induce a variation in conductivity. This can be trivially understood by examining equation $E=I/\sigma A$ (or simply, Ohm's law, where $E$ is the electric field, $I$ is the current, $\sigma$ conductivity, and $A$ the cross-sectional area), the conductivity difference directly influences the local electric field, thus creating the gradient.

#### 2.2.1 Field-amplified sample stacking/Field-amplified sample injection (FASS/FASI)

Field amplified sample stacking/sample injection has long been considered. It is one of the most commonly used and straight-forward mode of electrophoretic separation. The stacking effect can be achieved through a conductivity difference between samples and background electrolyte (usually the conductivity of background electrolyte is 10 times higher than that of the sample). When the voltage is applied, the electric field strength on the sample is higher compared to the background electrolyte, due to the lower conductivity. As a result, sample starts to stack in the boundary—the nominal location of the gradient.

The dynamics of this technique have been fully investigated by Bharadwaj et al. [18]. In that work, situations with and without electroosmotic flow (EOF) were studied. By building up the governing equations regarding convention, migration and diffusion, as well as considering the boundary conditions, the study provided a platform for a better understanding of FASS. In the following work, they calculated that the highest concentration enhancement achieved is 1100 fold [17].

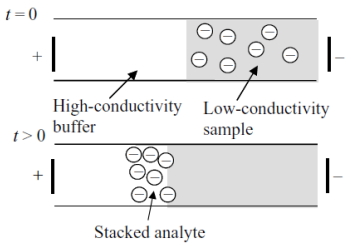


Figure 2.1 A schematic showing the basic principle of field-amplified sample stacking [18].

These techniques are not typically used alone, as it serves as an efficient sample introduction technique. They couple with a variety of other analytical methods for detection and identification on miniaturized-scales, including microchip electrophoresis, ICP-MS [47], ELISA [48], MEKC [49], and amperometry [50].

### 2.2.2 Isotachophoresis (ITP)

Isotachophoresis techniques have been common since the 1970's and, similar to field-amplified sample stacking method, ITP also uses conductivity difference to form gradient. The major difference is that amplified sample stacking relies on only one background electrolyte, while ITP uses two background electrolytes with different mobilities. The higher mobility is the leading electrolyte and the lower mobility the terminating electrolyte. The mobility of all the components of the sample must be between that of leading electrolyte and terminating electrolyte. Given the similarities between FASS and ITP, a comparison is tabulated (Table 2.1).

Table 2.1 A comparison between field-amplified sample stacking (FASS) and isotachophoresis (ITP).

| Techniques | FASS | ITP |
|---|---|---|
| Mobility requirement | Background electrolyte (BGE), sample (S), usually $\mu_{BGE} \geq 10\ \mu_S$ | Leading electrolyte (LE), terminating electrolyte (TE), sample (S), $\mu_{TE} < \mu_S < \mu_{LE}$ |
| Governing equations | $\frac{\partial C_i}{\partial t} + u \cdot \nabla C_i = -z_i v_i F \nabla \cdot (C_i E) + D_i \nabla^2 C_i$, $C_i$ is the concentration of ionic species $i$, $D_i$ is the molar diffusivity of species $i$, $v_i$ is the electromigration mobility, $z_i$ is the valence number, $F$ is Faraday's constant, $u$ is the fluid velocity, and $E$ is electric field; solution is approximately electrically neutral (except EDL); modified Stokes equation; a slip surface [16]. | $\frac{\partial C_i}{\partial t} + \alpha \vec{u} \cdot \nabla \overrightarrow{C_i} = -v_i \vec{\nabla} \cdot \left(C_i \vec{E}\right) + \frac{1}{Pe} D_i \nabla^2 C_i$, $C_i$ is the molar concentration of ion $i$, $v_i$ is the electrophoretic mobility, $E$ is the electric field, and $D_i$ is the diffusion coefficient, $\mathrm{Pe} = E_0 v_0 \delta / D_0$, $\alpha = -\epsilon \zeta_0 / (\mu v_0)$ (μ is viscosity, $\zeta_0$ is zeta potential, and $\delta$ is the length of stacked sample zone); EOF suppressed; diffusion dominates [48]. |
| Concentration enhancement | Based on the ratio of electric field in the sample and the BGE regions $\frac{C_{stacked}}{C_{Initial}} = \frac{E_S}{E_{BGE}}$, up to 1100-fold [43]. | Derived from Kohlrausch regulating function (KRF) $C_{Sample-plateau} = \frac{Z_{LE}(\lvert\omega_{LE}\rvert + \lvert\omega_{Counter-ion}\rvert)\omega_{Sample}}{Z_{Sample}\left(\lvert\omega_{Sample}\rvert + \lvert\omega_{Counter-ion}\rvert\right)\omega_{LE}} C_{LE}$ $Z$, ω, $C$ are charge, mobility, concentration respectively, up to 100,000 -fold [48]. |
| Coupled techniques | Mass spectroscopy [44], amperometry [47], ELISA [45], MEKC [46]. | GEITP [28], FFITP [49], EKS [50], CZE [51]. |

Bocek et al. has contributed a great deal to this area. They published reviews every two years describing new progress in the field of capillary isotachophoresis [26, 29,

33]. They also collaborated with Ivory's group and reported a review on microfluidic isotachophoresis [30]. Santiago's group has contributed a review on the development of ITP (in addition to his considerable original contributions, see below) [32].

This technique can be roughly divided into two categories, regular (mono-directional) and bidirectional. Here, mono-directional ITP refers to those isotachophoretic methods that only apply to enrich cations or anions. Bidirectional ITP aims at concentrating both cations and anions at the same time. Mono-directional ITP has been highly developed and most recent works have been focused on practical applications on biological samples. Below are some seminal examples among all the elegant applications.

Ivory's group selected biomarker cardiac troponin I (cTnI) as a model study. cTnI is produced in myocardium and is related to heart disease (also see Chapter 6). The phosphorylated level of cTnI can help to determine the risk and best treatment option. They started this work with a poly(methylmethacrylate) (PMMA) microdevice with a 50x reduction in the cross-sectional area [51]. The reduction in width or depth can give rise to a concentration increase. With this device, over 10,000 fold concentration of cTnI and R-phycoerythrin was achieved, and, with modifications, optimized their device to a 100x reduction [52]. With that device, labeled cTnI sample in depleted human serum was examined. Cationic ITP in a straight channel was investigated for a sample with more components in solution to mimic the situation even closer to human serum, such as NaCl, urea, and triton X-100 [53]. However, the results did not give as high efficiency as they previously demonstrated. They proposed it was mainly due to the surface adsorption and formation of bubbles from the sample loading procedures. To further explore and confirm their hypothesis, they conducted the numerical simulation. Future directions include

adapting this strategy to immunoassay for distinguishing of phosphorylated and unphosphorylated cTnI.

A)

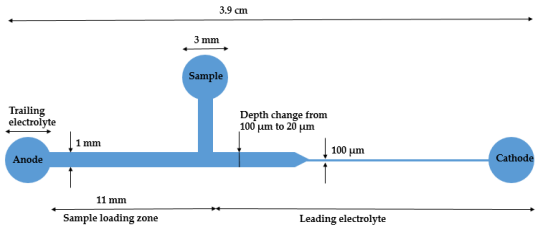


B)

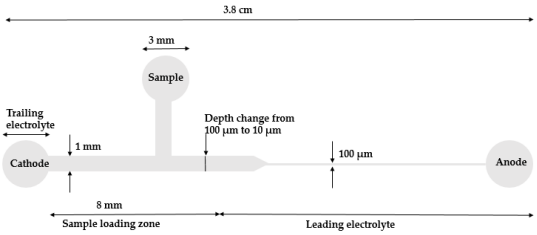


Figure 2.2 The schematics of reduction (A:50x [51], B:100x [52]) cross-sectional area PMMA ITP microdevices for cTnI concentration from Ivory's group. When samples passed through the reduction area, the sample concentration increased based on the reduction ratio.

Another excellent example is from Santiago and co-workers showing preconcentration of biomolecules, especially DNA and RNA [32]. In 2012, they reported a miniaturized system for extracting RNA from bacteria suspended in blood and avoided some contamination and degradation issues, achieving high sensitivity, up to 100,000 higher than some popular schemes [27]. The design was fairly simple, with a single straight channel and two ports. Terminating electrolytes (TE) were injected into the left port, while the leading electrolytes (LE) were injected into the right port. The samples were introduced directly into the left port after incubation. After separation they could be

easily coupled to PCR and other secondary detection methods. In that work, they validated their results with qPCR. They also published a modified design to simultaneously separate and concentrate RNA and DNA from single cells [54]. The design was implemented with branched channels, connecting to vacuum for sample loading. Coupling online pretreatment steps have also been accomplished. The whole process, including lysis, extraction and fractionation could be done in less than five minutes [55]. A similar design has also been applied to co-focus DNA and beads, which could potentially increase the DNA hybridization rate [56]. The complete process only took less than 20 minutes, a large reduction in the time required compared to conventional methods (20 hours) without significant concentration loss. In other work, a novel ITP device was designed to have two identically-shaped simple compartments connected with a thin channel [57]. The latter compartment contained some DNA probes. The sample underwent preconcentration via ITP, diffusion through the thin channel and entered the second compartment for hybridization. In a third design, both PMMA and cyclin olefin copolymer (COC) chips were fabricated to conduct ITP separation of DNA samples [58]. The design had a long turn channel and high aspect-ratio, which could potentially reduce dispersion and heat dissipation. A special structure for loading was incorporated in this device, which enabled the injection of 25 μL samples into device without waste. This method proved to have high recovery efficiency, well suited for precious and limited volume samples.

A) B)

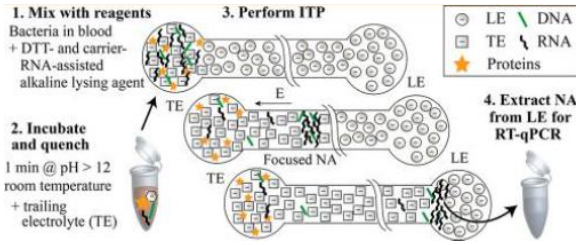


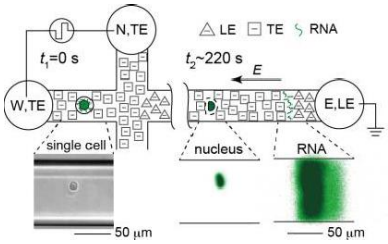


C) D)

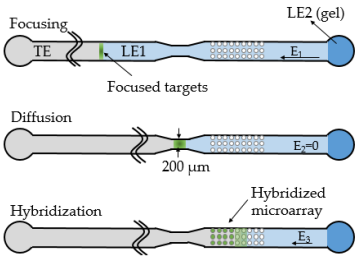


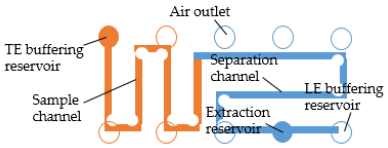


Figure 2.3 Four promising ITP devices from Santiago's group. A) Most typical design that has been used for DNA and/or RNA extraction by their group [54]. B) The modified version with branches facilitating sample loading [55]. C) Two identical shaped compartments for ITP and capture [57]. D) Long-wind channel for high performance ITP [58].

Santiago's group led the development of bidirectional ITP as well. In their work, they achieved bidirectional ITP in a straight channel through the application of shock wave [59, 60]. Different from mono-directional ITP, in their applications, four electrolytes were used, namely cationic leading electrolyte, cationic terminating electrolyte, anionic leading electrolyte and anionic terminating electrolyte. Using anionic analytes as an example, when voltage was applied, they formed distinct bands between leading electrolyte and terminating electrolyte, migrating in one direction. At the same time, the cationic electrolytes also underwent isotachophoresis, migrating in the opposite direction. When these two shock waves met, there would be a replacement of ions, so the conditions would dramatically change. In one of these applications, the ion exchanging

process eliminated the isotachophoresis condition. Then, it was switched to electrophoretic separation automatically without any treatment and non-focusing tracer method was used to visualize experimental results [59]. In another case, they have successfully generated the LE concentration cascade to further increase the sensitivity of ITP technique [60]. Their schemes could also achieve bidirectional ITP for protein and DNA purifications [61]. This bidirectional device was with one single input in the middle and two output reservoirs connected by two ‘C’ shaped channels for ITP separation of proteins and nucleic acids simultaneously. One channel conducted cationic ITP for enriching positively-charged proteins, the other channel performed anionic ITP for negatively-charged nucleic acids from human blood serum. This bidirectional ITP method was demonstrated to have high recovery efficiency and compatibility with PCR and other extraction methods.

Ross and co-workers have contributed to gradient elution ITP (GEITP) [31]. Compared to conventional ITP, it includes applied pressure-driven flow as a counterforce to the electrophoretic movement, generating precise position control and avoids introduction of contaminates. In their research, the capillary-based GEITP device was used to extract DNA from crude samples without significant pretreatment.

Free flow electrophoresis is another direction aimed at the improvement of current capillary electrophoresis [62]. Unlike most of the techniques addressed here, the field is applied perpendicular to the velocity direction, making the deflection of the species unique to their electrophoretic mobility. This technique is quite flexible and is hybridized with other electrophoretic separation techniques, such as isotachophoresis (FFITP). Prest and co-workers first miniaturized the FFITP device and applied this to

separation of bacteria. The design consisted of a rectangular chamber with nine inlets and nine outlets on short sides of the chamber as well as electrodes on long sides. The leading electrolytes were injected into the chamber from the left three inlets with a higher rate, while the terminating electrolytes from the right three inlets with a smaller flow rate and samples from the middle three inlets. Once the chambers were filled with a mixture of leading and terminating electrolytes, the separation started with the application of a constant current. Prior to bacteria separation, they first used this device on dyes. The results were quite promising. While dealing with bacteria samples, they made the visualization available by mixing the bacteria samples with a dye solution.

Electrokinetic supercharging (EKS) consists of field-amplified sample injection and isotachophoresis. Hirokawa and his co-workers designed a microdevice with three ports and a long curved channel for floating electrokinetic supercharging to separate, concentrate and analyze DNA samples [63]. The three ports were electronically floated to differ from conventional EKS and the long, turned channel was used for separation. Parameters and geometry were optimized for reducing band broadening effect. Fung and co-workers have realized two-dimensional transient scheme (t-ITP/CZE) for the detection of clinical urinary proteins [64]. Four urinary samples were successfully separated through a 2D t-ITP/CZE microdevice. The transient step was mainly used for desalting and preconcentration, while CZE was used for separation. The microdevice generated results in a short time, showing high enrichment and low LOC compared to standard clinical techniques.

Isotachophoresis can be performed in other mediums, paper-based microdevice serving as a prime example. In Bercovici's work, 1000-fold concentration enhancement

was demonstrated with porous media [65]. The device was easy to fabricate without complicated enclosure. The key point of designing this device was to minimize Joule heating and evaporation. This was achieved by printing shallow channels for a high heat dissipation efficiency. One major drawback was the dispersion effects. Another example was from Posner and co-workers [66]. A simple paper-based device was used to perform ITP concentration of fluorescent tracer. The results showed good agreement with numerical simulations. Moreover, the device can be powered by battery, showing the ability to be a portable device.

Separations based on ITP have been performed on commercialized all-in-one platform microdevices. Breadmore and co-workers explored some customized features of this instrument [67-69]. To evaluate the analytical potential of the system, the method was used for the quantitative analysis of benzoate in soft drinks. The results were validated with a CZE method with generally good agreement [68]. Using the same strategy on lactate in serum did not produce the same results, especially compared to the commercial chips [69]. In response, they designed a chip for ITP separation. With this customized chip, they performed lactate concentration determination in three different serum samples quantified by CZE and ITP individually using commercial systems. Both methods generated comparable results, demonstrating the platform was available for a diverse range of applications.

### 2.2.3 Conductivity gradient focusing

The early application of conductivity gradient for protein concentration came from Ivory's group [40]. They used a chamber that was divided into compartments by a dialysis membrane. Buffers of different conductivities were placed in each section. The

species with low molecular weight could pass through the membrane, creating the conductivity gradient when the voltage was applied. A convective force was employed to balance the electrophoretic velocity of proteins. The basic principles of this technique combining electric field, fluid field and mass transportation, were described as well.

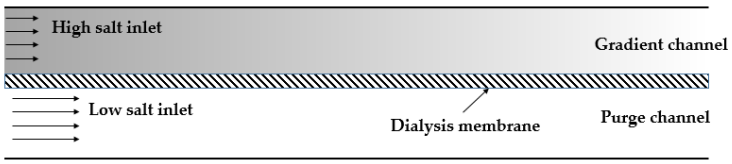


Figure 2.4 Schematic of conductivity gradient focusing from Ivory's group [40].

Inglis and co-workers have contributed to the development of this technique with a device that has a tapered channel, filled with low conductivity buffer on one side and high on the other side, creating gradient along the channel [70]. Once the electric field is applied, both electrophoretic velocity and the electroosmosis are induced. In the low conductivity zone, the electrophoretic velocity dominates, while at the high conductivity zone, the electroosmotic flow dominates, thus focusing different species at distinct locations based on their individual mobilities. Separation and concentration of two proteins were performed in this device, achieving 1000-fold concentration enhancement within 20 minutes. They also investigated the effects of altering the electric field [71]. Four different geometries, including rectangular channel and three tapered channels with different length ratios were studied. Based on the numerical simulations and experimental results, the tapered channel had the best performance. They proposed that in the rectangular channel focusing took place only when the flow direction was opposite to the conductivity gradient, since the electric field increased at low conductivity end. When flow direction and conductivity gradient were the same, the trapping was unstable. While

in the tapered channel, the electric field was higher at both ends and, with the channel width reduced, the field magnitude increased. A weakness was that, in the numerical simulation, it was assumed the electroosmotic flow was constant along the channel. In reality the electroosmotic flow was non-uniform due to gradients in the electric field and local electroosmotic mobility [72]. The non-uniformity of the electroosmotic flow changed the proposed mechanism and the varying electric field and the electric double layer thickness formed a counter electroosmotic flow at the low conductivity zone end of the device, increasing the trapping efficiency of proteins. With a new simulation, they re-examined the four geometries and the numerical results matched well with experimental results.

## 2.3 Counterflow electric field gradient

When electric field gradient is combined with another force to perform focusing in a single buffer, the strategy is commonly referred as counterflow electric field gradient (Figure 2.5). In most cases, one of the velocities holds constant while the other varies, the species focuses at the place where two velocities sum to zero.

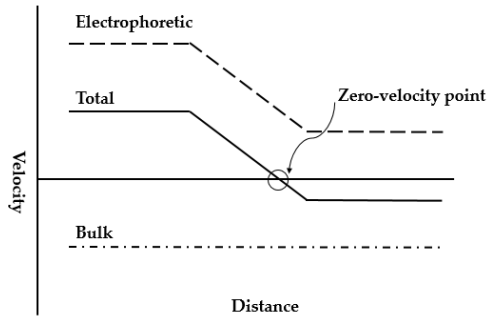


Figure 2.5 A universal schematic of counterflow electric field gradient focusing strategies [43].

### 2.3.1 Electric field gradient focusing/Dynamic field gradient focusing (EFGF/DFGF)

This technique employs an electric field and a pressure-induced flow. Ivory's group has made significant contributions to the development of EFGF. As early as 1996, they published an article introducing the strategy, where the electrophoretic force was countered by the convective force [39, 73]. The apparatus consisted of a chamber with varying cross-sectional area along the axis, inducing the electric field gradient. The flow was constant in the chamber. The chamber was split into two parts via a dialysis membrane, which allowed electric current to pass but not the convective flow. With this setup, they examined the focusing and separation of hemoglobin.

They also investigated a computer controlled array of electrodes to create a precise electric field gradient [74]. They termed this new branch dynamic field gradient focusing. From 2008 to 2010, they reported a variety of applications using this technique in preparative-scale apparatus [74-76]. The applications were all on preparative-scale and some were considered to be cumbersome and complicated.

Lee and colleagues contributed to analytical EFGF devices. They first proposed a device made of ionically conductive acrylic copolymer, which allowed ions to permeate but not proteins. A horn shape of the device enabled the creation of an electric field gradient [77, 78]. They successfully concentrated fluorescent protein 10,000-fold and demonstrated the separation of a mixture of proteins. The peak capacity and resolution of this device was relatively low, and the protein adsorption was a challenge. To ameliorate these problems, they used poly (ethylene glycol) (PEG)-functionalized acrylic plastic, which decreased protein adsorption. The PEG-functionalized monolith was also used to reduce dispersion [79]. The packed or monolithic column could disrupt the laminar flow profile (compared to an open channel), which flattened the parabolic shape of laminar

flow, thus increasing resolution. They optimized the device via switching to another buffer solution, which could produce a more linear electric field [80]. The results from this modified device showed narrower peak width and smaller standard deviation. With the optimized device, they investigated the ability to create bilinear electric field gradient focusing, which would enhance the resolving power and the peak capacity simultaneously [81].

In 2012, Breadmore and his co-workers developed a new strategy to generate electric field gradient by using a variable width polyaniline (PANI) electrode [82]. The idea was similar to Lee's work, replacing the horn-shape hydrogel with a PANI electrode. The width along the axial dimension varied to create variable resistances, thus generating an electric field gradient. The advantage of PANI electrode was that it relied on the low conductivity of PANI polymer, enabling the application of higher voltage with less current. With this technique, they were able to successfully concentrate two fluorescent dyes.

A) B)

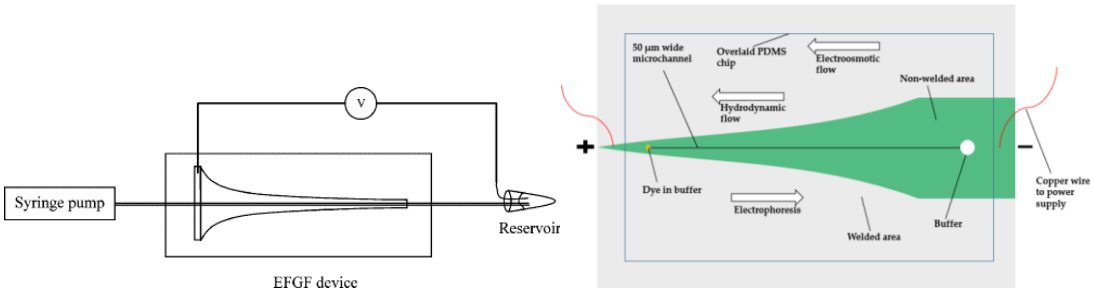


Figure 2.6 Schematics of two electric field gradient focusing techniques. A) Horn-shape design from Lee's group [77]. The device was fabricated with poly (ethylene glycol) (PEG)-functionalized acrylic plastic to reduce protein adsorption. Moreover, the PEG-functionalized monolith was incorporated in the device to reduce dispersion. B) Variable width PANI electrode design from Breadmore's group [82]. The dark-green area in the picture was made of PANI electrode with variable width.

More recent work on EFGF focused on theoretical foundations. A group in Canada, inspired by Lee's work, combined the bilinear gradient with swept counter-flow [83]. Numerical simulations were performed to assess the resolution using various parameters, including length, scan rate and potential. The results agreed well with the predicted valued from an existing literature.

Another direction of EFGF started with the observation of isotachophoretic phenomena within an EFGF device. The observations were supported by theoretical simulations. While DFGF is a somewhat unique. It does not necessarily scale linearly and therefore miniaturization must be done with care. Moreover, the technique typically has relied upon membranes. Ivory's group explored some major issues associated with semi-permeable membranes [84]. The membranes were removed and a novel DFGF design was developed [85]. To overcome the electrolysis in this design, an 'on-line degas' compartment was included. Compared to their previous design, the degas compartment was located at the bottom of the device and hooked to in-house vacuum. To prevent the collapse, the degas compartment and the main compartment—separation compartment with multiple electrodes—are connected only through a Teflon sheet as well as the porous ceramics. With this design, three dyes with lower molar weight were separated over 10 h without noticeable degradation.

### 2.3.2 Gradient elution moving boundary electrophoresis (GEMBE)

Ross' group proposed gradient elution moving boundary electrophoresis (GEMBE). Unlike EFGF with a constant convective flow, this technique used variable hydrodynamic flow from high to low opposing to a constant electrophoretic velocity. All the species were initially placed outside the entrance of the separation channel. Thus,

only when the bulk counter-flow velocity was smaller than the species' electrophoretic velocity, could they enter the channel. Sample could be injected without using any critical sample injection mechanisms.

This strategy was first made available on a CE platform in 2006 [38] with a pressure-controlled waste reservoir coupled to CE. As a model study, fluorescein and carboxyfluorescein were used to perform the separation. This apparatus could be miniaturized with only an all-in-one inlet port and one outlet port per analyte. With microfluidic apparatus, they studied linear pressure gradient, which successfully separated two fluorescent dyes. With a multistage (nonlinear) gradient, five dansyl-labeled amino acids were isolated. The method gave rise to stair-like data, and electropherogram-like data could be achieved by plotting the first derivative of the raw data.

To avoid some instrument-related issues, Ross' group used capacitively-coupled contactless conductively detection ($C^4D$). Post processing of the data was used to generate the electropherogram-like signal. With this detection method, numerous complex samples have been investigated, including dirt [86, 87], estuarine sediment, coal fly ash and leaves [87]. Samples were injected into the capillary-based apparatus filled with background electrolytes without any pretreatment. This idea has been adapted to a microfluidic device. The design was relatively simple, with one port for sample injection, and the other port for background electrolyte injection. The detection was performed around 1 mm from the sample reservoir. The pressure adjustment compartment was connected with buffer reservoir. With this device, dirt and whole blood samples were tested.

When implemented with a sample stacking technique, GEMBE could load preconcentrated samples continuously. Ross' group have successfully achieved substantial signal enhancement, which was not limited to just the conductivity ratio any more. The continuous sample loading process was accomplished by preparing samples in a lower conductivity buffer and using a higher concentration buffer for experiments.

### 2.3.3 Electrophoretic exclusion (EE)

Inspired from the techniques mentioned above as well as electrophoretic separation of biological samples is electrophoretic exclusion. It also exploits an electric field to establish a gradient and the pressure-driven hydrodynamic flow is used to counter. However, with the geometry of the apparatus, the electric field gradient is formed only at the entrance to the channel, making the exclusion take place in the immediate vicinity of the entrance and nowhere else.

The technique was started as a bench-top device by Polson et al., demonstrating exclusion on polystyrene spheres. Small molecule exclusion was shown by Meighan et al. with an in-house built instrument [88]. The setup was not complex. Separate sample and buffer vials were connected by a capillary. Two vials were placed at different heights to create pressure-driven flow. The electric field was applied cross the capillary with an integrated electrode exactly at the entrance and a standard electrode in the buffer vial. The spectrometer was placed near the entrance of the capillary. The principle of exclusion was confirmed by using a mixture of fluorescent dyes, namely methyl green and neutral red. Similar results were shown with proteins [89] by modifying the capillary with an inner surface polyimide coating to eliminate EOF. Myoglobin, as a model study, was concentrated 1000-fold in a short period of time. Moreover, separation of multiple

proteins was also shown, including mixtures of two positively charged species and one of mixed charge.

Kenyon et al. adapted this technique to a microfluidic device [90]. They investigated this miniaturized device using rhodamine 123 and 100 μm polystyrene beads. Images demonstrated the separation of these two species. They also investigated the theoretical limit of this technique, indicating that is very high resolution, can be run parallel, and separations can occur quickly [91].

Currently, a device with one entrance reservoir and three parallel functional units is used. To better understand how the microdevice works and how it can be optimized, investigation on asymmetric electrode placement (electrode only on one wall) was conducted. Numerical simulations were compared with the experimental results, showing a good agreement. The model constructed is believed to be beneficial for designing next-generation devices [92] and is discussed more fully in Chapter 4.

Table 2.2 A brief comparison between four common counterflow gradient focusing strategies.

| Techniques | EFGF-Ivory [36,72] | EFGF-Lee [76–80] | GEMBE [85–88] | EE [90–92,94] |
|---|---|---|---|---|
| Forces | Electrophoretic force, constant convective force | Electrophoretic force, constant bulk fluid flow | Bulk flow swept from high to low, electrophoretic migration constant | Hydrodynamic flow, electrophoretic velocity |
| Sample injection | A sample loop | Electrokinetic injection or pumped | Continuous introduction | Pipetting small volume or syringe pump |
| Pressure control | A back-pressure regulator | A syringe pump | A precision pressure controller | A rotatable board or syringe pump |
| Electric field gradient establishment | A shaped chamber | A horn-shaped chamber | Distal electrode and standard CE capillary | Electrode and sudden expansion channel-reservoir interface |
| EOF control | Not mentioned | Suppressed with poly(vinyl alcohol) coating the capillary wall | Coating DDAB on capillary surface | Suppressed with low pH buffer or polyimide |
| Detection method | UV detector | Laser-induced fluorescence detection | Fluorescence microscope, current, $C^4D$ | Fluorescence microscope |
| Concentration degree | 2~3-fold in ~7 h | Up to 14,000-fold in 60 min (bilinear) | 110× with a conductivity ratio of 8.21 | 1200 times in 60 s (bench-top), estimated more than 10-fold in 30 s (microdevice) |

## 2.4. Temperature gradient focusing (TGF)

An alternative technique, temperature gradient focusing (TGF) was described by Ross' group [93-95]. In this technique, the electric field gradient was created through a buffer with a temperature-dependent ionic strength and local heating. Pressure-driven

flow was balanced by varying electrophoretic velocity, and the targeted analytes can be focused at specific position.

They demonstrated external heating/cooling equipment to generate temperature gradient. However, the technique has limited peak capacity as well as the dependence of analytes and buffers to temperature. Some other groups found alternative ways to conduct temperature gradient. Normally, Joule heating should be eliminated for separations, as it causes internal convection within the channel or reservoir. However, in TGF regime, separation and concentration can take advantage of Joule heating and achieve excellent performance. The first attempt was by Hasselbrink's group [96]. Their work aimed to reduce the energy needed for the TGF device, as well as eliminate the usage of temperature-dependent buffer. The microchannel was wide at the end and narrow in the middle to establish the temperature gradient. Due to the smaller cross-sectional area in the middle, the current density was higher in this region, thus creating the highest temperature. Electroosmotic flow was used to counterbalance the electrophoretic velocity generated through temperature gradient. A mixture of two dyes were separated and concentrated in this device. However, the steady-state temperature profile was difficult to maintain, making the focused plug gradually move towards the anode side. This group further studied the Joule heating effect for temperature gradient generation with numerical simulations [97].

Instead of using the geometries mentioned above, Yang's research group designed a new system with sudden expansion. They started their investigation with numerical simulations and tested some parameters that might potentially affect the performance of the device, including voltage, buffer concentration, and channel width ratio, among

others. It turned out that all these factors influenced the concentration enhancement. The simulation results were comparable with experiments and showed higher concentration enhancement than the method developed by Ross. With this information, they further optimized the device by using combined AC and DC field to induce the Joule heating effect, thus suppressing electroosmotic flow and decreasing the required DC field. With this modification, the concentration could be enhanced to 2500 fold [98]. They performed concentration of DNA with the same setup, accomplishing 480-fold concentration enhancement in 40 s.

A) B)

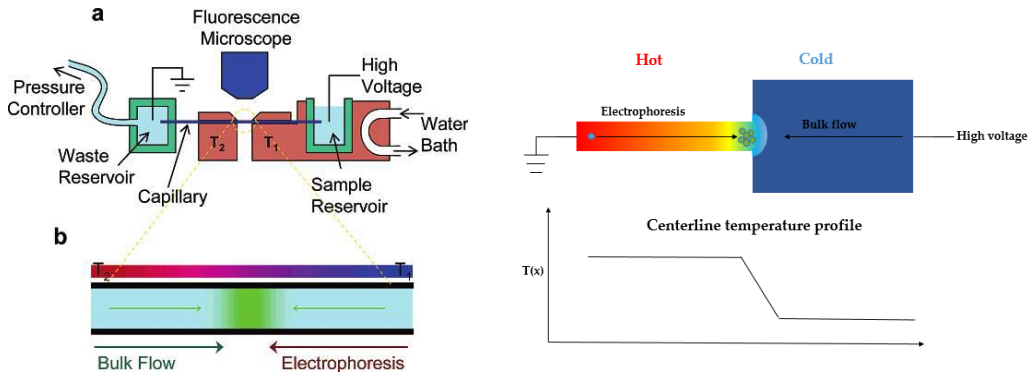


Figure 2.7 Two common schematics for temperature gradient focusing. A) Ross and co-workers design using external heating/cooling equipment for temperautre gradient generation [99]. B) Yang's work by using electroosmotic flow with a sudden expansion design for creating temperature gradient [100].

The usage of internal heater is also a trend for temperature gradient focusing, including Peltier element [35, 99], radiative heater [101], and optothermal accessories [102] among others. A miniaturized application focused on the use of liquid-metal [103]. In the work proposed by Liu and co-workers, they first filled the channel with liquid metal as heater, then with the application of voltage, Joule heating was generated from

this liquid-metal gallium-base alloy heater to form temperature gradient with low conductivity.

A) B)

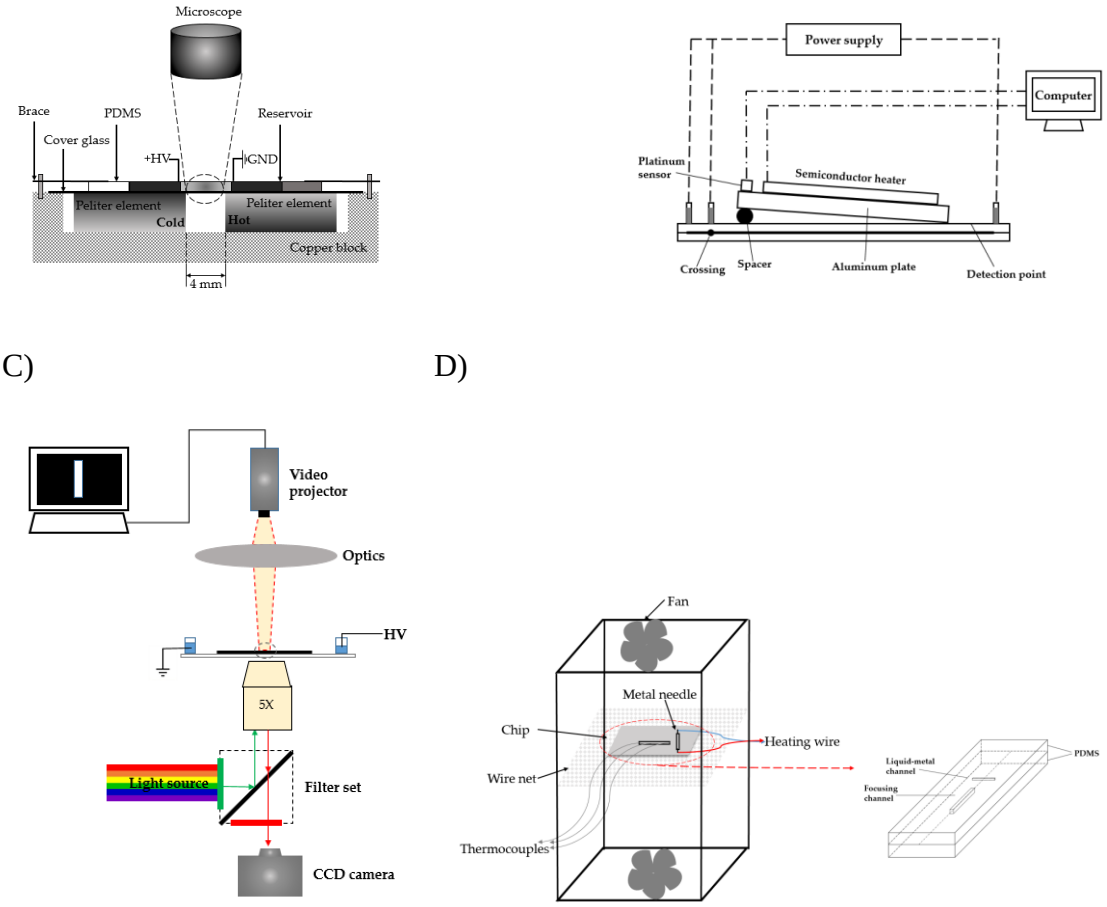


Figure 2.8 Different strategies for creating temperature gradient through an internal heater. A) Peltier elements were incorporated into the device, and applied by different temperatures. The area between two elements formed the temperature gradient [99]. B) A slantwise radiative heater was tilted and generated an angle with the plate, and the temperature gradient was generated along the channel [101]. C) The heated area was generated through the precise projection of a pattern onto the surface of microdevice [102]. D) Liquid metal was filled in the channel of microdevice for generating temperature gradient [103].

In temperature gradient focusing, bilinear gradient can also be applied to enhance the peak capacity and resolving power at the same time. Ren's group investigated the bilinear gradient formation in TGF device [83, 104, 105]. The basic idea was very similar

to what was proposed by Lee's team, namely combining a steep gradient followed by a shallow gradient. In order to achieve such a bilinear gradient, a heater was integrated into the microdevice. The heater was designed to have one large end and one small end to allow for the heat generation, thus creating a desired temperature profile. In order to obtain a broad temperature gradient, the large region was operated in cooled water at initial stage to enhance the temperature difference. The temperature profile was confirmed was finite element simulation software. A comparison between linear and bilinear experimental results were also made, and the bilinear method showed a fairly good resolving power when performing separation of three fluorescent labeled amino acids, while the linear method only showed two peaks.

## 2.5. Concentration polarization (CP)/Ion concentration polarization (ICP) and bipolar electrodes (BPE)

### 2.5.1 Concentration polarization (CP)/Ion concentration polarization (ICP)

Concentration polarization (CP) or ion concentration polarization (ICP) is well known to electrochemists, in many instances as a nuisance. ICP is commonly achieved purposefully through nanochannel structure and ion-permselective membrane.

The ICP phenomenon is generated by a gradient of ions and co-ions of differing mobilities across a nanopore that is small enough to allow for the electric double layer (EDL) overlaps or by permselective membrane. A nanostructure has pores small enough to allow the overlap of the electrical double layer from opposite sides of the opening. The overlapping of the electrical double layer causes the solution in the nanostructure to be charged, preventing transport of co-ions. The nanostructure then exhibits the permselectivity property, enriching ions or co-ions [106]. For the membrane, the

mismatch of mobile and stationary charge carriers across the membrane causes accumulation of ions.

Early work using nanochannel structures and charge-selective membranes for separation and preconcentration was from Sweedler and Bohn's research groups [107, 108]. In their work, two microfluidic channels were placed cross-wise in a layered device with a nanofluidic membrane in between. This design enabled the sorting of species between layers and enabled the possibility of using nanostructures and membranes as well as 3D multilayer constructions for preconcentration.

A novel nanostructure with the Nafion membrane for separation of salted species from seawater was shown by Han and his co-workers [109]. In their device, the nanostructure was located at the intersection of two branches. Due to the ion-depletion, the charged species were repelled to one branch, while the desalted species (mainly water) could flow through the other. Since the charged species were repelled, the nanoporous membrane did not foul. They showed that 99% of the salt could be removed and the energy consumption was low. However, recent work showed it was not as efficient as initial presented. But no doubt, this was a very successful trial and provided a convenient way to address the water shortage problem throughout the world. Later, the same device was used for separation of biomolecules and cells [110].

This design inspired other configurations. Kang's group using a Nafion membrane tilted 45 degree positioned between channels [111], where the ion-depletion zone formed near the one bottom edge of the membrane. The outlet region was expanded compared to the separation channel, amplifying the separation efficiency and acting as a

dimension sorter. The separation was demonstrated with two particles of differing diameters.

Sinton's group contributed a 3D design for its potential use of high-throughput detection and analysis related to desalination [112]. The device had three stacked vertical units, the top layer was a vertical membrane, the middle layer was a channel for purified water, and the bottom was used to transport charged species. Similar to Han and Kang's designs, when voltage was applied, the region near membrane formed an ion-depletion zone, deflecting the charged species. As a result, the neutral water molecules flow through the second layer, while the charged impurities passed through the bottom. It was noteworthy that the purified layer and bottom layer were not overlapped in space, making the visualization more convenient. The device had three-fold functional density and required less energy consumption than planar devices.

Preconcentration can also be achieved through a straight channel. Han and Kang's group collaborated in 2012 and developed a straight channel design with membrane located in the middle of the channel [113]. With the application of a sufficient flow, depletion and ion-enrichment zones formed. The spread of these zones was limited compared to conventional devices. They also coupled this to immunoassay for preconcentration and obtained a limit of detection of 1 ng/mL, which was 1000 times lower than classical strategies. Tang's group developed a similar single-channel device, achieving over 10,000-fold concentration enhancement of protein samples in one case and simultaneous accumulation of cells in another application [114]. Tang's group further investigated the theoretical basis of their scheme using numerical simulations [115].

Channel structures were expanded to a radial concentrator by Sinton's and his co-workers [116]. A vertical channel was placed in the center of a radial chamber covered by a Nafion membrane. Application of voltages created an ion-depletion zone around the membrane. The depletion zone spread until entering the middle vertical channel. No additional flow was required, and over 150-fold concentration was achieved in a short period of time.

A) B) C)

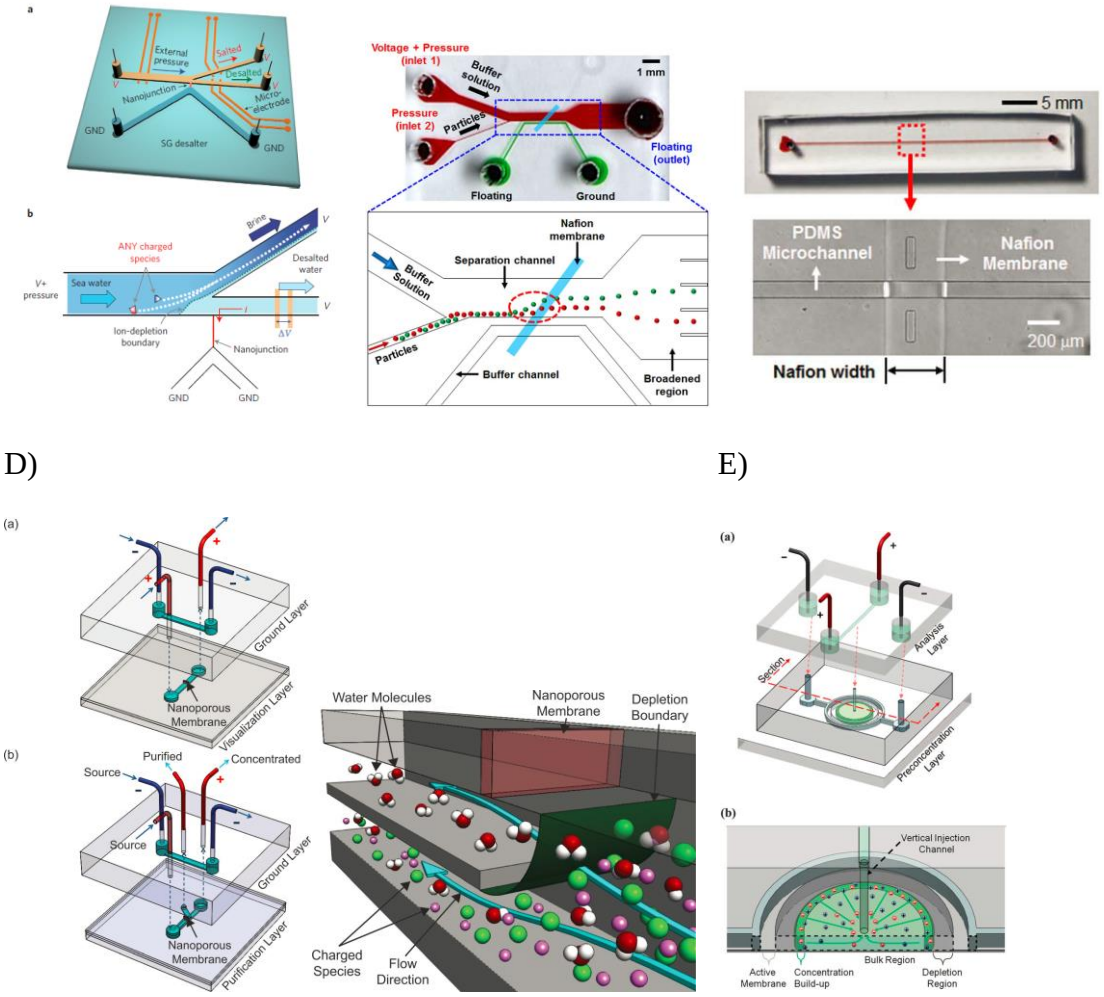


D) E)




Figure 2.9 Various ICP devices. A) Seawater purification device from Han's group [109]. B) Tilted Nafion membrane for particle sorting from Kang's group [111]. C) Single channel ICP [113]. D) Out-of-plane ICP for purification of seawater from Sinton's group [112]. E) Radial concentration from Sinton's group [116].

Most recent research has been focused on paper-based devices, easing fabrication requirements. A good example came from Wang's group in Taiwan. They tested several different geometries. Optimized converging device can result in ~20-fold increase, while straight channel only gave ~10-fold enhancement [117].

Another fabrication technique, called xurography can also be cleanroom-free [118]. Microchannels were created on a double-face adhesive-film, then adhered to a

glass slide. A strip of Nafion was placed above the film. A cutting plotter, which was formerly used industrially, was used for adjusting the shape of the channels and the Nafion membrane. With this simple device, a concentration factor of over 5000-fold was shown.

### 2.5.2 Bipolar electrodes (BPE)

Bipolar electrodes, mostly with respect to bipolar electrochemistry, have long been investigated. They did not receive much attention in electrophoretic separation and preconcentration until Crooks and co-workers reported competition between ionic conductance and electronic conductance in a microfluidic device [119]. A number of projects followed, first, they developed a theoretical model and studied the dynamics of species transportation and the electric field formation [120]. They then determined the rates of hydrolysis that led to the differences in conductivity, thus creating an electric field gradient. They extended the application to simultaneously enrich and concentrate three different species and the result was quite promising: within 200 s, they successfully enriched three negatively charged species over 200-fold [121]. The focusing mechanism was mainly due to the electric field generated by faradaic reactions. When a pH-sensitive buffer, for instance, Tris/Tris$H^+$, was used, the $OH^-$ generated at the cathodic pole of the BP could react with the Tris$H^+$ near that region, forming neutral Tris and reducing the conductivity regionally. The conductivity difference established the electric field gradient. In addition, the electroosmotic flow was used to counter the electrophoretic velocity, making the species accumulate at a specific position. They termed this phenomenon as ‘bipolar electrode focusing’ and investigated current and electric field

effects [122, 123]. Moreover, with the modification of the channel walls, the reversal EOF enabled the enrichment of cations in the BPE-based microdevices [124].

They also explored the depletion zone using bipolar electrodes [125]. The principle behind it was quite similar to that of bipolar electrode focusing, but the electrolyte was not pH-sensitive. As a result, the $OH^-$ at the cathodic pole and $H^+$ at the anodic pole increased the conductivity near these two regions. Consequently, the electric field was relatively low between BPE and high on both poles, making the anions migrated towards cathode. They further studied the ability of this device acting as a membraneless filter when one negatively charged dye and one neutral dye were combined together.

They also investigated both single-channel and dual-channel designs, leading to a discussion of faradic ion concentration polarization [126]. Compared to conventional ICP, which transports charged species through a nanostructure/membrane, the faradic ICP from BPE 'transported' species through electrochemical reactions on both cathodic and anodic poles of electrodes. As a result, conventional ICP was noted as mass-transport limited, while faradic ICP is electron-transfer limited.

With a clear understanding of faradic ICP, the dual-channel design has been used for enrichment and concentration of both cations and anions [127]. In this design, two channels were connected by a bipolar electrode with a $TrisH^+$ buffer in the top channel, and an acetate buffer in the bottom channel.

Building on this body of work, Song and co-workers developed a bipolar electrode-based microdevice combining the end-label free-solution electrophoresis for preconcentration and separation of DNA [128]. In their approach, a simple dual-channel

design was used. DNA was labeled by a protein tag to achieve different mass-to-charge ratio, which enabled the free-solution electrophoresis for separation and enrichment in a BPE-coupled dual-channel microdevice.

### 2.6. Concluding remarks

This review provides a distinctive view of electrophoretic separation and preconcentration strategies. Gradient-based approaches in electrophoretic methods are promising and continue to attract attention of the scientific community since they serve as selective preconcentration platform for complex matrices. Growing interest is visible in new fabrication procedures aiming to reduce the complicated and labor-intensive work with standard lithography procedures in the cleanroom. A remarkable trend can be seen in paper-based microdevices.

Among all the techniques mentioned in this review, isotachophoretic strategies might be the most practical ones as they can be applied to a variety of analytes including biological samples and inorganic components. Field-amplified sample stacking still serves as an important role in sample injection or introduction and may facilitate a better performance when combined with other techniques. Counterflow electric field gradient focusing remains as an effective separation and preconcentration method. Gradient elution moving boundary electrophoresis might be the most powerful tool in this category as it can be applied to raw samples even without prior treatment. Electric field gradient focusing maintains its advantage and can be used for some biosamples. Electrophoretic exclusion is still at an early phase and aims to provide new insight for next-generation design. Temperature gradient focusing continues to grow, with new fabrication or new materials facilitating further development of the technique.

The reviewed papers demonstrate that gradient-based electrophoretic approaches remain an effective tool for keeping CE techniques competitive, and in many cases superior, compared with other separation methods.

**2.7 References**


[1] Strohmeier, O., Keller, M., Schwemmer, F., Zehnle, S., Mark, D., von Stetten, F., Zengerle, R., Paust, N., *Chemical Society reviews* 2015, *44*, 6187-6229.

[2] Breadmore, M. C., *Electrophoresis* 2007, *28*, 254-281.

[3] Breadmore, M. C., Thabano, J. R., Dawod, M., Kazarian, A. A., Quirino, J. P., Guijt, R. M., *Electrophoresis* 2009, *30*, 230-248.

[4] Breadmore, M. C., Dawod, M., Quirino, J. P., *Electrophoresis* 2011, *32*, 127-148.

[5] Breadmore, M. C., Shallan, A. I., Rabanes, H. R., Gstoettenmayr, D., Abdul Keyon, A. S., Gaspar, A., Dawod, M., Quirino, J. P., *Electrophoresis* 2013, *34*, 29-54.

[6] Breadmore, M. C., Tubaon, R. M., Shallan, A. I., Phung, S. C., Abdul Keyon, A. S., Gstoettenmayr, D., Prapatpong, P., Alhusban, A. A., Ranjbar, L., See, H. H., Dawod, M., Quirino, J. P., *Electrophoresis* 2015, *36*, 36-61.

[7] Zeng, J., Deng, Y., Vedantam, P., Tzeng, T.-R., Xuan, X., *Journal of Magnetism and Magnetic Materials* 2013, *346*, 118-123.

[8] Han, X., Feng, Y., Cao, Q., Li, L., *Microfluidics and Nanofluidics* 2014, *18*, 1209-1220.

[9] Laurell, T., Petersson, F., Nilsson, A., *Chemical Society reviews* 2007, *36*, 492-506.

[10] Destgeer, G., Lee, K. H., Jung, J. H., Alazzam, A., Sung, H. J., *Lab Chip* 2013, *13*, 4210-4216.

[11] Li, P., Mao, Z., Peng, Z., Zhou, L., Chen, Y., Huang, P. H., Huang, T. J., *Proceedings of the National Academy of Sciences* 2015, *112*, 4970-4975.

[12] Kim, S. B., Yoon, S. Y., Sung, H. J., Kim, S. S., *Analytical chemistry* 2008, *80*, 2628-2630.

[13] Jung, J. H., Lee, K. H., Lee, K. S., Ha, B. H., Oh, Y. S., Sung, H. J., *Microfluidics and Nanofluidics* 2013, *16*, 635-644.

[14] Gongora, J. S. T., Fratalocchi, A., *Optics and Lasers in Engineering* 2016, *76*, 40-44.

[15] Song, J. Z., Chen, H. F., Tian, S. J., Sun, Z. P., *Journal of Chromtagraphy B:*

*Biomedical Sciences and Applications* 1998, *708*, 277-283.

[16] Yang, H., Chien, R. L., *Journal of chromatography. A* 2001, *924*, 155-163.

[17] Jung, B., Bharadwaj, R., Santiago, J. G., *Electrophoresis* 2003, *24*, 3476-3483.

[18] Bharadwaj, R., Santiago, J. G., *Journal of Fluid Mechanics* 2005, *543*, 57.

[19] Jung, B., Bharadwaj, R., Santiago, J. G., *Analytical chemistry* 2006, 2319-2327.

[20] Mala, Z., Gebauer, P., Bocek, P., *Electrophoresis* 2011, *32*, 116-126.

[21] Chen, Y., Lü, W., Chen, X., Teng, M., *Central European Journal of Chemistry* 2012, *10*, 611-638.

[22] Slampova, A., Mala, Z., Pantuckova, P., Gebauer, P., Bocek, P., *Electrophoresis* 2013, *34*, 3-18.

[23] Lian, D. S., Zhao, S. J., Li, J., Li, B. L., *Analytical and bioanalytical chemistry* 2014, *406*, 6129-6150.

[24] Mala, Z., Slampova, A., Krivankova, L., Gebauer, P., Bocek, P., *Electrophoresis* 2015, *36*, 15-35.

[25] Thormann, W., *Separation Science and Technology* 2006, *19*, 455-467.

[26] Gebauer, P., Mala, Z., Bocek, P., *Electrophoresis* 2011, *32*, 83-89.

[27] Rogacs, A., Qu, Y., Santiago, J. G., *Analytical chemistry* 2012, *84*, 5858-5863.

[28] Wen, Y., Li, J., Ma, J., Chen, L., *Electrophoresis* 2012, *33*, 2933-2952.

[29] Mala, Z., Gebauer, P., Bocek, P., *Electrophoresis* 2013, *34*, 19-28.

[30] Smejkal, P., Bottenus, D., Breadmore, M. C., Guijt, R. M., Ivory, C. F., Foret, F., Macka, M., *Electrophoresis* 2013, *34*, 1493-1509.

[31] Strychalski, E. A., Konek, C., Butts, E. L., Vallone, P. M., Henry, A. C., Ross, D., *Electrophoresis* 2013, *34*, 2522-2530.

[32] Rogacs, A., Marshall, L. A., Santiago, J. G., *Journal of chromatography. A* 2014, *1335*, 105-120.

[33] Mala, Z., Gebauer, P., Bocek, P., *Electrophoresis* 2015, *36*, 2-14.

[34] Petersson, F., Aberg, L., Sward-Nilsson, A. M., Laurell, T., *Analytical chemistry* 2007, *79*, 5117-5123.

[35] Becker, M., Mansouri, A., Beilein, C., Janasek, D., *Electrophoresis* 2009, *30*, 4206-4212.

[36] Turgeon, R. T., Bowser, M. T., *Analytical and bioanalytical chemistry* 2009, *394*, 187-198.

[37] Wildgruber, R., Weber, G., Wise, P., Grimm, D., Bauer, J., *Proteomics* 2014, *14*, 629-636.

[38] Benz, C., Boomhoff, M., Appun, J., Schneider, C., Belder, D., *Angewandte Chemie* 2015, *54*, 2766-2770.

[39] Koegler, W. S., Ivory, C. F., *Biotechnology progress* 1996, *12*, 822-836.

[40] Greenlee, R. D., Ivory, C. F., *Biotechnology progress* 1998, *14*, 300-309.

[41] Wang, Q., Tolley, H. D., LeFebre, D. A., Lee, M. L., *Analytical and bioanalytical chemistry* 2002, *373*, 125-135.

[42] Kelly, R. T., Woolley, A. T., *Journal of Separation Science* 2005, *28*, 1985-1993.

[43] Shackman, J. G., Ross, D., *Electrophoresis* 2007, *28*, 556-571.

[44] Ivory, C. F., *Electrophoresis* 2007, *28*, 15-25.

[45] Meighan, M. M., Staton, S. J., Hayes, M. A., *Electrophoresis* 2009, *30*, 852-865.

[46] Vyas, C. A., Flanigan, P. M., Shackman, J. G., *Bioanalysis* 2010, *2*, 815-827.

[47] Cheng, H., Han, C., Xu, Z., Liu, J., Wang, Y., *Food Analytical Methods* 2014, *7*, 2153-2162.

[48] Giri, B., Dutta, D., *Analytica chimica acta* 2014, *810*, 32-38.

[49] Sueyoshi, K., Kitagawa, F., Otsuka, K., *Analytical Sciences* 2013, *29*, 133-138.

[50] Won, S. Y., Chandra, P., Hee, T. S., Shim, Y. B., *Biosensors & bioelectronics* 2013, *39*, 204-209.

[51] Bottenus, D., Jubery, T. Z., Dutta, P., Ivory, C. F., *Electrophoresis* 2011, *32*, 550-562.

[52] Bottenus, D., Jubery, T. Z., Ouyang, Y., Dong, W.-J., Dutta, P., Ivory, C. F., *Lab on a Chip* 2011, *11*, 890.

[53] Jacroux, T., Bottenus, D., Rieck, B., Ivory, C. F., Dong, W. J., *Electrophoresis* 2014, *35*, 2029-2038.

[54] Shintaku, H., Nishikii, H., Marshall, L. A., Kotera, H., Santiago, J. G., *Analytical*

*chemistry* 2014, *86*, 1953-1957.

[55] Kuriyama, K., Shintaku, H., Santiago, J. G., *Electrophoresis* 2015, *36*, 1658-1662.

[56] Shintaku, H., Palko, J. W., Sanders, G. M., Santiago, J. G., *Angewandte Chemie* 2014, *53*, 13813-13816.

[57] Han, C. M., Katilius, E., Santiago, J. G., *Lab Chip* 2014, *14*, 2958-2967.

[58] Marshall, L. A., Rogacs, A., Meinhart, C. D., Santiago, J. G., *Journal of chromatography. A* 2014, *1331*, 139-142.

[59] Bahga, S. S., Chambers, R. D., Santiago, J. G., *Analytical chemistry* 2011, *83*, 6154-6162.

[60] Bahga, S. S., Santiago, J. G., *Electrophoresis* 2012, *33*, 1048-1059.

[61] Qu, Y., Marshall, L. A., Santiago, J. G., *Analytical chemistry* 2014, *86*, 7264-7268.

[62] Prest, J. E., Baldock, S. J., Fielden, P. R., Goddard, N. J., Goodacre, R., O'Connor, R., Treves Brown, B. J., *Journal of chromatography. B, Analytical technologies in the biomedical and life sciences* 2012, *903*, 53-59.

[63] Xu, Z., Murata, K., Arai, A., Hirokawa, T., *Biomicrofluidics* 2010, *4*, 14108.

[64] Wu, R., Yeung, W. S., Fung, Y. S., *Electrophoresis* 2011, *32*, 3406-3414.

[65] Rosenfeld, T., Bercovici, M., *Lab Chip* 2014, *14*, 4465-4474.

[66] Moghadam, B. Y., Connelly, K. T., Posner, J. D., *Analytical chemistry* 2014, *86*, 5829-5837.

[67] Smejkal, P., Breadmore, M. C., Guijt, R. M., Foret, F., Bek, F., Macka, M., *Electrophoresis* 2012, *33*, 3166-3172.

[68] Smejkal, P., Breadmore, M. C., Guijt, R. M., Grym, J., Foret, F., Bek, F., Macka, M., *Analytica chimica acta* 2012, *755*, 115-120.

[69] Smejkal, P., Breadmore, M. C., Guijt, R. M., Foret, F., Bek, F., Macka, M., *Analytica chimica acta* 2013, *803*, 135-142.

[70] Inglis, D. W., Goldys, E. M., Calander, N. P., *Angewandte Chemie* 2011, *50*, 7546-7550.

[71] Hsu, W. L., Inglis, D. W., Jeong, H., Dunstan, D. E., Davidson, M. R., Goldys, E. M., Harvie, D. J., *Langmuir : the ACS journal of surfaces and colloids* 2014, *30*, 5337-5348.

[72] Hsu, W. L., Harvie, D. J., Davidson, M. R., Jeong, H., Goldys, E. M., Inglis, D. W.,

*Lab Chip* 2014, *14*, 3539-3549.

[73] Koegler, W. S., Ivory, C. F., *Journal of Chromatography A* 1996, *726*, 229-236.

[74] Burke, J. M., Ivory, C. F., *Electrophoresis* 2008, *29*, 1013-1025.

[75] Tracy, N. I., Huang, Z., Ivory, C. F., *Biotechnology progress* 2008, *23*, 444-451.

[76] Tracy, N. I., Ivory, C. F., *Electrophoresis* 2008, *29*, 2820-2827.

[77] Humble, P. H., Kelly, R. T., Woolley, A. T., Tolley, H. D., Lee, M. L., *Analytical chemistry* 2004, *76*, 5641-5648.

[78] Liu, J., Sun, X., Farnsworth, P. B., Lee, M. L., *Analytical chemistry* 2006, *78*, 4654-4662.

[79] Sun, X., Farnsworth, P. B., Woolley, A. T., Tolley, H. D., Warnick, K. F., Lee, M. L., *Analytical chemistry* 2008, *80*, 451-460.

[80] Sun, X., Farnsworth, P. B., Tolley, H. D., Warnick, K. F., Woolley, A. T., Lee, M. L., *Journal of chromatography. A* 2009, *1216*, 159-164.

[81] Sun, X., Li, D., Woolley, A. T., Farnsworth, P. B., Tolley, H. D., Warnick, K. F., Lee, M. L., *Journal of chromatography. A* 2009, *1216*, 6532-6538.

[82] Trickett, C. A., Henderson, R. D., Guijt, R. M., Breadmore, M. C., *Electrophoresis* 2012, *33*, 3254-3258.

[83] Shameli, S. M., Glawdel, T., Ren, C. L., *Electrophoresis* 2015, *36*, 668-674.

[84] Burke, J. M., Ivory, C. F., *Electrophoresis* 2010, *31*, 893-901.

[85] Burke, J. M., Smith, C. D., Ivory, C. F., *Electrophoresis* 2010, *31*, 902-909.

[86] Strychalski, E. A., Henry, A. C., Ross, D., *Analytical chemistry* 2009, *81*, 10201-10207.

[87] Sikorsky, A. A., Fourkas, J. T., Ross, D., *Analytical chemistry* 2014, *86*, 3625-3632.

[88] Meighan, M. M., Keebaugh, M. W., Quihuis, A. M., Kenyon, S. M., Hayes, M. A., *Electrophoresis* 2009, *30*, 3786-3792.

[89] Meighan, M. M., Vasquez, J., Dziubcynski, L., Hews, S., Hayes, M. A., *Analytical chemistry* 2011, *83*, 368-373.

[90] Kenyon, S. M., Weiss, N. G., Hayes, M. A., *Electrophoresis* 2012, *33*, 1227-1235.

[91] Kenyon, S. M., Keebaugh, M. W., Hayes, M. A., *Electrophoresis* 2014, *35*, 2551-2559.

[92] Zhu, F., Hayes, M. A., *Electrophoresis* 2019, *40*, 304-314.

[93] Balss, K. M., Vreeland, W. N., Phinney, K. W., Ross, D., *Analytical chemistry* 2004, *76*, 7243-7249.

[94] Balss, K. M., Vreeland, W. N., Howell, P. B., Henry, A. C., Ross, D., *Journal of the American Chemical Society* 2004, *126*, 1936-1937.

[95] Munson, M. S., Meacham, J. M., Locascio, L. E., Ross, D., *Analytical chemistry* 2008, *80*, 172-178.

[96] Kim, S. M., Sommer, G. J., Burns, M. A., Hasselbrink, E. F., *Analytical chemistry* 2006, *78*, 8028-8035.

[97] Sommer, G. J., Kim, S. M., Littrell, R. J., Hasselbrink, E. F., *Lab Chip* 2007, *7*, 898-907.

[98] Schwarzkopf, F., Scholl, T., Ohla, S., Belder, D., *Electrophoresis* 2014, *35*, 1880-1886.

[99] Matsui, T., Franzke, J., Manz, A., Janasek, D., *Electrophoresis* 2007, *28*, 4606-4611.

[100] Ge, Z., Wang, W., Yang, C., *Lab Chip* 2011, *11*, 1396-1402.

[101] Zhang, H. D., Zhou, J., Xu, Z. R., Song, J., Dai, J., Fang, J., Fang, Z. L., *Lab Chip* 2007, *7*, 1162-1170.

[102] Akbari, M., Bahrami, M., Sinton, D., *Microfluidics and Nanofluidics* 2011, *12*, 221-228.

[103] Gao, M., Gui, L., Liu, J., *Journal of Heat Transfer* 2013, *135*, 091402.

[104] Shameli, S. M., Glawdel, T., Liu, Z., Ren, C. L., *Analytical chemistry* 2012, *84*, 2968-2973.

[105] Shameli, S. M., Glawdel, T., Fernand, V. E., Ren, C. L., *Electrophoresis* 2012, *33*, 2703-2710.

[106] Holtzel, A., Tallarek, U., *Journal of separation science* 2007, *30*, 1398-1419.

[107] Kuo, T. C., Cannon, D. M., Shannon, M. A., Bohn, P. W., Sweedler, J. V., *Sensors and Actuators A: Physcial* 2003, *102*, 223-233.

[108] Kuo, T. C., Cannon, D. M., Chen, Y., Tulock, J. J., Shannon, M. A., Sweedler, J. V., Bohn, P. W., *Analytical chemistry* 2003, *75*, 1861-1867.

[109] Kim, S. J., Ko, S. H., Kang, K. H., Han, J., *Nature nanotechnology* 2010, *5*, 297-301.

[110] Kwak, R., Kim, S. J., Han, J., *Analytical chemistry* 2011, *83*, 7348-7355.

[111] Jeon, H., Lee, H., Kang, K. H., Lim, G., *Scientific reports* 2013, *3*, 3483.

[112] MacDonald, B. D., Gong, M. M., Zhang, P., Sinton, D., *Lab Chip* 2014, *14*, 681-685.

[113] Ko, S. H., Song, Y. A., Kim, S. J., Kim, M., Han, J., Kang, K. H., *Lab Chip* 2012, *12*, 4472-4482.

[114] Kim, M., Jia, M., Kim, T., *The Analyst* 2013, *138*, 1370-1378.

[115] Jia, M., Kim, T., *Analytical chemistry* 2014, *86*, 10365-10372.

[116] Scarff, B., Escobedo, C., Sinton, D., *Lab Chip* 2011, *11*, 1102-1109.

[117] Yang, R. J., Pu, H. H., Wang, H. L., *Biomicrofluidics* 2015, *9*, 014122.

[118] Yuan, X., Renaud, L., Audry, M. C., Kleimann, P., *Analytical chemistry* 2015, *87*, 8695-8701.

[119] Dhopeshwarkar, R., Hlushkou, D., Nguyen, M., Tallarek, U., Crooks, R. M., *Journal of the American Chemical Society* 2008, *130*, 10480-10481.

[120] Hlushkou, D., Perdue, R. K., Dhopeshwarkar, R., Crooks, R. M., Tallarek, U., *Lab Chip* 2009, *9*, 1903-1913.

[121] Laws, D. R., Hlushkou, D., Perdue, R. K., Tallarek, U., Crooks, R. M., *Analytical chemistry* 2009, *81*, 8923-8929.

[122] Anand, R. K., Sheridan, E., Hlushkou, D., Tallarek, U., Crooks, R. M., *Lab Chip* 2011, *11*, 518-527.

[123] Perdue, R. K., Laws, D. R., Hlushkou, D., Tallarek, U., Crooks, R. M., *Analytical chemistry* 2009, *81*, 10149-10155.

[124] Sheridan, E., Hlushkou, D., Knust, K. N., Tallarek, U., Crooks, R. M., *Analytical chemistry* 2012, *84*, 7393-7399.

[125] Sheridan, E., Knust, K. N., Crooks, R. M., *The Analyst* 2011, *136*, 4134-4137.

[126] Anand, R. K., Sheridan, E., Knust, K. N., Crooks, R. M., *Analytical chemistry* 2011, *83*, 2351-2358.

[127] Knust, K. N., Sheridan, E., Anand, R. K., Crooks, R. M., *Lab Chip* 2012, *12*, 4107-4114.

[128] Song, H., Wang, Y., Garson, C., Pant, K., *Analytical methods : advancing methods and applications* 2015, *7*, 1273-1279.

# CHAPTER 3

# GENERAL OVERVIEW OF ELECTROPHORETIC EXCLUSION

## 3.1 Introduction

Previous chapters have discussed the role of separations in protein biomarker analysis and provided an overview for a variety of electrophoretic separation techniques.

Current electrophoretic separation strategies can be divided into two categories. The first type is migration-based techniques, such as isotachophoresis (ITP), field-amplified sample stacking (FASS), and sweeping [1-6]. While the second type is focusing techniques. Compared with migration-based techniques, focusing approaches employ a counter-flow, so that analytes could be concentrated and allows for increased peak capacity and resolution. This idea was initially proposed by O' Farrell [7]. In his work termed as counteracting chromatographic electrophoresis (CACE), the column was packed with two different materials of different porosities, and the target protein could accumulate in the junction of two materials. Later Giddings and Dahlgren [8] summarized equilibrium gradient methods, in which the analytes could reach an equilibrium point where the net force summed to zero. In addition, similar to Hooke's Law, the deviation from the equilibrium point could result in a restoring force, which caused the analytes to be concentrated in narrow bands. These efforts led to new applications on electrophoretic separation such as flow counterbalanced capillary electrophoresis (FCCE) [9], electric field gradient focusing (EFGF) [10-20], temperature gradient focusing (TGF) [21, 22], and gradient elusion moving boundary electrophoresis (GEMBE) [23-28]. Most of these elegant electrophoretic separation techniques have been discussed in Chapter 2.

Similar to these techniques, and pre-dating some, is electrophoretic exclusion. [29-33]. Consistent with other techniques, it exploits an electric field ($E$) to establish a gradient and a pressure-driven flow ($v$) to counter the electrophoretic force. Since the electrophoretic velocity ($u$) is equal to the product of the electrophoretic mobility ($\mu$) and the electric field strength ($E$), each analyte accumulates at the point where the electrophoretic velocity of the analyte is equal and opposite to the bulk fluid flow ($v=u=\mu E$). With the geometry of the apparatus, the electric field is formed at the entrance to the channel where the gradient is established, resulting in the exclusion taking place out of the channel.

This technique was started as a bench-top device. Polson et al. first demonstrated the capability of exclusion with this technique [29]. Later, a theoretical study was presented with the collaboration of Hayes group and Chen group, through whose work the electrophoretic exclusion conditions were examined [30]. Meighan et al. showed the exclusion phenomenon with in-house built instrument. To better control and minimize the electroosmotic flow (EOF), an acidic buffer was used. The principle of exclusion was confirmed with a mixture of methyl green and neutral red dyes [31]. Later, this apparatus was used for the separation of proteins. The capillary was modified with polyimide coating to eliminate the EOF. Myoglobin was concentrated 1000-fold in a short period of time. Moreover, multiple proteins were also separated on the apparatus, including a mixture of two positively charged species, and another mixture of one positively and one negatively charged species [32].

Compared to other methods, this new technique has some advantages. First, with this technique a species can be excluded by employing carefully chosen electric field

strengths. The flow rate is designed to be relatively slow, which does not acquire a high electric field to conduct separations, minimizing bubble formation. Second, there is no need for critical injection and sample loading is no longer a major problem; this does not cause band broadening, which simplifies the sample injection. Third, species are separated in bulk solution based upon their native properties without the need for a binding step or other pretreatment, which makes it possible for coupling with various downstream techniques for detection, such as mass spectrometry and electron microscopy. Since the exclusion takes place outside the channel, unlike those of chromatography, or capillary electrophoresis, this technique is independent of the length of the channel, which makes this technique adaptable for use in microfluidic devices. In addition, this technique does not depend upon usage of membranes for isolation, which could avoid any issues associated with the retention of small molecules or the non-uniformities of the fields.

More recently, Kenyon et al. adapted this technique to a microfluidic device. As microfluidic devices gained popularity recently due to their superior properties compared to bench-top devices, such as miniaturized operation systems, reduced reagents consumption, reduced wastes formation, and decreased time consumption [34]. This microdevice was a complete hybrid glass/PDMS chip with nine single separation channels. The principle of this technique on this miniaturized device was studied with exclusion of Rhodamine 123 and 100 μm polystyrene beads. Visual evidence of images from fluorescent microscope were used to demonstrate the separation of these two species [33].

In the simple format as a single-channel separation interface, the separation capability of electrophoretic exclusion is limited as the analytes could either enter the reservoir or be excluded at the entrance to the channel. In order to achieve higher separation capability, the coupling of multiple channel entrances in series and in parallel could be advantageous. Considering the non-linear, punctuated microgradient property of this technique, it is possible to allow for customizable separation for specific analytes with known electrophoretic mobilities by adjusting the electric field applied. As a result, an array-based design was proposed by Dr. Kenyon. This array-based design consists of a large reservoir for sample loading, followed by three individual separation units. Each unit comprises a central reservoir and an exit reservoir (Figure 3.1).

In the present work, this array-based microfluidic device format was tested. With this geometry, analytes of different mobilities were separated spatially and simultaneously. Results from individual dye solutions showed they exhibited different behaviors when varying the applied electric field strength. Moreover, when the voltage was released, a bright concentration bolus would flow through the channel, indicating the device capabilities for exclusion, enrichment, and separation. The separation of a mixture of two dye solutions was demonstrated through images/videos of fluorescence microscopy. Centerline concentration profile was established for studying the mechanism of exclusion. The phenomenon of partial exclusion was also observed from the centerline concentration profile. The obtained results indicated that electrophoretic exclusion is a promising technique, which could be further used for more applications.

## 3.2 Experimental

### 3.2.1 Microfluidic device fabrication

A photograph of the device as well as schematics with isometric view and top view were shown in Figure 3.1. The hybrid glass/PDMS array was used for all experiments. Each device contained a large entrance reservoir, three central reservoirs and three exit reservoirs connected by separation channels. The development of this device is briefly discussed below.

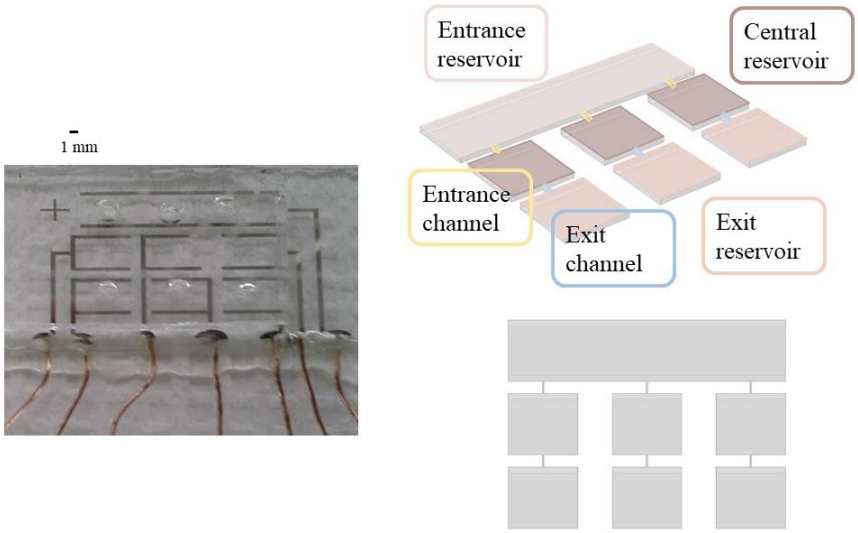


Figure 3.1 A photograph of the actual device is included on the left. Top right shows a schematic with isometric view, and all the reservoirs and channels are labeled with terminology. Bottom right presents a schematic with top view.

### 3.2.1.1 PDMS casts fabrication

This array-based microdevice consisted of an entrance reservoir connected to three central and exit reservoirs through separation channels. The dimension of the entrance reservoir was 19 mm x 5 mm, central and exit reservoirs were 5 mm x 5 mm, and the channels were 1 mm in length, 100 μm in width, and 10 μm in depth. Masks were designed using Illustrator (Adobe, San Jose, CA, USA) and printed on transparency using a resolution of 65,000 dpi (Fine Line Imaging, Colorado Springs, CO, USA). Positive photoresist AZ 4620 was spun onto a silicon wafer and exposed using an EVG®620

Automated UV-NIL, μ-CP System (EV Group, Austria) at 500 mJ/cm$^2$ with the transparency as a mask.

The microdevice was then fabricated using common soft lithography techniques. Using Sylgard 184 (Dow Corning, Midland, MI, USA), polymer and curing agent was prepared as a 10:1 mass ratio, and the mixture was poured onto the wafer at a thickness of roughly 5 mm. The crude mixture with wafer was allowed to sit at room temperature for 15 minutes to remove all the air bubbles and cured at 70-80°C for 60 min in the oven. The cured PDMS cast was peeled off from the wafer and 3 mm diameter holes were punched in the entrance and exit reservoirs using a Harris Uni-Core quill (Shunderson Communications Inc., Orleans, Ontario, Canada).

**3.2.1.2 Electrode fabrication**

Ti/Pt electrodes were plated on standard glass microscope slides (VWR International). A mask was designed using Adobe Illustrator and printed on transparency using a resolution of 8000 dpi (Fine Line Imaging, Colorado Springs, CO USA). Electrodes were plated 500 μm in width and bracketed three sides of each reservoir to produce a flat potential. A schematic of the electrode design is shown (Figure 3.1, left). Positive photoresist AZ 4330 was spun onto glass microscope slides and then exposed with the EVG®620 Automated UV-NIL, μ-CP System at 150 mJ/cm$^2$ using the transparency mask. Two layers of metal were deposited on the glass slides using electron beam physical vapor deposition (PVD75, Kurt J. Lesker Company, Jefferson Hills, PA, USA). A 30 nm layer of Ti was deposited onto the slides, followed by 50 nm of Pt. Copper wires were attached to the deposited metal stripes on the glass slides using silver conductive epoxy to create electrical connection to an external high voltage power supply

(Series HV5448, LabSmith Inc., Livermore, CA, USA) through an in-house built voltage divider.

### 3.2.2 Materials

Aspartic acid, hydrochloric acid (1 M), Rhodamine 123 stock solution (2 mM), Rhodamine 6G stock solution (2 mM), 8-Hydroxypyrene-1,3,6-trisulfonic acid (HPTS) stock solution (2 mM), True Blue chloride stock solution (~10 mM) were used as received. Aspartic acid buffer solution was prepared to 5 mM with a pH around 2.95 using 18 MΩ Milli-Q water (hydrochloric acid was used to adjust the pH value). Rhodamine 123, Rhodamine 6G, HPTS, and True blue stock solution were diluted to 10 µM, 40 µM, 60 µM, 1.5 mM, respectively, using aspartic acid buffer solution on the day of the experiment. Under acidic buffer solution conditions, HPTS is a negatively charged dye, while the other three are positively charged. Rhodamine 123, Rhodamine 6G and HPTS show green fluorescence under microscope, while True Blue shows blue fluorescence.

### 3.2.3 Experimental setup

The upper PDMS layer and the electrode slide were bound together after surface treatment with oxygen plasma operated at high radio frequency (RF) for 60 s (Plasma Cleaner, Harrick Plasma). The copper wires of the device were connected to an in-house fabricated voltage divider. The voltage divider was further linked to a high voltage power supply. An Olympus IX70 microscope with a mercury light source was used to monitor the experiment.

The array was filled with a solution containing fluorescent dye molecules by pipetting the solution into the entrance reservoir. Channels were filled through capillary

action and bulk flow was directed towards the exit reservoirs by the difference in height between the menisci of the entrance and exit reservoirs. A total of 21 μL of solution was added to each device. Properly selected electric fields were applied so that exclusion of dye molecules could be observed near the entrance to exit channel.

For each trial with the microdevice, the general procedure for data collection was designed as: for the initial 10 s, the device filled with sample was placed on the stage of microscope without voltage applied; next 15 s, a low voltage configuration was applied manually for voltage accuracy checking with a voltage meter; at 25 s, the voltage was triggered through a programmable voltage sequence from the voltage power supply to a desired value and left on for another 20 s; at 45 s, the voltage was released, and videos were recorded for another 15 s. The images from the videos were saved as .tiff files from the camera software.

### 3.2.4 Data processing

ImageJ software (NIH, Bethesda, MD, USA) was used for intensity measurements. For the centerline concentration profile, pre-selected images were imported into the software. A centerline was established within the channel of each image and the intensity of each pixel along this line was achieved through the command 'Analysis'→'Plot profile'.

## 3.3 Results and discussion

### 3.3.1 Exclusion principle

As discussed before, electrophoretic exclusion takes place when the electrophoretic velocity of a charged analyte is larger than the counteracting hydrodynamic flow. Three main factors are required to achieve exclusion: hydrodynamic

flow, positive or negative charge, as well as an electric field. Due to the punctuated feature of electrophoretic exclusion, the charged target analyte, with the application of a proper electric field, is expected to be excluded in the interface between channel and reservoir, while other species could still flow through the channel. For a given set of experiments as well as the device, the electrophoretic mobility of the analyte remains constant (giving the same buffer condition and analyte concentration). While the pressure-driven hydrodynamic flow does not change significantly within the time frame of experiment, so the electric field strength can be manipulated to achieve exclusion for different analytes.

This array-based microchip is expected to separate and concentrate three different species with various electrophoretic mobilities. The principle of electrophoretic exclusion is illustrated below with schematics (Figure 3.2). As the hydrodynamic flow direction points down, it is necessary for have a negative electric field to counterbalance the negatively charged species (Figure 3.2 A). With a positively charged species with a higher mobility, a relatively small electric field is sufficient to achieve exclusion (Figure 3.2 B); while a positively charged species with a lower mobility needs a higher electric field to be excluded (Figure 3.2 C).

A) B)

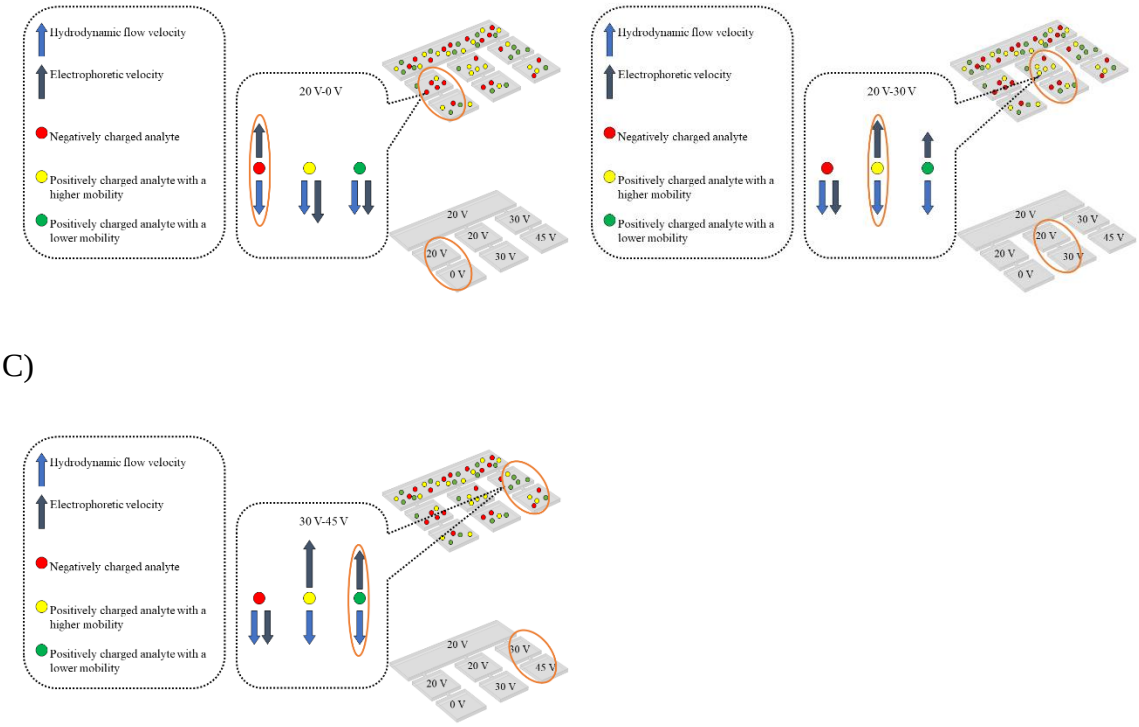


C)




Figure 3.2 Detailed exclusion conditions for an array-based device. Three different colors, red, yellow, and green represent the three different species: A) negatively charged, B) positively charged with a higher mobility, C) positively charged with a lower mobility, respectively. Different electric field strengths are required to exclude different types of species, making electrophoretic exclusion a good strategy for separation.

### 3.3.2 Demonstration of exclusion phenomenon

To demonstrate the exclusion phenomenon in the microdevice, behaviors of dye molecules were investigated. Images focused on the exit channels were captured, presenting the various dye behaviors with the voltage on and off.

The individual fluorescent dyes, including HPTS (negatively charged), True Blue, Rhodamine 6G and Rhodamine 123 (all positively charged) behaved in predictable manners as discussed in section 3.3.1. The successful exclusion of Rhodamine 6G in the exit channel 2 region was shown below as an example (Figure 3.3). In the experiment, the

bulk flow was from top to bottom. Before any electric field was applied, the dye molecules could travel through the channel due to the bulk flow, so the channel area was quite bright (Figure 3.3 A). When sufficient voltage was applied, the opposing electrophoretic velocity induced the dye molecules to be excluded, and the channel area was almost dark (Figure 3.3 B). When the voltage was off, the channel area was bright again, suggesting the excluded dye had collected near the entrance. It was again allowed to flow through the system once the electric field was removed from the channel and the hydrodynamic flow dominated (Figure 3.3 C).

However, in the exit channel 1 region, when a different electric field was applied, no obvious change was observed (pictures not shown), indicating only with the specific voltage configuration, exclusion could take place. This pattern of intensity changes was also observed for all the other experiments with other dye molecules as visual evidence of exclusion at the entrance area and demonstrated the exclusion can be achieved through manipulation of proper electric fields.

A) B) C)

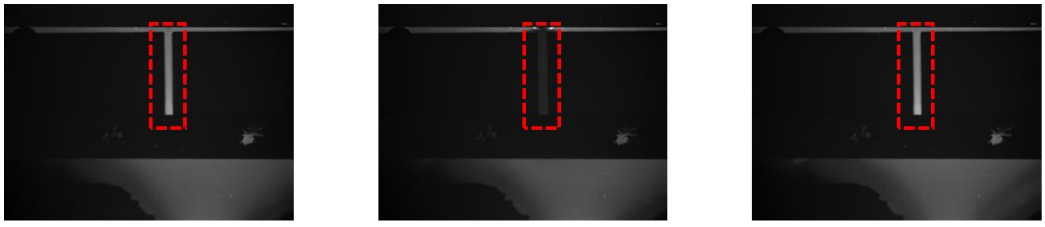

Figure 3.3 Exclusion for Rhodamine 6G. A) Before potential was applied, the channel area was still bright. B) Potential was applied, the channel area was completely dark. C) Potential was released, the intensity of the channel recovered. Red rectangle highlighted the channel area.

### 3.3.3 Concentration profiles within channel

With qualitative evidence demonstrating the exclusion phenomena, more quantitative results were pursued, especially for the dynamics of dye molecules in the channels between reservoirs. The intensity along the centerline of the channel was quantitated as a method to assist in describing the exclusion behavior. Logically, very low electric field strength is not sufficient to exclude dye molecules, and very high electric field strength can completely exclude species from the channel in a short period of time. While for the intermediate electric field strength, when the electrophoretic velocity is higher than hydrodynamic flow velocity, the dye molecules can be pushed backwards gradually, thus excluding from the channel with a longer period of time.

Several trials focused on the channel area, seeking to quantitate the behaviors. Two representative data sets (Figure 3.4) are shown to allow discussion. For Figure 3.4 A, the same voltage (400 V) was applied to the exit channel region, and the intensity of channel centerline was depicted at different time scales; while for Figure 3.5 B, different voltages were applied for the same period of time (15 s). Control experiments were performed with no electric field applied, no hydrodynamic flow, or no charged analytes, respectively. No exclusion phenomenon was observed (results not shown), as these three factors were required to achieve exclusion.

For experiments with the same voltage (electric field) applied for different amounts of time, the intensity change was observed (Figure 3.4 A). Initially, when the voltage was applied for a short period of time, the intensity was relatively steady, as the amount dye molecules entering and leaving the channel was close to equilibrium. When the voltage was on for several seconds, the dye molecules were excluded from the end of the channel area as indicated by the curves with decreased intensities. This was

interpreted as evacuation of the charged dye from the channel and being replaced by the buffer that has had the dyes electrophoretically removed. At a longer time from 4.3 s to 15.7 s, the excluded species grew from a small amount to occupying most of the channel, which supported the expectation that species were quickly and efficiently excluded. Moreover, with the species pushed backwards more and more, the shapes of the curves were approximately the same. The largest intensity change was observed for about 15 s after voltage was applied, indicating that at about 15 s, the amount of Rhodamine 6G that was excluded was the most. As time further increased to 20 s, the amount of excluded dye molecules did not rise as expected (data not shown), this was mainly due to the diffusion and penetration of concentrated bolus.

In addition, the voltage applied was varied to study the exclusion process in the channel area (Figure 3.4 B) while the amount of time was held constant (15 s) based upon the discussion above to achieve more exclusion. When the voltage was relatively low (250 V), there was no measured change for the intensity within the channel, indicating the electric field was not sufficient to counterbalance the hydrodynamic flow. As the voltage increased to 300 V, the intensity near the end of the channel was decreased, consistent with the species moving backwards due to the high electrophoretic velocity. Still, at this time, the hydrodynamic flow velocity was competing with electrophoretic velocity, as well as the diffusion of the concentrated species and other intermolecular interactions. The concentration profile in the channel did not show a sudden change, instead, it was a gradual shift. While the voltage was even higher, the electrophoretic velocity dominated, and the species could be pushed backwards faster. As a result, after

15 s, the centerline profile differences between 500 V and 550 V did not present significant changes in intensity.

The intensity change from either time or electric field influence was non-linear, mainly due to the complex and asymmetric interface between channel and electrode, which will be further discussed in Chapter 4.

A) B)

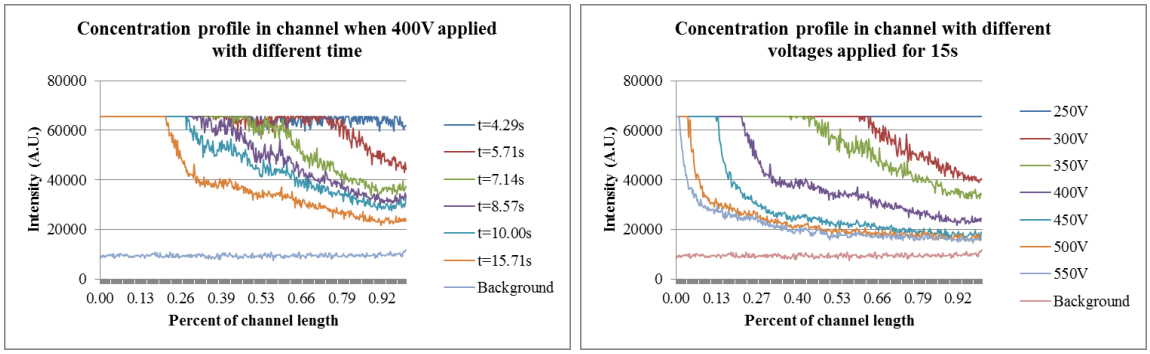


Figure 3.4 Concentration profile in channel: A) When 400 V applied with different time scales; B) Different voltages applied for 15 s.

### 3.3.4 Separation of two fluorescent dyes

Experiments were performed to demonstrate the capability of this technique to differentiate two charged fluorescent dyes.

A mixture of HPTS (-) and Rhodamine 123 (+) was tested on the microdevice with a negative electric field applied on exit channel 1 area to exclude HPTS and a positive electric field on exit channel 2 area to exclude Rhodamine 123. Exclusion phenomena were observed in both channel areas, and were similar to those presented in section 3.3.1, while the individual dye molecule could only result in exclusion in one specific area with the applied electric fields (i.e. HPTS alone could only be excluded at

the entrance to exit channel 1, and Rhodamine 123 could only be excluded at the entrance to exit channel 2 with the same voltage configuration applied).

Intensity in the central reservoir was also measured to confirm the exclusion taking place in the area to the exit channel. As a result, the dye molecules accumulated in the central reservoir area, leading to an increased intensity change. However, the intensity in the central reservoir 1 did not give rise to a significant enhancement, and even reduced in intensity as compared to the central reservoir 2 (Figure 3.5 A), which was mainly due to the photobleaching effect of HPTS (Figure 3.5 B). It was clear that within 30 s, the intensity in the reservoir area decreased more than half with HPTS loaded.

A) B)

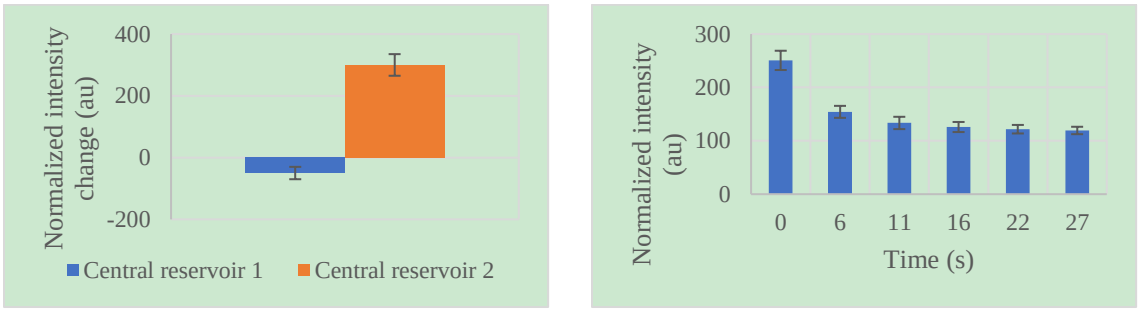


Figure 3.5 Intensity change in the central reservoir of different dye molecules. A) Intensity difference in the central reservoirs when a mixture of HPTS and Rhodamine 123 were excluded after 15 s (n=3, error bar stands for standard deviation). B) Intensity of the central reservoir when HPTS was loaded in the device for half a minute (n=3, error bar stands for standard deviation).

### 3.4 Concluding remarks

In summary, a miniaturized array-based device for this novel counter-flow gradient focusing technique, electrophoretic exclusion, has been tested. Images captured via fluorescence microscopy allow investigation of the microdevice and help to understand the behaviors of excluded species with applied electric fields. Moreover, the data extracted from the centerline of the channel indicates the dynamics of exclusion is

time-dependent and a higher voltage facilitates the complete exclusion of the species. This work is expected to achieve high resolution separation and can be potentially applied to biological samples.

### 3.5 References


[1] Breadmore, M. C., *Electrophoresis* 2007, *28*, 254-281.

[2] Breadmore, M. C., Thabano, J. R., Dawod, M., Kazarian, A. A., Quirino, J. P., Guijt, R. M., *Electrophoresis* 2009, *30*, 230-248.

[3] Breadmore, M. C., Dawod, M., Quirino, J. P., *Electrophoresis* 2011, *32*, 127-148.

[4] Breadmore, M. C., Shallan, A. I., Rabanes, H. R., Gstoettenmayr, D., Abdul Keyon, A. S., Gaspar, A., Dawod, M., Quirino, J. P., *Electrophoresis* 2013, *34*, 29-54.

[5] Breadmore, M. C., Tubaon, R. M., Shallan, A. I., Phung, S. C., Abdul Keyon, A. S., Gstoettenmayr, D., Prapatpong, P., Alhusban, A. A., Ranjbar, L., See, H. H., Dawod, M., Quirino, J. P., *Electrophoresis* 2015, *36*, 36-61.

[6] Breadmore, M. C., Wuethrich, A., Li, F., Phung, S. C., Kalsoom, U., Cabot, J. M., Tehranirokh, M., Shallan, A. I., Abdul Keyon, A. S., See, H. H., Dawod, M., Quirino, J. P., *Electrophoresis* 2017, *38*, 33-59.

[7] O'FARRELL, P. H., *Science* 1985, *227*, 1586-1589.

[8] Giddings, J. C., Dahlgren, K., *Separation Science* 1971, *6*, 345-356.

[9] Culbertson, C. T., Jorgenson, J. W., *Analytical chemistry* 1994, *66*, 955-962.

[10] Koegler, W. S., Ivory, C. F., *Biotechnology progress* 1996, *12*, 822-836.

[11] Koegler, W. S., Ivory, C. F., *Journal of Chromatography A* 1996, *726*, 229-236.

[12] Greenlee, R. D., Ivory, C. F., *Biotechnology progress* 1998, *14*, 300-309.

[13] Huang, Z., Ivory, C. F., *Analytical chemistry* 1999, *71*, 1628-1632.

[14] Humble, P. H., Kelly, R. T., Woolley, A. T., Tolley, H. D., Lee, M. L., *Analytical chemistry* 2004, *76*, 5641-5648.

[15] Kelly, R. T., Woolley, A. T., *Journal of Separation Science* 2005, *28*, 1985-1993.

[16] Burke, J. M., Ivory, C. F., *Electrophoresis* 2008, *29*, 1013-1025.

[17] Tracy, N. I., Huang, Z., Ivory, C. F., *Biotechnology progress* 2008, *23*, 444-451.

[18] Tracy, N. I., Ivory, C. F., *Electrophoresis* 2008, *29*, 2820-2827.

[19] Sun, X., Farnsworth, P. B., Woolley, A. T., Tolley, H. D., Warnick, K. F., Lee, M. L., *Analytical chemistry* 2008, *80*, 451-460.

[20] Sun, X., Farnsworth, P. B., Tolley, H. D., Warnick, K. F., Woolley, A. T., Lee, M. L., *Journal of chromatography. A* 2009, *1216*, 159-164.

[21] Hoebel, S. J., Balss, K. M., Jones, B. J., Malliaris, C. D., Munson, M. S., Vreeland, W. N., Ross, D., *Analytical chemistry* 2006, *78*, 7186-7190.

[22] Shackman, J. G., Munson, M. S., Ross, D., *Analytical and bioanalytical chemistry* 2007, *387*, 155-158.

[23] Shackman, J. G., Munson, M. S., Ross, D., *Analytical chemistry* 2007, *79*, 565-571.

[24] Strychalski, E. A., Henry, A. C., Ross, D., *Analytical chemistry* 2009, *81*, 10201-10207.

[25] Ross, D., Romantseva, E. F., *Analytical chemistry* 2009, *81*, 7326-7335.

[26] Strychalski, E. A., Henry, A. C., Ross, D., *Analytical chemistry* 2011, *83*, 6316-6322.

[27] Sikorsky, A. A., Fourkas, J. T., Ross, D., *Analytical chemistry* 2014, *86*, 3625-3632.

[28] Ross, D., Munson, M. S., *Electrophoresis* 2014, *35*, 770-776.

[29] Polson, N. A., Savin, D. P., Hayes, M. A., *Journal of Microcolumn Separations* 2000, *12*, 98-106.

[30] Pacheco, J. R., Chen, K. P., Hayes, M. A., *Electrophoresis* 2007, *28*, 1027-1035.

[31] Meighan, M. M., Keebaugh, M. W., Quihuis, A. M., Kenyon, S. M., Hayes, M. A., *Electrophoresis* 2009, *30*, 3786-3792.

[32] Meighan, M. M., Vasquez, J., Dziubcynski, L., Hews, S., Hayes, M. A., *Analytical chemistry* 2011, *83*, 368-373.

[33] Kenyon, S. M., Weiss, N. G., Hayes, M. A., *Electrophoresis* 2012, *33*, 1227-1235.

[34] Ng, J. M., Gitlin, I., Stroock, A. D., Whitesides, G. M., *Electrophoresis* 2002, *23*, 3461-3473.

# CHAPTER 4

# SIMULATION AND EXPERIMENT OF ASYMMETRIC ELECTRODE PLACEMENT FOR ELECTROPHORETIC EXCLUSION IN A MICRODEVICE

## 4.1 Introduction

Investigations towards better separation have been the focus of research for many decades, as separation science serves as the preliminary step before identification and quantification for many workflows. As research focuses on more and more complex samples, increasingly sophisticated separation methods with sufficient high resolution are required [1].

Electrophoretic exclusion (EE) was developed to meet this demand. The basic premise of EE is derived from capillary electrophoresis (CE) and counterflow gradient focusing techniques, aimed at retaining the advantages of both types of techniques.

CE has been widely used in complex sample analysis. However, it is restricted by a poor concentration limit of detection and reproducibility issues. Several strategies have been examined to improve the technique. Examples, which increase concentration, are isotachophoresis (ITP) [2-5], field amplified sample stacking (FASS) [6], sweeping [7], and counterflow gradient focusing (CFG) [8]. Among them, the counterflow technique offers external control of focus locations with variable restoring forces to enhance peak capacity and resolution, in addition to the increased concentration.

Several groups have contributed to the development of CFG techniques. Ivory's group established an electric field gradient by changing cross-sectional area and used convective force to counter electrophoresis [9, 10]. They also created a precise electric

field gradient by employing an array of actively controlled electrodes. However, the strategy was limited by large and complex instruments [11-13]. Lee's group developed a horn-shaped geometry, with the varying cross-sectional area on the longitudinal axis creating the electric field gradient. Several species were separated using pressure-driven flow as the balancing force [14-17]. However, sample absorption and degradation on the membrane restricted its further development, among other issues [18]. Alternatively, gradient elution moving boundary electrophoresis uses a constant flow while temporarily varying the electric field. This has been applied to complex 'real-world' samples, such as milk, whole blood, and leaves among others without pretreatment [19-23]. A gradient can also be formed using buffer which varies its ionic strength with temperature. Temperature gradient focusing (TGF) was developed using this concept, coupling a heating element and pressure-driven flow to create the gradient [24, 25]. The technique is limited by buffer matching issues and resulting in a modest range of analytes.

EE exploits an electric field to establish a gradient and a pressure-driven flow to counter the electrophoretic force. This technique was first demonstrated as a bench-top device, where Polson et al. demonstrated exclusion using a traditional capillary entrance in 2000 [26]. Fundamental field and fluid effects were modeled [27] and proteins and small molecules have since been effectively manipulated [28, 29]. Experimental and theoretical descriptions of the flow and electric fields about the capillary entrance have been established [30]. Kenyon et al. adapted this technique to a microfluidic device, demonstrating separations of Rhodamine 123 and 100 μm polystyrene beads [31]. Theoretical work of EE technique on capillary-based apparatus noted that the resolving power as a minimum electrophoretic mobility difference could be as small as $10^{-13}$

$cm^2/Vs$. While the format and purpose of EE differs significantly, this value is comparable to best results from channel and capillary electrophoresis systems [32]. A typical capillary zone electrophoresis system enables the separation of closest resolvable species differ by approximately $10^{-10}$ $m^2/Vs$.

To understand the significance of the current work, a brief summation of EE is required. The unique feature underlying all EE is the geometry of the apparatus, where the electric field is formed at the entrance to the channel, causing the exclusion to occur near to, but outside of the channel. Specific analytes can be excluded by an easily adjustable parameter of the electric field strength. Species are held in bulk solution based upon their native properties without the need for a binding step or other pretreatment, and it can be easily coupled to various techniques for detection, such as mass spectrometry. The exclusion taking place outside the channel (unlike chromatographic or other CE-related systems) allowing independence of channel length, which makes it adaptable for use in microfluidic devices. An optimized system with low flow, short channel length and small magnitude applied voltage can minimize electrolysis and bubbles. Due to the high surface to volume ratio of the entrance area and micro-channels, the heat dissipation is efficient.

The performance of the microdevice is expected to differ significantly compared to the radially-symmetric capillary device. Further, the location of the electrode for the capillary-based system is limited to the face of the capillary and could not be varied. With a microdevice, the dispersive force and flow rate are reduced as the decreased size of device, and the position of the electrodes can be varied with asymmetric interfaces, which may possibly increase the resolution of this technique. Subtle changes in interface is

expected to generate different behaviors under such a sensitive system. 3D simulations are created on commercial finite element mesh software. The results of the models can be compared directly to the experimental evidence because of the ease of monitoring afforded by the 3D microfluidic device. Significant and obvious changes are expected in the concentration profiles with relatively small alterations of the location of the electrode, thus providing a robust test for the theoretical assessments.

For the modeling, finite element numerical simulation method is used. Numerical simulations have been developed as a useful and efficient tool to study microfluidics phenomena because it enables the integration of multiphysics, such as fluidics, transportation, electrics, and mechanics. However, to solve these simulations, the coupling of multiple components is required, adding a layer of complexity. Another challenge arises from highly varied length scales of most microfluidic devices. They vary by several orders of magnitude in geometrical scales: reservoirs length and width in millimeter scale, channels dimensions in micrometer scale, and thickness of electric double layer in nanometer scale [33].

The work presented here is built upon a strong fundamental foundation of numerical simulations. Various numerical schemes and techniques have been developed to solve these problems. As early as 1986, Saville et al. presented a 1D model on monovalent, soluble materials in electrophoresis without considering the bulk flow influence and boundaries [34]. Quasi-1D models to simulate nonlinear electrokinetic processes have also been addressed by Santiago and co-workers more recently [35]. Ramsay and co-worker came up with a 2D mathematical model to investigate the influence from electroosmotic flow, electrophoretic motion, and diffusion on sample

mass transport in microchip channels, and finite-difference algorithms on finite volume method in structured grids were employed to solve the problem [36, 37]. Girault et al. developed a 2D model for an electroosmotic driven flow at a T-junction of rectangular microscale channel and a numerical software Flux Expert was used to assess the performance of the model [38]. A fully coupled model for electrokinetic flow and transport in an electrophoresis microdevice was reported by Ehrhard et al. with time-dependent and two-dimensional Finite Element (FEM) simulations [39]. A generalized and unified model on 3D dimension was reported by Chatterjee and a specific example of electrophoretic transport of weak analytes was also given in the work with the application of multi-block finite-volume scheme [40]. Kler et al. performed 3D finite element model for the simulation of electrophoretic flow and transport in different microgeometries with parallel computations and domain decomposition techniques [33, 41-43].

Our work, which reflects all of the developments noted, was greatly simplified by the introduction of commercial finite element mesh software. With the usage of commercial finite element mesh software, the numerical simulation was more accessible and convenient. An elegant example was from Mansouri et al. with the study of transient streaming potential using a commercial code, Femlab, and the results were confirmed with existing analytical results [44].

The work presented here is a detailed investigation of an inherently asymmetric microfluidic interface. In this study, the interface was varied by moving the glass-deposited electrode to various positions near and within a channel entrance: leading electrode placed outside of channel entrance, leading electrode aligned with entrance, and leading electrode within channel. The different electrode placement has a significant

impact on the exclusion behavior of the interface. Full 3D numerical simulation was built in finite element multiphysics commercial software. Simulation results were validated with known microfluidic and electrochemical interfaces giving results quantitatively equal to systems with analytical solutions. Using the same approach, the simulations were applied to the problem at hand and then compared experimental data with generally good agreement. Combined with previous studies, this work on electrode placement provides a foundation for examining new geometries and parameters for next-generation designs.

## 4.2 Experimental

### 4.2.1 Microfluidic device fabrication

The microdevices is a hybrid system using a glass base plate with deposited electrodes and a PDMS cover plate with channels embedded. Standard soft lithography methods were used to fabricate the upper PDMS layer [31]. Punched holes on the surface of PDMS layer were used to create access ports for sample injection. Electrodes consisting of 300 nm Ti and 500 nm Pt were deposited on microscope slides using electron beam evaporation (PVD75, Kurt J. Lesker Company, Clairton, PA, USA). The upper PDMS layer (Figure 4.1 A) and electrode slide (Figure 4.1 B) were bound together after pretreatment using oxygen plasma with high RF setting and a pressure of approximately 500 mTorr for 60 s (Harrick, Ithaca, NY, USA). The device consists of one large reservoir and six small reservoirs (Figure 4.1 C), forming three parallel units, and within each unit, reservoirs are interconnected with channels. The size of large reservoir is 20 mm × 5 mm, small reservoir is 5 mm × 5 mm. The channels are 1 mm in length and 0.1 mm in width. All channels and reservoirs are 10 μm in depth.

### 4.2.2 Materials

Aspartic acid and hydrochloric acid stock solution (1 M) were used as received (Sigma-Aldrich, St. Louis, MO, USA). Aspartic acid buffer solution was prepared to 5 mM with a pH of 2.95 (pH adjusted with hydrochloric acid). Rhodamine 6G (R6G) stock solution was prepared by dissolving the pure material (Sigma-Aldrich, St. Louis, MO, USA) into deionized water (Millipore, Bedford, MA, USA) to 20 mM. The stock solution was diluted to 1 mM, using aspartic acid buffer for each experiment. R6G exhibits green fluorescence (excitation: 495 nm, emission: 570 nm) and is positively charged under the acidic buffer solution conditions.

### 4.2.3 Experimental setup

Copper wires were attached to the electrodes using silver epoxy (Sigma-Aldrich, St. Louis, MO, USA) to ensure continuity. The wires of the device were connected to a high voltage power supply (HVS448-3000D LabSmith, Livermore, CA, USA) through an in-house constructed voltage divider (1:100 or 1:10) for each channel. An Olympus IX70 microscope (Olympus, Japan) with mercury arc lamp (HBO, OSRAM, Germany), and a 12-bit fast cooled monochrome CCD camera (Qimaging, Canada) was used to monitor experiments and capture images/videos.

### 4.2.4 Device operation

The microdevice was filled with R6G solution through the entrance ports, and rested on the bench for 2 minutes. Differing liquid levels from between entrance and exit ports were used to generate pressure-driven hydrodynamic flow. The device was then placed on the microscope stage, connected to the voltage divider and a high voltage

configuration applied. The voltage for each channel was confirmed through a digital multimeter (DM-4400A Sperry, Menomonee Falls, WI, USA). The captured data contained a whole process including 10 s before voltage was applied, a simple and quick step to trigger the voltage on with an easy programmed sequence from the high voltage power supply, 30 s when voltage was applied, and another 10 s when voltage was released. The process was repeated greater than five times for each experimental setting.

The florescent intensity for each series of images was quantified through ImageJ (publicly available, National Institute of Health) by loading a stack of images, drawing a centerline, and obtaining the pixel value along this centerline. The intensity of the images from the first 10 s was averaged as the baseline for each set of data, and was subtracted from the data images.

### 4.2.5 Theoretical modeling

A mathematical model was used to simulate 3D and time-dependent electrokinetic flow and transport phenomena in an electrophoretic exclusion microdevice.

#### 4.2.5.1. Governing equations

Governing equations for electrokinetics, fluid mechanics and species transport are used [45-48]. Definition and value of each parameter are given below.

Table 4.1 Physical parameters/constants used.

| Parameter/Constant | Symbol | Value | Unit |
|---|---|---|---|
| Density | ρ | 1000 | $kg/m^3$ |
| Viscosity | μ | $10^{-3}$ | kg/m s |
| Ionic valence | z | 1 | - |
| Electric field | E | 350 | V/cm |
| Temperature | T | 300 | K |
| Gas constant | R | 8.31 | J/mol K |
| Faraday constant | F | 96500 | C/mol |
| Permittivity | ε | $80x8.85x10^{-12}$ | F/m |
| Diffusion coefficient | D | $5x10^{-9}$ | $m^2/s$ |
| Mobility | ν | $5x10^{-9}$ | $m^2/V$ s |
| Pressure | p | 25 | Pa |
| Concentration | c | $10^{-3}$ | mol/L |

The flow in a typical microfluidic device is considered as laminar flow due to the low Reynolds number caused by small dimension and low flow velocity. The velocity field can be described by Navier-Stokes and continuity equations, which includes the conservation of mass for incompressible fluids:

$$\nabla \cdot \boldsymbol{u} = 0 \tag{1}$$

where *u* is fluid velocity.

As well as the conservation of momentum for Newtonian fluids (Navier-Stokes equation):

$$\rho\left(\frac{\partial \boldsymbol{u}}{\partial t} + \boldsymbol{u} \cdot \nabla \boldsymbol{u}\right) = \nabla \cdot \sigma + \rho_e \boldsymbol{E} \tag{2}$$

$\rho$ and $\mu$ represent density and viscosity, respectively. They are considered consistent over all the domain during the whole process. Stress tensor σ is described as $\sigma = -p\boldsymbol{I} + \mu(\nabla \boldsymbol{u} + \nabla \boldsymbol{u}^T)$, where *p* is pressure, and *I* is identity matrix. The last term on the right side is for momentum balance denoted by electric forces. $\rho_e$ is the electric charge density of

the electrolyte solution, which can be obtained from $\rho_e = F\sum z_j c_j$, where $z_j c_j$ represents valence and molar concentration respectively, and F is the Faraday constant.

The equation describing the relation between electric field and charge distributions in the fluid of permittivity $\varepsilon$ is given as (Poisson equation):

$$\nabla \cdot (\varepsilon \boldsymbol{E}) = \rho_e \tag{3}$$

Mass transport of moderately or weakly concentrated sample ions as well as buffer electrolyte can be expressed as below (the reactive term is neglected with the assumption of strong electrolytes existing in the system):

$$\frac{\partial c_i}{\partial t} + \boldsymbol{u} \cdot \nabla c_j = D_j \nabla^2 c_j - \nabla \cdot \left(v_j z_j c_j F \boldsymbol{E}\right) \tag{4}$$

which describes the transportation of diluted species $j$, with a concentration of $c_j$. $D_j$ is the diffusion coefficient, $\nu_j$ is the mobility, and F is Faraday constant.

In order to accurately solve the situation, Eqs. (1)– (4) need to be fully coupled. Kostiuk and co-workers' work offered an insight on solving fully coupled system[44]. First, the electric potential distribution was solved in stationary study. Using the electric fields and the calculated charge densities, velocity profile was solved with the applied pressure. With these initial steps, all the governing equations were solved together in a time-dependent mode.

#### 4.2.5.2 Simulation geometry and boundary conditions

A 3D model (Figure 4.1 E) of electrophoretic exclusion was generated with finite element multiphysics commercial software (COMSOL Multiphysics v.5.0a, COMSOL, Palo Alto, CA, USA) to obtain the electric field, the velocity field, and the fluorescent

dye concentration profile. The graphical user interface (GUI) and pre-programmed modules of COMSOL Multiphysics allow for rapid creation of different interfaces and/or electrode placement as the subdomains and boundary conditions can be easily setup.

The simulated geometry was a simplified module with two 5 mm × 5 mm reservoirs connected by one 1 mm × 0.1 mm channel. Two electrodes were 0.5 mm × 5 mm, placed at the bottom surface of the device. The device height was set to 10 $\mu$m, while the electrode height was 0.1 μm according to the actual device.

For the area not close to electrode and channel, a mapped mesh was used with extremely fine setting. For the area close to electrode and channel, a triangular mesh was applied with maximum element size as 50 μm and minimum element size a 5 μm. For the channel area, even more fine triangular mesh was exploited, with maximum element size as 10 μm and minimum element size as 1 μm. A swept mesh was used for both the reservoir layer (swept from the top of reservoir layer to the boundary between reservoir and electrode) and electrode layer (swept from the boundary between reservoir and electrode to bottom of electrode layer).

Materials, including liquid, silica glass, and copper were selected from the built-in library and assigned to the respective geometric entities. With the usage of a diluted solution, the liquid viscosity, density and other parameters were close to those of water. The electrical conductivity was modified to 0.03 S/m, reflecting the aspartic acid buffer used in the experiments.

Equation (1) and (2) can be implemented into COMSOL Multiphysics with steady-state, laminar flow (spf) module. The no-slip boundary condition was applied. The

pressure at the inlet was set to 25 pa, and 0 pa at outlet in order to maintain a flow rate similar to experimental values in the channel.

Equation (3) can be realized with the application of electric current (ec) module. Electric field was applied to the two electrodes to reach a 350 V/cm electric field strength. Electric insulation condition was assumed on the channel walls and surfaces.

Equation (4) can be solved with transport of diluted species (chds) module in COMSOL Multiphysics. For the initial condition, buffer solution was 5 mM aspartic acid, and the microdevice was filled with a fluorescent dye of the 0.001 mol/L concentration with +1 charge, $5x10^{-9}$ $m^2/Vs$ in mobility and $5x10^{-9}$ $m^2/s$ as diffusion coefficient.

The electric field was solved first, followed by the velocity field. The simulation results of velocity were compared to the results solved by Hagen Poiseuille equation for rough validation. With stored solution of electric field and velocity field, the concentration distribution was solved with a time-dependent study.

The simulations were run on a Windows Server Win7 Professional Enterprise (64-bit) operating system that included 64 GB of installed memory (RAM).

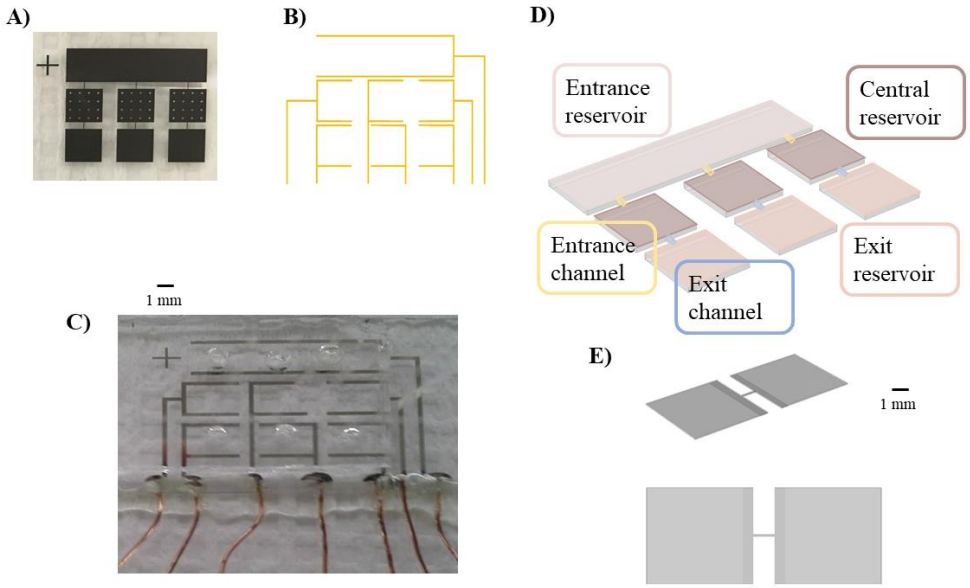


Figure 4.1 Photographs and schematics of the microdevice. A) A shadow pattern photograph for PDMS cast. B) A schematic of glass slide with electrodes, gold lines indicate electrodes (not to the scale). C) A photograph of the microdevice with PDMS cast and electrode slide sealed together. D) Isometric view with highlighted area of entrance reservoir, entrance channel, central reservoir, exit channel and exit reservoir from top to bottom. Channels are present between each vertical set of reservoirs. E) Isometric and top view of the simplified model used in simulation with single channel, electrodes and reservoirs system.

## 4.3 Results & Discussion

### 4.3.1 Strong changes in the profile of concentration with small changes in electrode placement

Dramatic differences in the concentration profiles near channel entrances were observed in response to small changes in the placement of the electrodes. Three conditions were quantitatively investigated with numerical modeling and device testing: leading electrode outside the channel entrance, leading electrode align with channel entrance, and leading electrode within channel entrance. The distance between two

electrodes were kept constant. Generally good agreement between simulation and experiment was observed.

For an asymmetric (three walls insulating, one wall electrode) channel entrance, vertical and lateral asymmetries between flow and electric fields dramatically affect the behavior of concentration profiles. These affects are investigated using fluorescence microscopy of operating devices and quantitatively compared to finite-element based models. A stringent study is presented here, where any discrepancies between models and data are well articulated in the visual representations of the concentration profiles. This study includes two-dimensional *z*-axis views of the device and models for three electrode placements at three time-points each (and a modeled side view of flow and electric fields), and a centerline concentration profile for each at a set time and single voltage.

Qualitative observations of the data and model include (Figure 4.2). For leading electrode outside the channel, only a small concentration increase is observed outside the channel and an evacuated zone lies in between the channel exit and the trailing electrode (Figure 4.2 A). For the edge of the leading electrode coinciding with the channel entrance, the evacuation of dye is initiated at the exit of the channel (Figure 4.2 B). No evacuated zone forms at the entrance, just an increase in local concentration. Note that the evacuation zone and increased concentration zones are not observed directly in experiments, but the intensity within the channel is greatly diminished, consistent with the simulation. For leading electrode placed within channel entrance, the electric field is initiated well with the channel entrance, where the charged dye molecules are evacuated at unique areas for the entrance and the exit in both simulations (Figure 4.2 C, top) and experiments (Figure 4.2 C, bottom). The evacuation is initiated at the edge of the trailing

electrode. Eventually, the charged dye is accumulated to the edge of the leading electrode. The increased concentration is located directly above the electrode.

The model and experimental results qualitatively matched well, even with regards to some tiny details. These details include the evacuation area between the leading electrode and trailing electrode for all three electrode placements, the formation of semi-circle shape at the entrance to the channel when the leading electrode is placed outside of the channel entrance (Figure 4.2 A), and the triangular shape between the channel and the trailing electrode, as well as the extremely bright spot at the front of channel when the leading electrode is placed within the channel (Figure 4.2 C).

Examining the side view of the modeling results can inform some of these behaviors (Figure 4.3). The lateral spreading of the electric field (Figure 4.3 A, top and middle) and reduced average flow velocity (Figure 4.3 A, bottom) from the increased cross-sectional area can account for the semi-circle shape of the evacuated zone under the condition of leading electrode outside the channel. The electric field lines are parallel in the rectangular channel region, but laterally spread in the 'T'-shaped region between the electrode and channel. This creates a curvature to the local electric field resulting in the observed/modeled isotropic exclusion of depletion zone within the region. Even though the local electric field is somewhat reduced, reflected by the spreading electric field lines, the flow rate is also reduced, such that exclusion occurs.

The spreading field lines shown in the side view can also account for the triangular evacuated zone under the condition of trailing electrode outside the channel. Similar to the condition of leading electrode outside the channel, the intensity of the

laminar flow profile is reduced (the maximum versus average velocity, Figure 4.3 C, bottom). The spreading electric lines (Figure 4.3 C, top) indicate the lower electric field strength. In this case, however, the net transport is towards the channel, and the molecules in the center are evacuated more so, while those off-center undergo a smaller electrophoretic force in the vertical direction. The further the molecules are from the center, the smaller the vertical movement, so in the middle the depletion zone penetrates to a greater extent. Near the channel wall, there is almost no depletion, creating a triangular shape.

A)

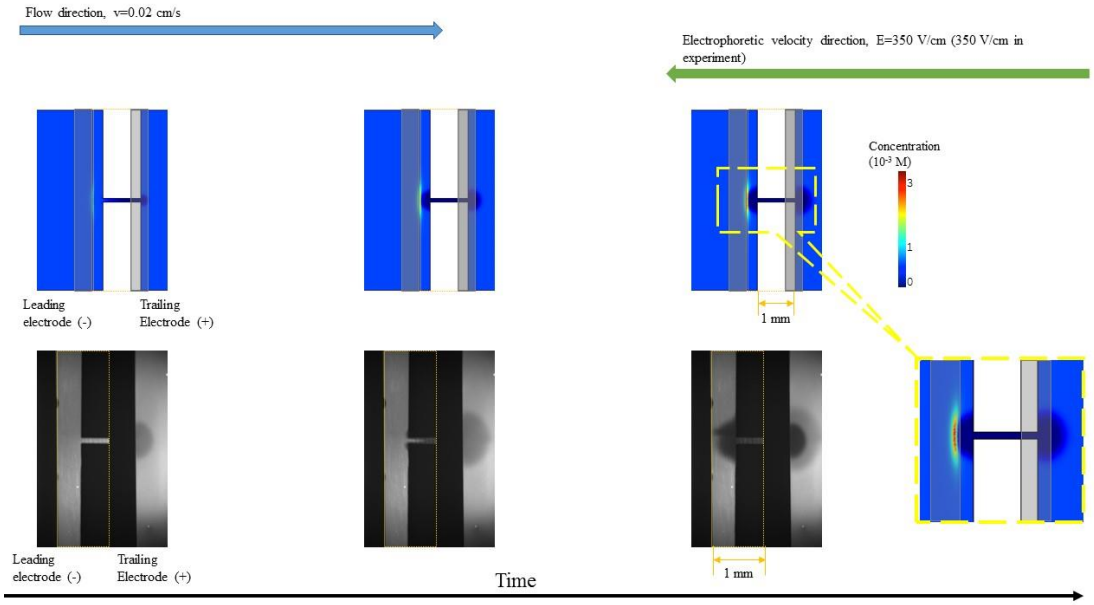


(see figure legend on Page 89)

B)

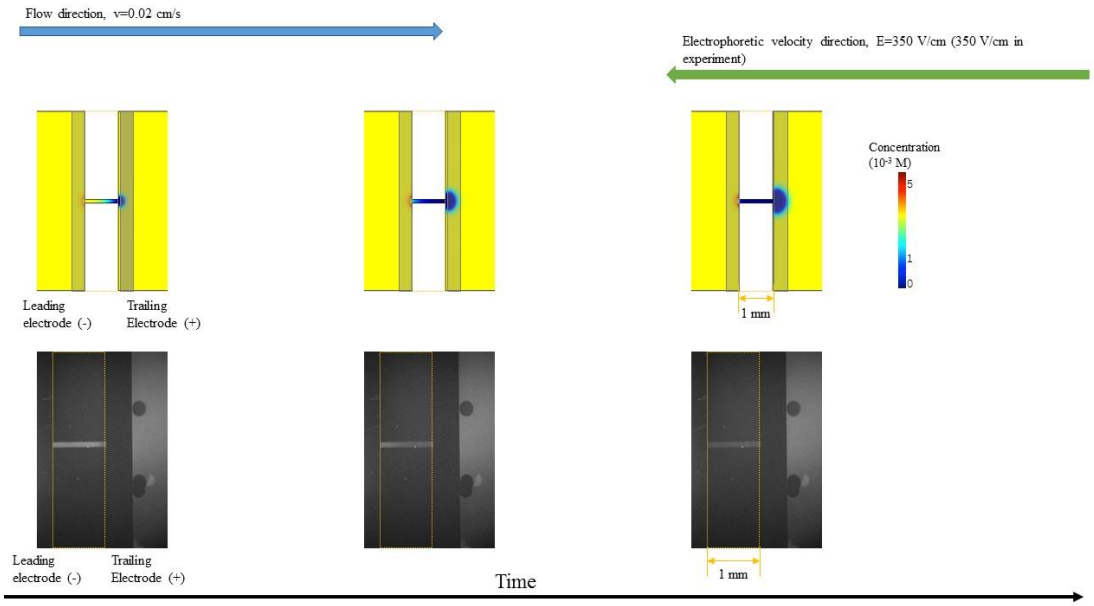


(see figure legend on Page 89)

C)

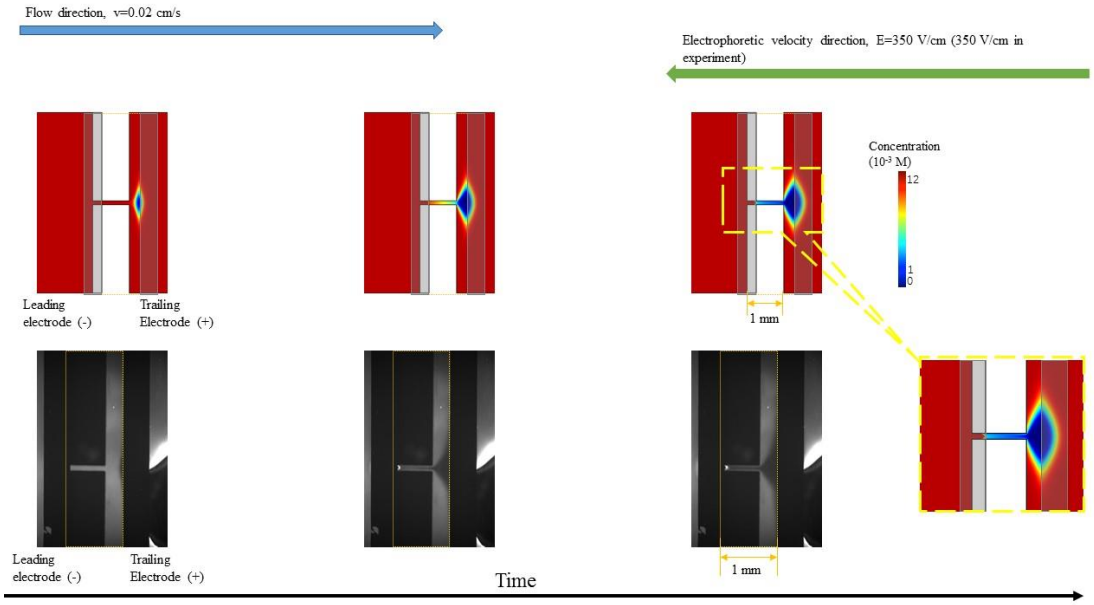


Figure 4.2 Experimental data exploring qualitative spatial-temporal features of modeling for all three entrance configurations. Calculated concentration changes and fluorescence measurements of A) leading electrode placed outside of channel entrance, B) leading electrode aligned with entrance, and C) leading electrode within channel. All simulations (top, each section) created with finite element multiphysics commercial software. Thick grey vertical lines (labeled leading electrodes, trailing electrode) represent the electrode placement. Dashed orange zones indicate the locations that can be experimentally observed via microscopy and similar locations are also shown in simulations. Zoom-in area of A) and C) indicate the semi-circle pattern and triangular shape pattern. Dominant color differences between A, B and C are due to the varying degrees of concentration changes for each electrode placement. Black parts in all experimental results (bottom, each section) are electrodes. The placement of the electrodes has a significant effect on the features and patterns of 2D concentration distribution for electrophoretic exclusion.

A) B) C)

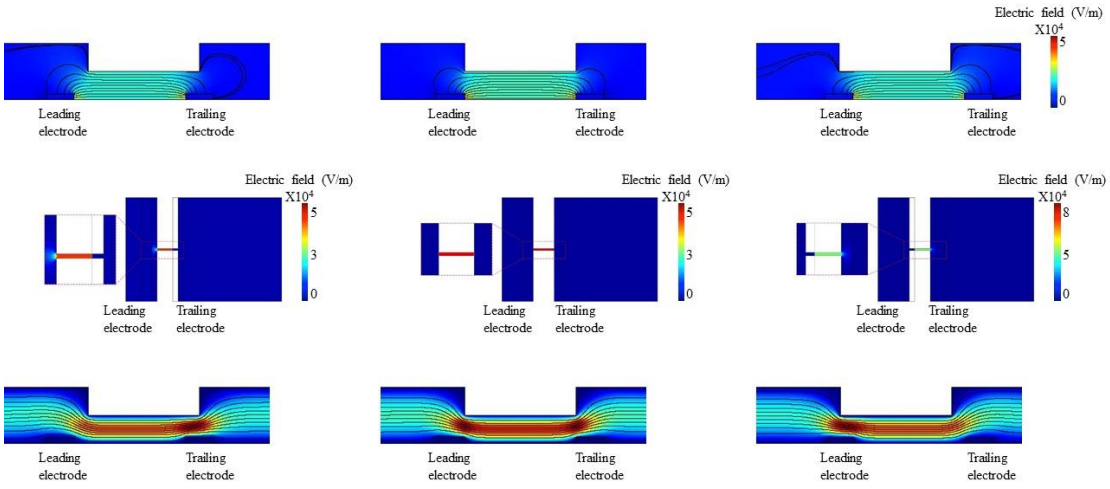


Figure 4.3 Detailed plots of qualitative features for simulations of electric field strength (side-view, top sections), electric field strength (top-view, middle sections), and velocity (side-view, bottom sections) along x-axis of A) leading electrode placed outside of channel entrance, B) leading electrode aligned with entrance, and C) leading electrode within channel. Red color and more intense streamlines indicate higher velocity fields (blue is low intensity flow) or electric fields. There are clearly observable changes for these fields in response to small changes in electrode placement.

Another method to explore the dramatic differences from subtle electrode position change is to examine the concentration profile along the longitudinal axis centerline. In plotting these values (Figure 4.4, bottom of each section), three distinct patterns emerge. Here, all plots were from the same electric field (350 V/cm) and the electric field was applied for the same amount of time (5 s).

For the electrode placed outside the channel (Figure 4.4 A, bottom), a small concentration enhancement is present, coupled with a depletion zone. For the electrode aligned with the entrance (Figure 4.4 B, bottom), a concentration enhancement is present again near the entrance, however, not as significant. With the leading electrode placed within the channel (Figure 4.4 C, bottom), a significant concentrated zone is apparent

near the entrance. Moreover, by comparing these three patterns, the electrode placed within the channel (Figure 4.4 C, bottom) creates a little bit depletion in 5 s, while electrode aligned with the entrance (Figure 4.4 B, bottom) has some material remaining at the boundary of leading electrode and channel, and electrode placed outside the channel (Figure 4.4 A, bottom) has more exclusion in the channel.

One issue that is obvious when examining this representation of the data is that the concentration increase associated with the electrode region does not fully compensate for the concentration decrease within the channel area (apparently conflicting with conservation of mass). This is simply due to the univariate view not being sufficient to depict the whole concentration distribution in a 3D model. That notwithstanding, the investigation with a centerline is informative, when combined with other assessments, since most of the concentration enhancement is taking place along the centerline.

Among all the three placements, the leading electrode within channel entrance gives rise to the highest local concentration increase. Several factors contribute to this result. First, the concentrated dyes molecules are accumulated in a confined region with less diffusion. The region within channel contributes to the amount of dye captured within the concentrated zone. The flow rate is high in that region. The electric field is also high, and net transport is still towards the leading electrode. Second, the electric field at the edge of the electrode is high and concentrated near the bottom of the reservoir, adding to local transport. In addition, the total current across the electrode/channel system is slightly higher, since there is reduced resistance within the reservoir area from an increased cross-sectional area and the length of the channel between conductors is reduced.

For the channel entrance aligned configuration, the overall current is the lowest of the three conditions and the flow and electric fields are essentially aligned and counter one-another. The only materials are those transported to the channel entrance and the within-channel initial concentration.

For the leading electrode outside the channel entrance, no significant concentrated bolus is observed. The total resistance is slightly reduced, similar to the leading electrode within channel and thus electrophoretic velocity somewhat is reduced. The penetration of the reduced electric field in the vertical dimension is apparently insufficient to prevent the bleed-through associated with the velocity laminae as well as lateral diffusion.

In addition to the two-dimensional spatial assessment, time-dependent simulation allows comparison of the dynamics of the exclusion. The concentration profile along the longitudinal axis centerline provides a good representation of the system. All plots are chosen at the time point when the electric field is applied for 1, 2, 3, 4 and 5 s, respectively (Figure 4.4 D).

The data and simulation results show the exclusion starting from the end of the channel, and gradually moving towards to the front of the channel, reaching exclusion. When the voltage is applied for a short period of time, the concentration/intensity drops beginning at the exit, which could be observed from both simulation and experimental results (Figure 4.4 D). This configuration also gives rise to a similar concentration factor, as consistent with mentioned in previous sections.

A)

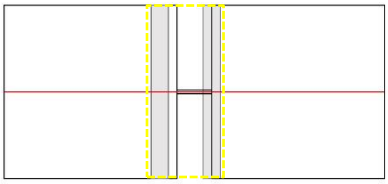

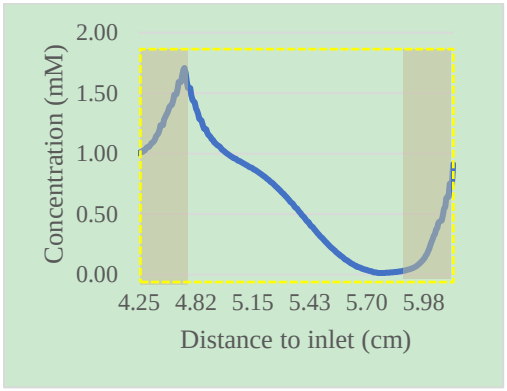
Concentration (mM)
2.00
1.50
1.00
0.50
0.00
4.25 4.82 5.15 5.43 5.70 5.98
Distance to inlet (cm)

B)

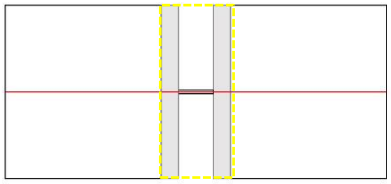

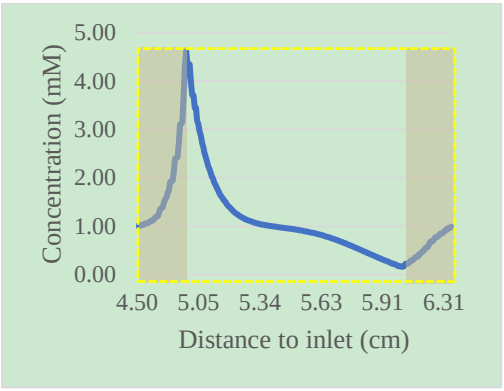
Concentration (mM)
5.00
4.00
3.00
2.00
1.00
0.00
4.50 5.05 5.34 5.63 5.91 6.31
Distance to inlet (cm)

C)

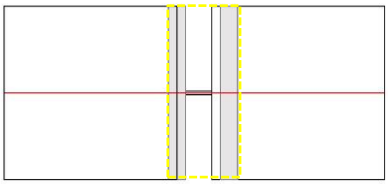

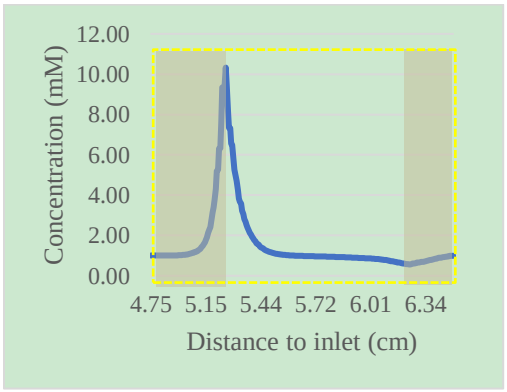
Concentration (mM)
12.00
10.00
8.00
6.00
4.00
2.00
0.00
4.75 5.15 5.44 5.72 6.01 6.34
Distance to inlet (cm)

D)

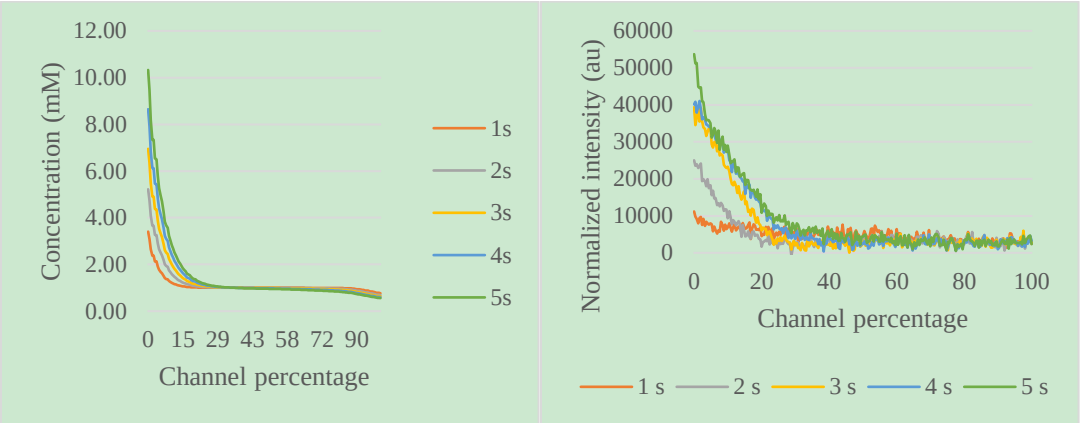


Figure 4.4 A-C: Concentration profile from simulation along the centerline for various electrode alignments: A) electrode outside of channel entrance, B) electrode aligned with entrance, and C) electrode within channel. Black line in each schematic (top, each section) outlines the top-view shape of the reservoirs (2) and channel (1) used in the model. Total length of the device is 11 mm, with reservoir length of 5 mm and channel length of 1 mm. Grey rectangles present electrodes and their locations indicate the positions in the model. The electric field is applied to the electrodes. Red line across the device highlights the centerline used for each plot. Yellow dash boxes are chosen left end of the left electrode to right end of the right electrode. Values along x-axis are the relative length to the left side of the device. D) Simulations and representative experimental results for the electrode within the channel entrance pattern, demonstrates semi-quantitative, temporal differences in concentration along the centerline, showing consistent features.

### 4.3.2 Resolution characterization of current interfaces and impact on design of next-generation devices

With this work, a model which captures observed experimental behaviors has been built to assess asymmetric interfaces with varying electrode placement. The accuracy with which this model reflects even the tiny details of the experimental concentration profiles instills confidence that a similar modeling strategy for evolving designs will reflect experimental performance. The observation that small changes make a big difference in concentration distribution and a model which faithfully reflects those

distributions suggests the modeling capability will enable significantly higher resolution interfacial designs.

Resolution description of electrophoretic exclusion is defined significantly different than standard linear separations schemes. Kenyon et al.'s theoretical work provided a fundamental basis of resolution assessment on capillary-based EE apparatus and other similar techniques. One method to compare interfaces and estimate resolution is to compare the concentration at consistent point in the channel. For a fully excluded species, the concentration is zero and a non-excluded species is still at the nominal concentration.

Based on this approach, exclusion efficiency of three interfaces described above are solved as 50%, 30% and 10% for leading electrode outside the channel, leading electrode aligned with channel, leading electrode within channel, respectively. Based on this brief assessment, this can be compared to the capillary-based radially symmetric entrances, and the current interface does not provide high separation resolution.

Building on the previous simulations and experiments with capillaries and rotational symmetry [27, 30], this work expands to an asymmetric geometry. This system is of high complexity and subtle variations result in significantly different behaviors captured in both the simulations and experiments. This suggests that the simulation strategy is useful for complex geometries. These studies build a foundation for exploration using modeling for new electrode geometry and placement and channel entrance configuration. New designs promise to improve efficiency of exclusion and begin to reach theoretical limits recently described [32].

In addition, the ability of building 3D structures potentially benefits to the development of mimicking physiological features. Combined with newly emerged fabrication techniques, it can result in a better understanding of physiological micro-environment [49].

### 4.4 Concluding remarks

Numerical and experimental studies as well as resolution characterization of an electrophoretic separation technique with three different interfaces has been investigated. The simulation constructed in 3D reflects the experimental effects of three patterns resulting from electrode placement. It was found that the placement of the electrodes in relation to the separation channel had a large impact on the concentration properties. The comparisons between calculated profiles and experimental results generated excellent qualitatively agreement. The development of a 3D numerical simulation provides a convenient tool for examining current design constraints and enables predicting future design features. It is believed that the device and the analysis presented here can serve as a guide to the design of next-generation device with enhanced concentration ability and increased resolving power.

### 4.5 References

[1] Issaq, H. J., *Electrophoresis* 2001, *22*, 3629-3638.

[2] Smejkal, P., Bottenus, D., Breadmore, M. C., Guijt, R. M., Ivory, C. F., Foret, F., Macka, M., *Electrophoresis* 2013, *34*, 1493-1509.

[3] Gebauer, P., Mala, Z., Bocek, P., *Electrophoresis* 2011, *32*, 83-89.

[4] Mala, Z., Gebauer, P., Bocek, P., *Electrophoresis* 2013, *34*, 19-28.

[5] Mala, Z., Gebauer, P., Bocek, P., *Electrophoresis* 2015, *36*, 2-14.

[6] Lian, D. S., Zhao, S. J., Li, J., Li, B. L., *Analytical and bioanalytical chemistry* 2014, *406*, 6129-6150.

[7] Quirino, J. P., Kim, J. B., Terabe, S., *Journal of Chromatography A* 2002, *965*, 357-373.

[8] Shackman, J. G., Ross, D., *Electrophoresis* 2007, *28*, 556-571.

[9] Koegler, W. S., Ivory, C. F., *Biotechnology progress* 1996, *12*, 822-836.

[10] Koegler, W. S., Ivory, C. F., *Journal of Chromatography A* 1996, *726*, 229-236.

[11] Huang, Z., Ivory, C. F., *Analytical chemistry* 1999, *71*, 1628-1632.

[12] Tracy, N. I., Huang, Z., Ivory, C. F., *Biotechnology progress* 2008, *23*, 444-451.

[13] Tracy, N. I., Ivory, C. F., *Electrophoresis* 2008, *29*, 2820-2827.

[14] Humble, P. H., Kelly, R. T., Woolley, A. T., Tolley, H. D., Lee, M. L., *Analytical chemistry* 2004, *76*, 5641-5648.

[15] Liu, J., Sun, X., Farnsworth, P. B., Lee, M. L., *Analytical chemistry* 2006, *78*, 4654-4662.

[16] Sun, X., Farnsworth, P. B., Tolley, H. D., Warnick, K. F., Woolley, A. T., Lee, M. L., *Journal of chromatography. A* 2009, *1216*, 159-164.

[17] Sun, X., Farnsworth, P. B., Woolley, A. T., Tolley, H. D., Warnick, K. F., Lee, M. L., *Analytical chemistry* 2008, *80*, 451-460.

[18] Burke, J. M., Ivory, C. F., *Electrophoresis* 2008, *29*, 1013-1025.

[19] Strychalski, E. A., Henry, A. C., Ross, D., *Anal Chem* 2011, *83*, 6316-6322.

[20] Shackman, J. G., Munson, M. S., Ross, D., *Analytical chemistry* 2007, *79*, 565-571.

[21] Ross, D., Munson, M. S., *Electrophoresis* 2014, *35*, 770-776.

[22] Sikorsky, A. A., Fourkas, J. T., Ross, D., *Analytical chemistry* 2014, *86*, 3625-3632.

[23] Strychalski, E. A., Henry, A. C., Ross, D., *Analytical chemistry* 2009, *81*, 10201-10207.

[24] Hoebel, S. J., Balss, K. M., Jones, B. J., Malliaris, C. D., Munson, M. S., Vreeland, W. N., Ross, D., *Analytical chemistry* 2006, *78*, 7186-7190.

[25] Shackman, J. G., Munson, M. S., Ross, D., *Analytical and bioanalytical chemistry* 2007, *387*, 155-158.

[26] Polson, N. A., Savin, D. P., Hayes, M. A., *Journal of Microcolumn Separations* 2000,

*12*, 98-106.

[27] Pacheco, J. R., Chen, K. P., Hayes, M. A., *Electrophoresis* 2007, *28*, 1027-1035.

[28] Meighan, M. M., Keebaugh, M. W., Quihuis, A. M., Kenyon, S. M., Hayes, M. A., *Electrophoresis* 2009, *30*, 3786-3792.

[29] Meighan, M. M., Vasquez, J., Dziubcynski, L., Hews, S., Hayes, M. A., *Analytical chemistry* 2011, *83*, 368-373.

[30] Keebaugh, M. W., Mahanti, P., Hayes, M. A., *Electrophoresis* 2012, *33*, 1924-1930.

[31] Kenyon, S. M., Weiss, N. G., Hayes, M. A., *Electrophoresis* 2012, *33*, 1227-1235.

[32] Kenyon, S. M., Keebaugh, M. W., Hayes, M. A., *Electrophoresis* 2014, *35*, 2551-2559.

[33] Kler, P. A., López, E. J., Dalcín, L. D., Guarnieri, F. A., Storti, M. A., *Computer Methods in Applied Mechanics and Engineering* 2009, *198*, 2360-2367.

[34] Saville, D. A., Palusinski, O. A., *AIChE Journal* 1986, *32*, 207-214.

[35] Bahga, S. S., Bercovici, M., Santiago, J. G., *Electrophoresis* 2012, *33*, 3036-3051.

[36] Ermakov, S. V., Stephen C. Jacobson, and J. Michael Ramsey. , *Analytical chemistry* 1998, *70*, 4494-4504.

[37] Ermakov, S. V., Jacobson, S. C., Ramsey, J. M., *In Proc. Conf. Modeling Simulation Microsyst* 1999, 534-537.

[38] Bianchi, F., R. Ferrigno, and H. H. Girault., *Analytical chemistry* 2000, *72*, 1987-1993.

[39] Barz, D. P. J., Ehrhard, P., *Pamm* 2005, *5*, 535-536.

[40] Chatterjee, A., *Journal of Micromechanics and Microengineering* 2003, *13*.

[41] Cardona, A., Nigro, N., Sonzogni, V., Storti, M., *Mecanica Computacional* 2006, *25*, 2573-2583.

[42] Kler, P., Guarnieri, F., Berli, C., *Mecanica Computacional* 2008, *27*, 3367-3380.

[43] Kler, P. A., Berli, C. L. A., Guarnieri, F. A., *Microfluidics and Nanofluidics* 2010, *10*, 187-198.

[44] Mansouri, A., Scheuerman, C., Bhattacharjee, S., Kwok, D. Y., Kostiuk, L. W., *J Colloid Interface Sci* 2005, *292*, 567-580.

[45] Stone, H. A., Stroock, A. D., Ajdari, A., *Annual Review of Fluid Mechanics* 2004, *36*, 381-411.

[46] Li, D., *Electrokinetics in microfluidics*, Elsevier 2004.

[47] Squires, T. M., Quake, S. R., *Reviews of modern physics* 2005, *77*, 977.

[48] Tabeling, P., *Introduction to microfluidics*, Oxford University Press on Demand 2005.

[49] Hwang, Y., Candler, R. N., *Lab on a chip* 2017.

# CHAPTER 5

# PREPARING DILUTE SMALL VOLUME PROTEIN SAMPLES WITH ELECTROPHORETIC EXCLUSION FOR ELECTRON MICROSCOPY DETECTION

## 5.1 Introduction

The function of cellular macromolecules, such as proteins, is linked to their three-dimensional architectures. High resolution, atomic level structural information not only provides clues for protein function, interactions, and conformational changes, but also offers insights for the development of potential therapeutic medicine and treatment [1, 2].

Over the last several decades, X-ray crystallography and NMR spectroscopy were quite successful and largely dominated the field of determination of atomic resolution protein structures. However, even with a very high level of development, there are some drawbacks to these techniques. For X-ray crystallography, proteins must be crystallized. It is often challenging, labor-intensive, and time-consuming to achieve crystals which generate good diffraction patterns. Moreover, not all the proteins can be easily crystallized. NMR spectroscopy, on the other hand, does not require protein crystallization. It is primarily used for proteins with relatively low molecular weight (< 50 kDa) and relatively large pure and concentrated samples are used [3].

Transmission electron microscopy (TEM) has been an alternative method for structure determination of biological samples spanning several decades, and it has provided many important insights into fundamental biological processes and diseases. Unlike X-ray crystallography or NMR spectroscopy, it does not require protein crystallization, nor a large sample amount [4].

While great strides have been made in EM data collection and processing, sample preparation is still performed using decades old techniques [5, 6]. Optimal samples have a high density of well-separated biomolecular complexes embedded in ice within the voids of the EM grid support film. This sample preparation method has been enormously successful and has been used to produce the majority of the high-resolution EM structures. However, this method relies on extensive macroscale benchtop purification and concentration to achieve homogeneity suitable for high-resolution analysis. It is extremely challenging when dealing with target proteins in low abundances among complex matrices. One significant example was from the early detection of Alzheimer's diseases (AD). Patients with AD suffer from memory impairment, disorientation, and executive dysfunction [7] and lead to death within 3 to 9 years after diagnosis [8]. Recent studies suggest that therapy and treatment in the early stages of AD may be more effective [9]. The biomarkers of AD play an important role and the 3D structures of biomarkers provide great insights into the mechanism of diseases, and thereby allowing rational design of novel diagnostic and therapeutic agents. However, the concentrations of such markers in biofluids (such as cerebral spinal fluid) are so low in the early stages that they cannot be identified accurately [10]. Therefore, it is often necessary to conduct a purification and preconcentration step before effective imaging can be achieved.

Conventional preconcentration techniques, such as centrifuge or chromatography, often do not help with purification and concentration in a rapid time frame with enhanced efficiency and throughput. Gel-electrophoresis has been used for protein isolation and purification in most cases [11]. However, this conventional protein isolation and purification strategy is time-consuming and labor-intensive. The conventional techniques

with poor efficiency require an adapted methodology in EM for selective sample preconcentration prior to applying samples onto grids, while still keeping grid complete/undamaged, electron microscopy detectable, and data interpretable.

A novel electrophoretic separation and preconcentration technique could be potentially applied to enhance the efficiency and facilitate selective preconcentration. This electrophoretic isolation and preconcentration technique, electrophoretic exclusion, is a counterflow gradient focusing technique which exploits hydrodynamic flow to counterbalance the electrokinetic force, thus focusing target molecules to a specific location [12-22]. The gradient is established between the boundary of the channel and an expanded reservoir. Electrophoretic exclusion can be achieved at the entrance to a channel in bulk solution when the electrokinetic velocity (electric field-induced) is larger than or equal to the hydrodynamic flow (pressure-induced). The electrokinetic velocity depends on the mobility and the electric field, so by manipulating the applied voltage (or the electric field), separation of different species with various mobilities can be achieved. Selective preconcentration and isolation of different protein samples and dye molecules has been demonstrated with this technique [15, 17, 18].

As TEM imaging does not require a large sample amount, microfluidic devices could potentially help promote the performance of electron microscope imaging. Beginning in the early 1990s, microfluidics has since been widely adopted in various fields of analytical chemistry and life sciences. This expansion is due to microfluidics having advantages over bench-top devices, such as portability, flexibility in design, miniaturization of operating systems, reduced reagent consumption, decreased run time, minimized sample dilution, and accelerated mass and heat transfer [23]. Several groups

have begun to recognize this natural fit between TEM imaging and microfluidics. Giss and co-workers presented a microfluidic approach for a fast protein isolation method to separate untagged target protein from a complex cell lysate background and achieved relative or even absolute quantification of protein levels [24]. Roper et al. demonstrated a microfluidic device to deal with the variability issues of manual staining of EM grids by confining grids into a chamber performing reagent delivery and drying. With their device, negative staining could be achieved in a controlled manner with reproducible results and minimized artifacts [25]. Other investigations focused on the cryo-EM grid preparation. Arnold et al. developed a method by directly depositing a small volume of sample (3-20 nL) on to the grid through a microcapillary, without blotting steps, and achieved resolution between 0.3 and 0.6 nm [26]. Feng et al. came up with a fast and effective microfluidic spraying-plunging method for cryo-EM to have a better control of the ice thickness of the droplet. With this strategy, they solved the structure of apoferritin to 0.3 nm resolution [27]. A more recent work by Ashtiani applied surface acoustic wave (SAW) to deliver femtoliter (30-200 fL) droplets from a microfluidic chip in the form of aerosol and the delivered droplets spread on the surface of grid to form a film. The main difference in mechanism is that SAW drives the atomization instead of a fluid, so the system can be simplified to a capillary without using pumping, which further decreases the volume of the sample required [28].

Advances have been made by these strategies, but selective concentration has not been addressed, especially for samples with complex matrices. An approach is investigated here that uses electrophoretic exclusion in a microfluidic chip as a sample preparation strategy for TEM imaging. Grids are directly embedded into the central

reservoir of the microfluidic device, where the samples are preconcentrated in the upstream area of the reservoir. As proof-of-usefulness, preconcentration of single protein and selective isolation and concentration of one protein in a mixture of two are presented. The results are monitored with fluorescence microscopy and TEM imaging.

## 5.2 Experimental

### 5.2.1 Materials

Acetone, isopropanol, sodium hydroxide, 4-(2-hydroxyethyl)-1-piperazineethanesulfonic acid (HEPES), dimethyl sulfoxide (DMSO), and human immunoglobin M (IgM) were obtained from Sigma-Aldrich (St. Louis, MO). NHS-rhodamine and NHS-fluorescein were purchased from Thermo Scientific (Waltham, MA). Horse spleen apoferritin was received from the collaborator (Nannenga, Engineering ASU) with a concentration of 25 mg/ml in glycerol. Formvar coated grids, stabilized with evaporated carbon film (FCF300-Cu-SB, 10 nm formvar and 3-4 nm carbon) were purchased from Electron Microscopy Sciences (Hatfield, PA). Uranyl acetate for negative staining was prepared as 2% by staff in Eyring Materials Center at Arizona State University. For all solutions, ultrapure deionized water was used (Barnstead International, Inc., Dubuque, IA).

HEPES stock solution (0.1 M, pH 7.2) was freshly prepared prior to each experiment by dissolving 2.38 g of HEPES with 100 mL distilled water and adding one NaOH pellet to raise the pH to around 7.2. The solution was then sterile-filtered and stored in the refrigerator temporally if necessary.

### 5.2.2 Protein labeling

NHS-rhodamine was dissolved in DMSO to concentrations of 10 mg/mL. Horse spleen apoferritin stock sample used was prepared as 25 mg/mL in glycerol. Glycerol was removed from a 50 μL sample by transferring it to a dialysis tube unit (Thermo Fisher Scientific, Waltham, MA) placed in 1000 mL distilled water for more than 15 minutes. The content in the dialysis tube was transferred into a centrifuge tube, and 1.6 μL of NHS-rhodamine-DMSO mixture was added according to instruction provided by kit manufacturer (Thermo Fisher Scientific, Waltham, MA). The tube was gently shaken in dark for one hour to allow the reagents fully react. Afterwards, the content in the tube was again placed into a dialysis unit and dialyzed against about 250 mL 20 mM HEPES solution overnight. Final concentration was 10 mg/mL. Sample were diluted to certain concentrations upon use.

NHS-fluorescein was dissolved in DMSO to concentrations of 10 mg/mL. IgM was commercially available with a concentration of 1 mg/mL. 50 μL sample was transferred to a dialysis tube unit and placed in 250 mL 20 mM HEPES solution for more than 4 hours to allow buffer exchange. The content in the dialysis tube was then transferred into a centrifuge tube, and 1 μL of NHS-fluorescein-DMSO mixture was added into the tube according to manual instruction. The tube was gently shaken in dark for one hour to let the reagents fully react. Afterwards, the content in the tube was again placed into a dialysis unit and dialyze in 250 mL 20 mM HEPES solution overnight. Final concentration was 0.5 mg/mL, and diluted to certain concentrations upon use.

### 5.2.3 Microdevice fabrication

Devices were fabricated according to an established procedure [18, 22], and the procedure was described in previous chapters.

### 5.2.4 Microdevice operation

For a common microdevice (without grids embedded) operation, the sample was loaded into device prior to voltage application. When voltages were applied, a certain part of the device was monitored with fluorescence microscopy, and results were recorded.

For a microdevice of TEM applications, grids were pretreated in the glow discharger unit (Harrick, Ithaca, NY, USA) for 60 seconds with medium RF setting and a pressure of approximately 1000 mTorr on both sides. Then the grids were placed on glass slide within the area of central reservoir (Figure 5.1). A PDMS cast was placed on top. The microdevice was filled with HEPES buffer solution by placing the liquid into the entrance ports and allowed to fill the channels and reservoirs though capillary action. The buffer was pipetted from the entrance ports after 2 minutes. The device was then placed on the microscope stage, connected to the voltage divider and a high voltage configuration was applied. The voltage for each channel was confirmed through a digital multimeter (DM-4400A Sperry, Menomonee Falls, WI, USA). Afterwards, samples were loaded into each entrance port. After 3 minutes, voltage was released. Right before releasing voltage, exit ports of unit 1 and/or 2 were filled with DI water and channels were blocked by collapsing with external physical pressure to prevent any further movement of fluid.

After experiments, grids were removed from the microdevice and negative stained. The procedures of negative staining in this particular case were: on a clean piece of parafilm place two drops of distilled water and two drops of staining solution (uranyl acetate), around 5 µL each. The grid with the carbon-side down was placed on the first

drop of water stain and let it rest for 10-15 seconds. The excess was blotted to remove the excess stain by touching the edge of the grid to a piece of filter paper. The same operation was used for the next drop of water and the other two drops of staining solution. The grid was then placed carbon-side down on a piece of dry filter paper and let it dry for five minutes before viewing in the electron microscope.

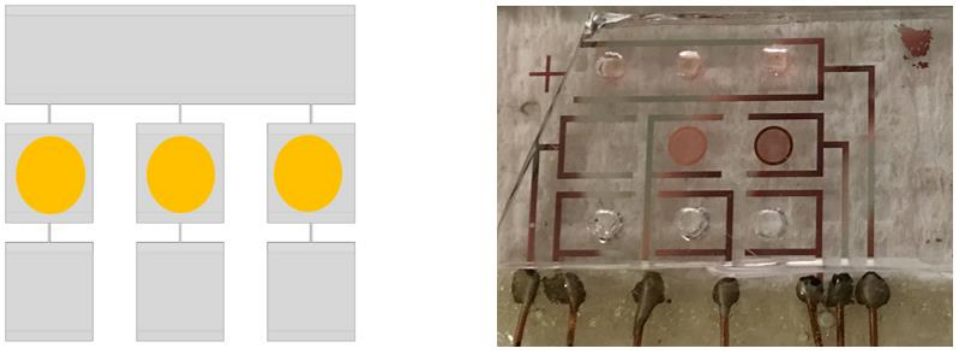

Figure 5.1 The integrated microdevice with grids embedded (left: schematic; right: photograph).

### 5.2.5 TEM imaging

Philips CM12 TEM was used for detection. Micrographs were taken with desired field and magnification using the software DigitalMicrograph (Gatan, Pleasanton, CA). Intensity was adjusted to set EXP TIME as 2.0-3.0 seconds before taking the micrographs.

### 5.2.6 Data processing

The acquired micrographs were processed with ImageJ (NIH). For images from fluorescence microscopy, a region of interest was chosen for each image in the grid area, and the averaged intensity was measured with the software. For a chosen micrograph, the contrast, brightness, and/or background was adjusted to make the particles of interest

more visible and clearer. The threshold of the micrograph was then adjusted to distinct analytes and create a binary image. Analyze particle command was used to count the number of particles. The area with aggregations (black area) was outlined with *Wand* function and the surface area was estimated from the software. Based on the area and the average protein size (10-12 nm), the number of particles in the black region can be estimated by assuming the particles tile one layer in that region.

### 5.3. Results and Discussion

#### 5.3.1 Preconcentration

Electrophoretic exclusion technique is extended to concentration and deposition of proteins directly to grids for TEM detection. The grids were embedded into a device, allowing for easier operation and less contamination (Figure 5.1). Horse spleen apoferritin was used a standard proof-of-principle sample. It has a distinctive hollow sphere shape when visualized in the TEM and it has been used to benchmark many new EM methods [27, 29]. Apoferritin samples were prelabeled with NHS-rhodamine for direct visualization during concentration via fluorescence microscopy, showing red fluorescence under these conditions.

A set of electric fields were determined to achieve sample preconcentration and provide control experimental condition. The field strengths used were somewhat lower than conventional electrophoretic methods, due to a relatively low flow rate in the system. The criteria for the choice of electric fields was that the electric field cannot be exceedingly large, which may cause damage to the biological samples, nor too low to not be sufficient for exclusion. Three conditions were selected for apoferritin enrichment: a smaller electric

field (10 V/mm), a higher electric field (20 V/mm), and no electric field as control (Figure 5.2).

Average intensity of the grids before and after electric field applied was compared and representative images were presented (n=3) (Figure 5.2). Images were captured from central reservoir before electric field was applied (left of each set), central reservoir after electric field was applied (right of each set), and grids removed from the microdevice (top of each set). With no electric field applied, the intensity of the images did not change; while with an electric field applied, the intensity increased. When a relatively higher electric field (20 V/mm) was applied, a higher intensity enhancement was obtained and a significant red color on the grid was observed. This is consistent with more sample being accumulated on the grid, suggesting a suitable electric field for operation.

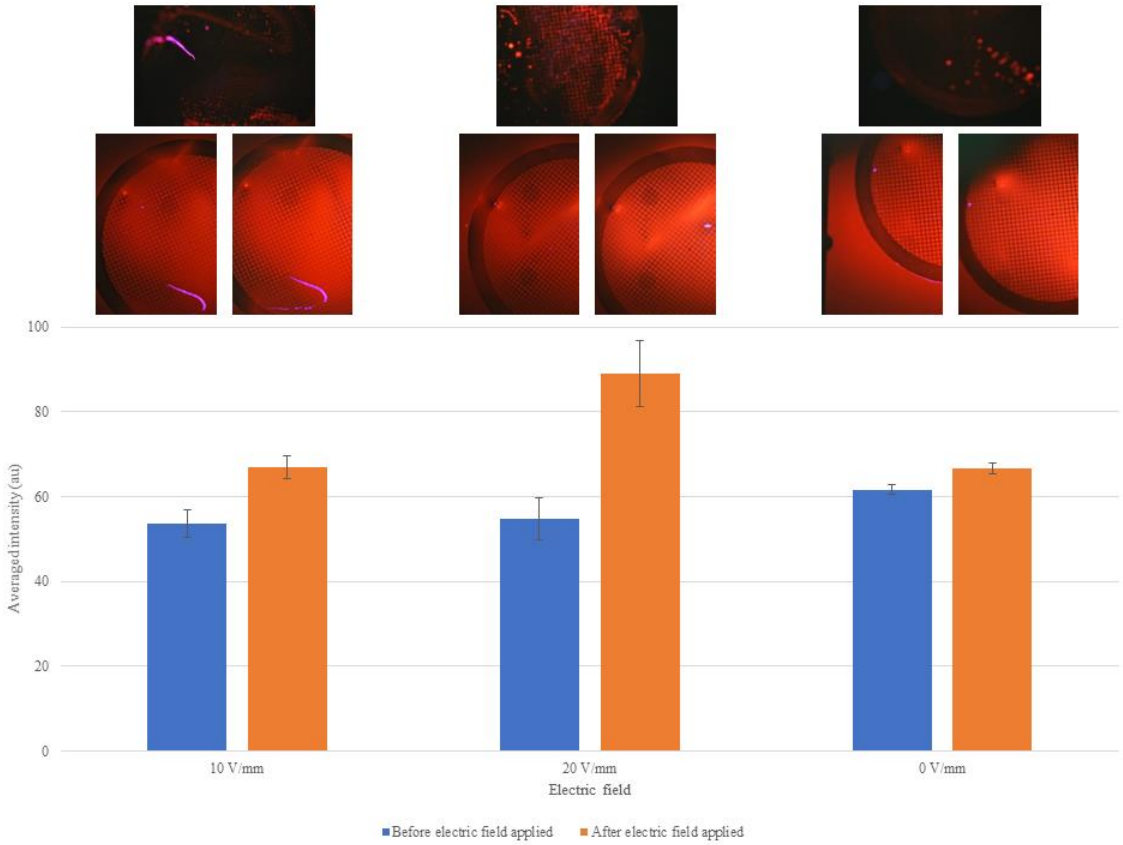


Figure 5.2 Electric field strength was varied to examine the optimal exclusion condition (n=3, error bar stands for standard deviation). Samples were loaded into each individual unit under different conditions. Left: with a smaller electric field (10 V/mm); Middle: with a higher electric field (20 V/mm); Right: with no electric field as control. Results were detected under fluorescence microscopy coupled with an SLR camera.

Proteins will adsorb immediately to a clean grid surface and this can complicate monitoring the effects of electrophoretic exclusion. This is evidenced by the absorption of analytes on the grid (Figure 5.2) with 10 V/mm and 0 V/mm applied (top of each set). Both images show similar levels of intensity, indicating analytes attached on the grids in both cases, even though the grid with 10 V/mm had experienced preconcentration while the grid with 0 V/mm did not. For regular operation of the device (consistent with previous uses), when sample was injected throughout the device prior to applying voltage

configurations, the absorption effect on the grid dominated. This loading was reflective of the initial concentration of analytes prior to any electrophoretic effects.

To avoid an initial adsorption event, a voltage configuration was designed to concentrate analytes in the upstream reservoir. The concentrated bolus was then allowed to flow onto the grids (Figure 5.3). The device was filled with buffer with no analyte to prevent collapse and maintain flow. After 3 minutes of sample accumulation, the concentrated bolus was released to the grid in the downstream reservoir. One unit was set as control and sample was allowed to flow through during the whole experiment. Another unit was blocked immediately prior to the voltages were released.

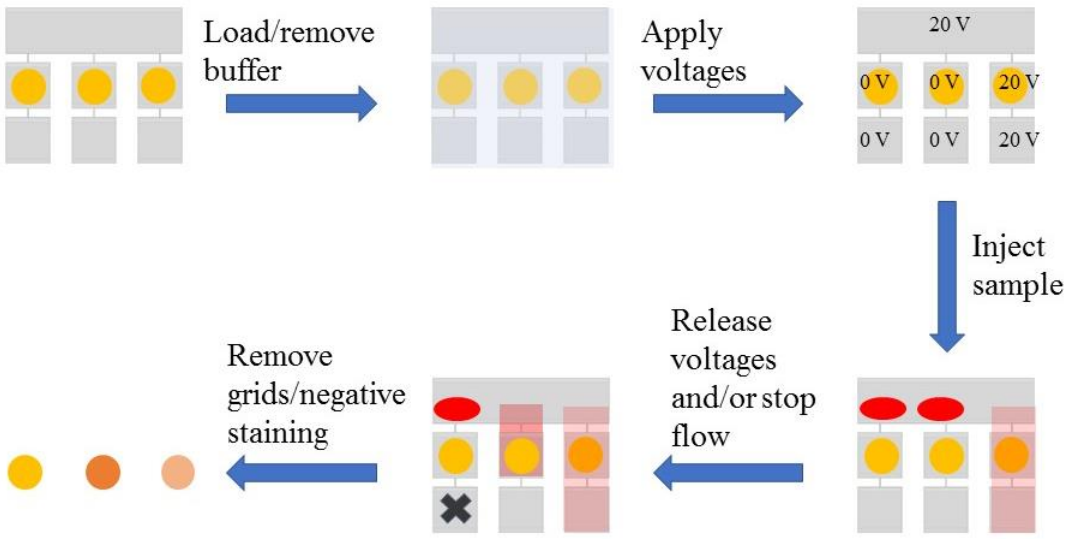


Figure 5.3 Strategy for capture high quality TEM data of protein from solutions that are too dilute to detect without enhancement. Fluorescent labels on protein are used to monitor the process.

Micrographs were captured (n=3) from TEM using this strategy (Figure 5.4). For these images, the grey area nominally represents protein, while the less grey or white area is background. At closer inspection or high magnification (bottom), the characteristic

hollow doughnut shape of apoferritin is apparent. The micrograph from central reservoir 3 acted as a control without taking any preconcentration action and an intermediate amount of proteins observed on the grid, presumable due to absorption. The micrograph from central reservoir 1 showed more white area and less grey area, indicating fewer proteins were accumulated on the grid. This also suggested that with this strategy, samples were able to effectively preconcentrate in the upstream reservoir. The micrograph from central reservoir 2 accumulated more protein samples, evidenced by even more grey area compared to the control.

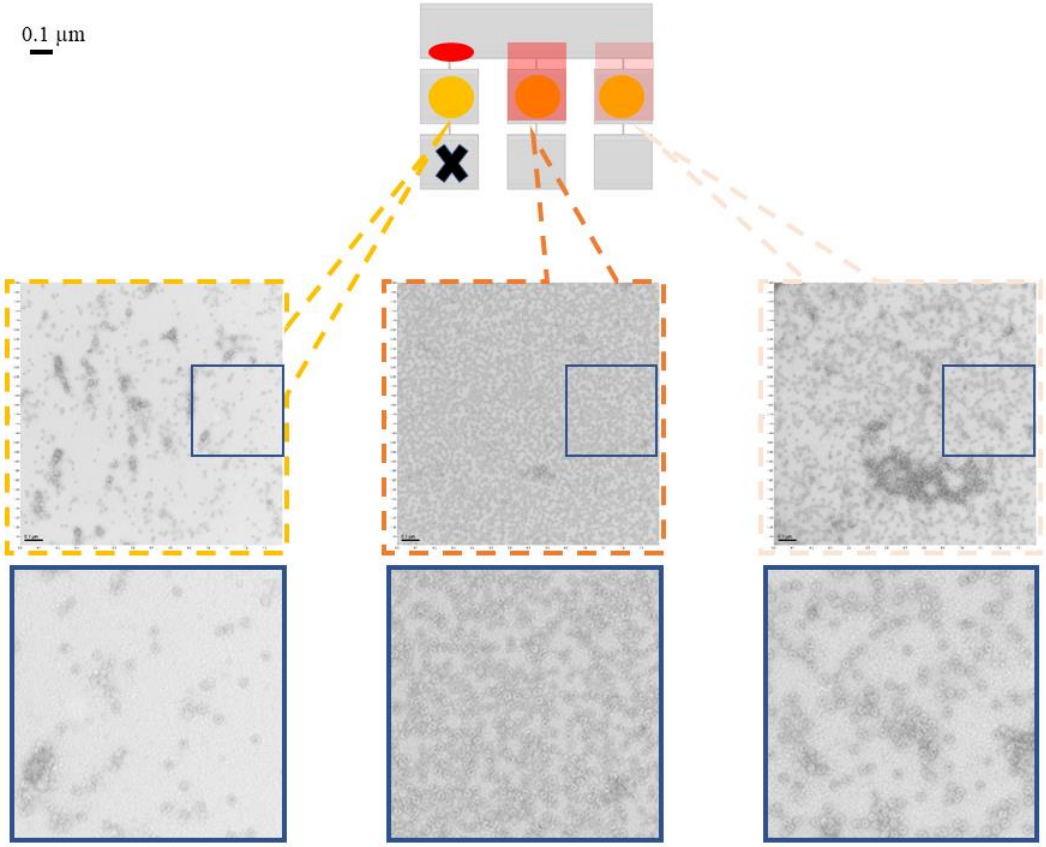


Figure 5.4 Representative images for grids from different reservoirs. Gray area nominally represents protein with a characteristic doughnut shape. Less gray or white area is background. Grid 3 acts as a control, Grid 2 appears to have accumulated more proteins, while Grid 1 accumulates fewer. An area in each micrograph (highlighted in blue) was magnified to present results in a better resolution.

### 5.3.2 Dilute samples

Using the strategy to minimize the effects of adsorption of sample onto the grids, the concentration of the original sample was varied to investigate the ability to gain high quality TEM from dilute solutions of protein. A typical EM sample contains biological species at concentration about 0.1 mg/mL to 3 mg/mL [30]. With the electrophoretic exclusion component applied, the available concentration for detection is expected to be much lower.

To develop a data set for comparison to the electrophoretic exclusion experiments, conventional negative staining treatment was performed on a range of apoferritin concentrations (Figure 5.5). The concentration ranged from 0.2 mg/mL to 0.01 mg/mL were prepared and applied directly onto the grids (n=10). After incubation, 2 drops of stain were applied sequentially. The grids were examined under TEM.

For concentration ranges between 0.1 mg/mL and 0.01 mg/mL, the number of particles observed exhibited a relatively linear relationship with concentration. From the graphical information, a reasonable detection limit is 0.007 mg/mL. The linearity of the quantification falls off at concentrations somewhat above 0.1 mg/mL and below 0.2 mg/mL, indicating a saturating imaging field (Figure 5.5).

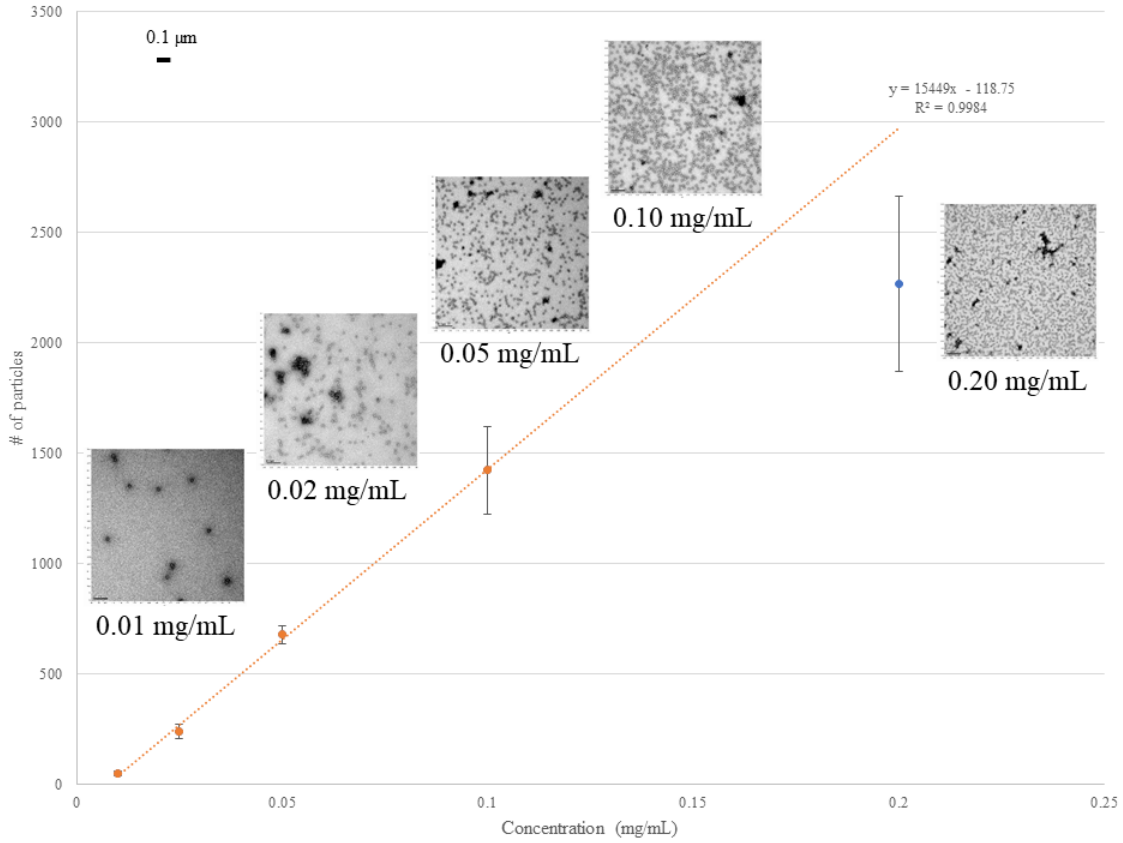


Figure 5.5 Calibration curve of apoferritin particles versus concentration (n=10, error bar stands for standard deviation) with representative micrographs. The curve was extended to 0.2 mg/mL, whereas the data point for 0.2 mg/mL was significantly lower than the curve, indicating the grid was saturated with particles.

Using the adsorption avoidance process again, three concentrations, 0.05, 0.005 and 0.0005 mg/mL, of apoferritin were tested (n=3) for effects from electrophoretic exclusion. We note that a concentration of 0.05 mg/mL is considered low for a conventional TEM test. However, with an electrophoretic exclusion microdevice treatment, this resulting sample was too concentrated as the representative TEM image gave rise to a largely grey featureless image. The concentration increase is estimated to be two-fold (Figure 5.6 A). With lower concentration, 0.005 mg/mL, for which it is almost impossible to achieve meaningful micrographs with conventional TEM, results

from imaging produced circular proteins evenly distributed (Figure 5.6 B). By comparing this result with the calibration curve (Figure 5.5), the concentration is estimated to be increased by four-fold. For a more diluted sample (0.0005 mg/mL), the image was taken under low magnification and there was almost no sample on the grid (Figure 5.6 C).

The lower concentration enhancement when a higher concentration of apoferritin sample was applied was mainly due to the lower ability of the complex interfacial zone to hold concentrated bolus when the concentration got higher as the concentrated bolus tended to diffuse laterally and breakthrough the channel area [19, 20].

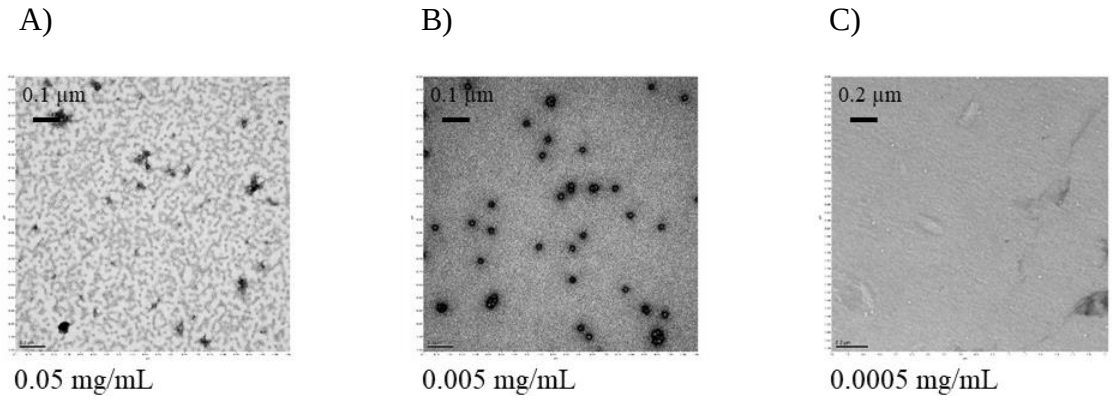


Figure 5.6 Representative micrographs containing samples with different concentrations.

However, it is worth mentioning that the concentration of specimen was not the higher, the better in TEM applications as the micrographs need a reasonable particle density to facilitate the particle selection step in further structural determination. The micrograph with a concentration of 0.05 mg/mL (Figure 5.6 A), although with plenty of particles on it, was not considered as a good example as the particle density was too large. Electrophoretic exclusion was more powerful on the diluted sample side as it enabled preconcentration and allowed conventional low concentrations to be detectable with a reasonable particle density.

### 5.3.3 Selective concentration on a mixture of apoferritin and IgM

Selective concentration of one component can be achieved from a protein mixture with the electrophoretic exclusion. The protein IgM was prelabeled with NHS-fluorescein (green fluorescence) and apoferritin was unlabeled as it demonstrated consistent behaviors in TEM imaging for the experiments performed.

A voltage configuration was designed to exclude apoferritin in Unit 1, exclude IgM in Unit 2, and take Unit 3 as a control (Figure 5.7 A). Results (n=3) (Figure 5.7 B) from fluorescence microscopy were used to test the applicability of this modified strategy. According to the results, both central and exit reservoir area of Unit 1 and Unit 3 showed green color, as IgM was expected to flow through Unit 1 and Unit 3 based on the modified strategy; while Unit 2 did not exhibit any green color, indicating IgM was excluded in the upstream reservoir.

TEM imaging was used to further characterize this strategy. Data from the central reservoir 3 grid was the control and both apoferritin and IgM can be observed. The representative micrograph from the grid in central reservoir 1 showed dark black particles, which were mostly IgM particles (Figure 5.7 C, bottom right) as compared to the IgM control (Figure 5.7 C, top left), since apoferritin has been effectively excluded to the entrance of the central reservoir 1. The representative micrograph from the central reservoir 2 grid showed round particles with doughnut shape, indicating they were mostly apoferritin particles (Figure 5.7 C, bottom middle).

Under the conditions of this strategy, there is a concentrated bolus outside of the exclusion area of the channel entrance. This was investigated with another set of trials (n=3) where the voltage was released without collapsing channels after the

electrophoretic exclusion was applied. As a result, the central reservoir 1 grid had image features consistent with IgM at a normal concentration level and apoferritin at a higher concentration level (Figure 5.7 D, bottom left). In a similar fashion, the grid from central reservoir 2 contained apoferritin at a normal level and IgM at a higher concentration level (Figure 5.7 D, bottom middle).

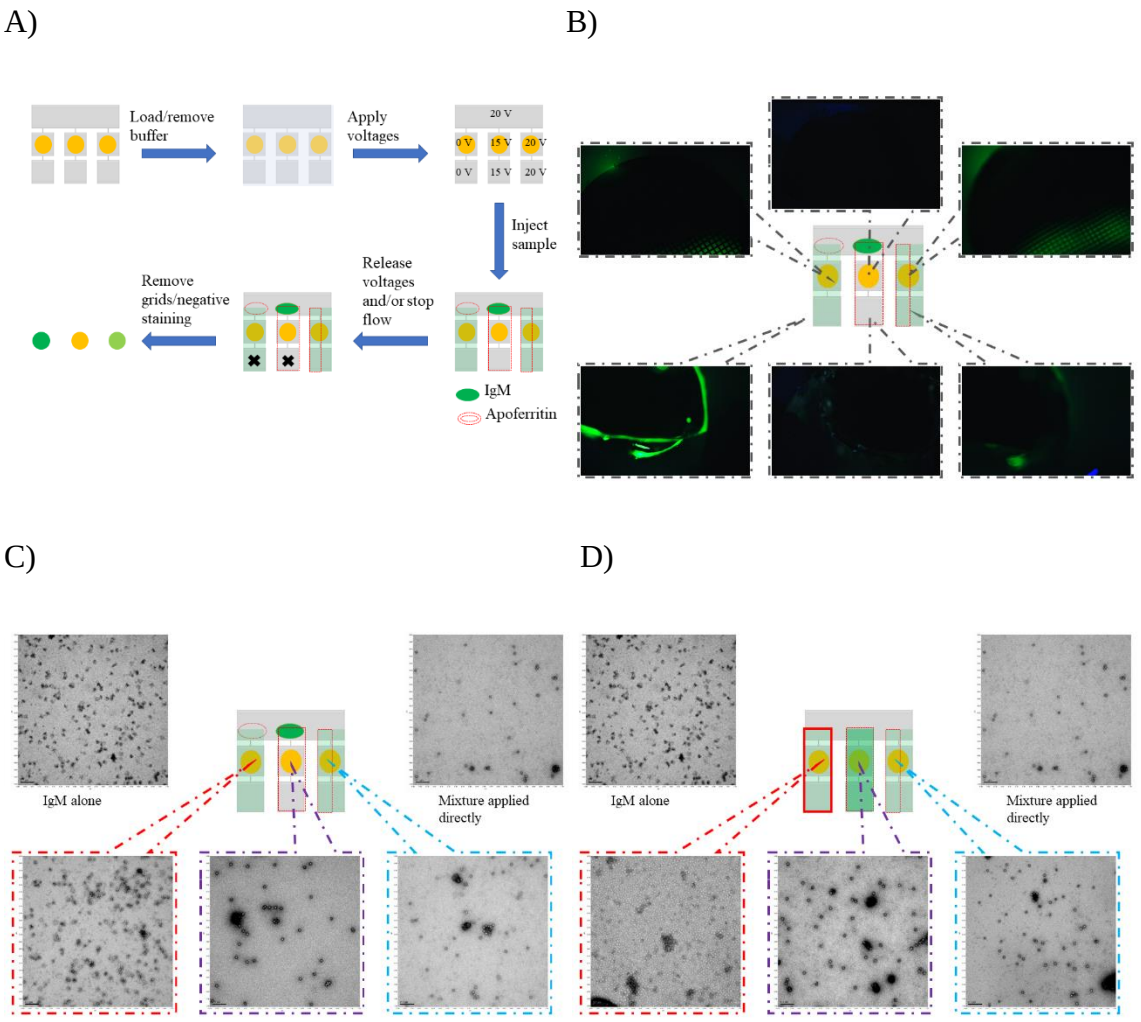


Figure 5.7 Results for selective concentration of a protein mixture. A) Illustration for selective concentration of protein from a simple mixture using electrophoretic exclusion. B) Results from fluorescence microcopy. C) Results from TEM. Top left corner: IgM only as a control; top right: mixture applied directly on the grid; bottom left: grid from central reservoir 1, IgM only; bottom middle: grid from central reservoir 2, apoferritin only; bottom right: grid from central reservoir 3, control. D) Results from TEM without collapsing all the channels. Bottom left: grid from central reservoir 1, IgM and a higher level of apoferritin; bottom middle: grid from central reservoir 2, apoferritin and a higher level of IgM; bottom right: grid from central reservoir 3, control.

When leaving the channel open upon release of the voltage (not collapsed), apoferritin which was being held back entered the grid chamber. By comparing micrographs from central reservoir 1 grids of channel collapsed (Figure 5.8 A, top) and

open (Figure 5.8 A, bottom), there is an obvious increase in apoferritin (round particles). Particle counting indicates the concentration of apoferritin is enhanced approximately two-fold. Similarly, but less straight forward, features consistent with IgM changed between the open and collapsed channel states.

The comparison between central reservoir 2 grids with collapsed (Figure 5.8 B, top) and open (Figure 5.8 B, bottom) did give rise to a difference, but the contrast is less straightforward than for apoferritin. The degradation of IgM made it difficult to quantitatively differentiate IgM from the background as the degraded protein lead to amorphous shapes without clear edges, although figures still showed significant difference in the background (note three image locations with enhanced contrast). The micrograph with apoferritin only had a more consistent background (Figure 5.8 B, top, three highlighted locations), while the micrograph with a mixture of apoferritin and IgM showed uneven background (Figure 5.8 B, bottom, three highlighted locations), indicating the presence of IgM. After adjusting the parameters of micrographs, the surface plots presented that the background was relatively clean and homogeneous with apoferritin samples only as there were almost no random peaks expect for apoferritin peaks (Figure 5.8 C); it was very noisy with IgM and apoferritin on the grid together as more peaks showed up besides apoferritin peaks (Figure 5.8 D). The uneven background is interpreted as an indication of the presence of IgM particles.

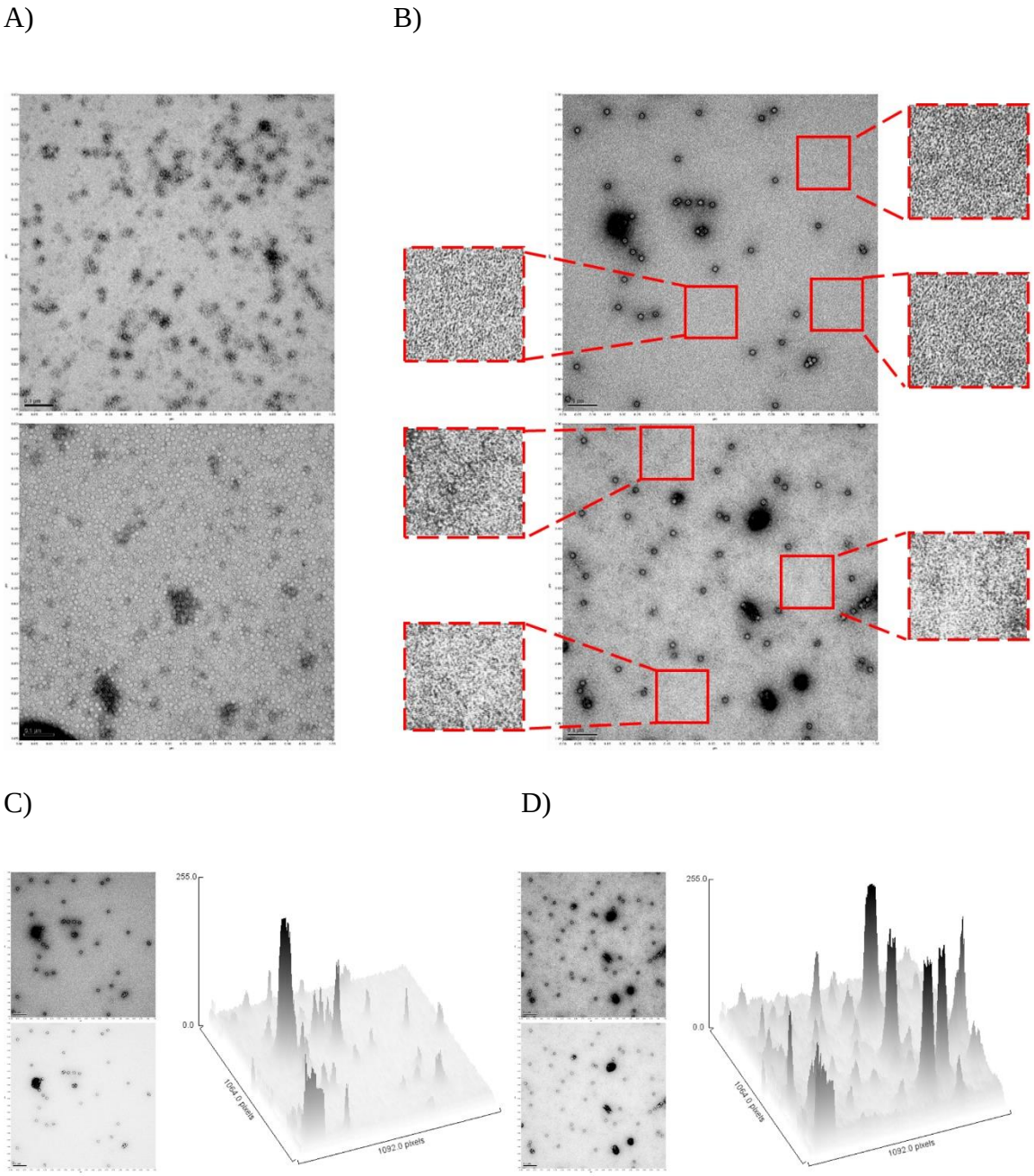


Figure 5.8 Comparison between results with and without channels collapsed. A) Higher magnification micrographs of grids from central reservoir 1 with channels collapsed (top) and without channels collapsed (bottom). B) Micrographs from central reservoir 2 with (top) and without (bottom) channels collapsed. Insets: higher magnification with enhanced contrast. C) Surface plot of micrograph from central reservoir 2 with channels collapsed. D) Surface plot of micrograph from central reservoir 2 without collapsing channels.

The preliminary example discussed above showed successful selective concentration of a mixture of two proteins. With other targets or buffer conditions, more qualitative selective concentration results can be accomplished. In addition, in most TEM applications, the specific sample of interest needs to be carefully purified so that only one single band appeared on PAGE, indicating no contaminants or other traces existed. Based on the general procedure of structural determination, acquisition of high-quality micrographs is followed by particle selection and 2D classification of selected particles. Theoretically, it is possible to conduct structural determination with a mixture of samples as long as the sample of interest can be easily recognized by some algorithms and can generate enough images of high quality. The selective concentration feature of electrophoretic exclusion can be integrated into TEM sample pretreatment to simplify the purification step and facilitate the detection capability.

### 5.4 Concluding remarks

Embedding grids into microdevice and using electrophoretic exclusion as a preconcentration step before applying samples on the grids broadens the capability of the TEM technique. Results of one model protein from both fluorescence microscopy and TEM demonstrate this work is promising. With the grids embedded into the device, a new strategy was established, a lower detection limit was achieved, and selective concentration was demonstrated. It is believed that with a refined next-generation, electrophoretic exclusion will be able to manipulate with more diluted samples or more complicated mixtures for structural determination and facilitate future clinical applications. In addition, designs for cryo-EM applications are also under investigation. Cryo-EM is experiencing an explosion in popularity and can achieve resolution down to a

few Å, which allows the proper placement of amino acid side-chains and develops atomic models of these biomolecules. This technique combined with electrophoretic exclusion is expected to achieve higher resolution for structural determination.

**5.5 References**


[1] Arnold, S. A., Muller, S. A., Schmidli, C., Syntychaki, A., Rima, L., Chami, M., Stahlberg, H., Goldie, K. N., Braun, T., *Proteomics* 2018, *18*, e1700176.

[2] Quentin, D., Raunser, S., *J Mol Med (Berl)* 2018, *96*, 483-493.

[3] Krishnan, V. V., Rupp, B., 2012.

[4] Murata, K., Wolf, M., *Biochim Biophys Acta Gen Subj* 2018, *1862*, 324-334.

[5] Thompson, R. F., Walker, M., Siebert, C. A., Muench, S. P., Ranson, N. A., *Methods* 2016, *100*, 3-15.

[6] Dubochet, J., Adrian, M., Chang, J. J., Homo, J. C., Lepault, J., McDowall, A. W., Schultz, P., *Q Rev Biophys* 1988, *21*, 129-228.

[7] Barber, R. C., *The Journal of the American Osteopathic Association* 2010, *110*, S10-15.

[8] Querfurth, H. W., Laferla, F. M., *N Engl J Med* 2010, *362*, 329-344.

[9] Hajipour, M. J., Santoso, M. R., Rezaee, F., Aghaverdi, H., Mahmoudi, M., Perry, G., *Trends Biotechnol* 2017, *35*, 937-953.

[10] Georganopoulou, D. G., Chang, L., Nam, J. M., Thaxton, C. S., Mufson, E. J., Klein, W. L., Mirkin, C. A., *Proc Natl Acad Sci U S A* 2005, *102*, 2273-2276.

[11] Schagger, H., Cramer, W. A., Vonjagow, G., *Analytical biochemistry* 1994, *217*, 220-230.

[12] Polson, N. A., Savin, D. P., Hayes, M. A., *Journal of Microcolumn Separations* 2000, *12*, 98-106.

[13] Pacheco, J. R., Chen, K. P., Hayes, M. A., *Electrophoresis* 2007, *28*, 1027-1035.

[14] Meighan, M. M., Staton, S. J., Hayes, M. A., *Electrophoresis* 2009, *30*, 852-865.

[15] Meighan, M. M., Keebaugh, M. W., Quihuis, A. M., Kenyon, S. M., Hayes, M. A., *Electrophoresis* 2009, *30*, 3786-3792.

[16] Kenyon, S. M., Meighan, M. M., Hayes, M. A., *Electrophoresis* 2011, *32*, 482-493.

[17] Meighan, M. M., Vasquez, J., Dziubcynski, L., Hews, S., Hayes, M. A., *Analytical chemistry* 2011, *83*, 368-373.

[18] Kenyon, S. M., Weiss, N. G., Hayes, M. A., *Electrophoresis* 2012, *33*, 1227-1235.

[19] Keebaugh, M. W., Mahanti, P., Hayes, M. A., *Electrophoresis* 2012, *33*, 1924-1930.

[20] Kenyon, S. M., Keebaugh, M. W., Hayes, M. A., *Electrophoresis* 2014, *35*, 2551-2559.

[21] Keebaugh, M. W., Hayes, M. A., *Electrophoresis* 2016.

[22] Zhu, F., Hayes, M. A., *Electrophoresis* 2019, *40*, 304-314.

[23] Tabeling, P., *Introduction to microfluidics*, Oxford University Press on Demand 2005.

[24] Giss, D., Kemmerling, S., Dandey, V., Stahlberg, H., Braun, T., *Analytical chemistry* 2014, *86*, 4680-4687.

[25] Mukhitov, N., Spear, J. M., Stagg, S. M., Roper, M. G., *Analytical chemistry* 2016, *88*, 629-634.

[26] Arnold, S. A., Albiez, S., Bieri, A., Syntychaki, A., Adaixo, R., McLeod, R. A., Goldie, K. N., Stahlberg, H., Braun, T., *J Struct Biol* 2017, *197*, 220-226.

[27] Feng, X., Fu, Z., Kaledhonkar, S., Jia, Y., Shah, B., Jin, A., Liu, Z., Sun, M., Chen, B., Grassucci, R. A., Ren, Y., Jiang, H., Frank, J., Lin, Q., *Structure* 2017, *25*, 663-670 e663.

[28] Ashtiani, D., Venugopal, H., Belousoff, M., Spicer, B., Mak, J., Neild, A., de Marco, A., *J Struct Biol* 2018, *203*, 94-101.

[29] Russo, C. J., Passmore, L. A., *Science* 2014, *346*, 1377-1380.

[30] Arnold, S. A., Albiez, S., Opara, N., Chami, M., Schmidli, C., Bieri, A., Padeste, C., Stahlberg, H., Braun, T., *ACS Nano* 2016, *10*, 4981-4988.

# CHAPTER 6

# PROTEIN BIOMARKER SEPARATION VIA ELECTROPHORETIC EXCLUSION AND PRELIMINARY QUANTIFICATION ON MICROFLUIDIC DEVICES

## 6.1 Introduction

A spectrum of diseases begins with biomarkers at clinically undetectable levels, stochastically increasing concentration until symptoms eventually appear. When a disease is fully developed, it is sometimes too late to treat and potentially cure. The earlier that the disease is diagnosed, the more diverse therapies can be applied in curing, treating and even reversing the progress of the disease, thus larger possibility for survival. Early detection of diseases has therefore assumed an essential role in modern medical therapy. Surveillance and monitoring of the progression and/or the management of the disease, and individually assessing the response to treatment are becoming the hallmarks of personalized medicine [1].

Biomarkers are cellular, biochemical or molecular alterations that are measurable in biological media, such as cells, body fluids [2]. They have proven their scientific and clinical value and are commonly used in the practice of medicine. This value and use notwithstanding, detection of biomarkers still facing challenges and can be improved. For instance, an ideal sample source is serum for noninvasive disease diagnosis for early stage screening. Serum proteomics is often used for the identification of disease biomarkers. Serum contains species ranging from proteins, electrolytes, waste products, dissolved gases and water. Additionally, some tissue leakage proteins and various immunoglobulins are present in abundance. This is very challenging due to the presence of wide dynamic range of proteins over 10 orders of magnitude and probability of the low

abundance proteins being important biomarkers [3]. Moreover, many diseases biomarkers may have high sensitivity for the clinical stage, when it comes to early detection, few of them will still maintain high sensitivity for preclinical, which adds a layer of complexity for early detection [4].

Successful early detection of these low-abundance disease biomarkers will depend upon the development of sophisticated methods for separation prior to robust detection techniques with high sensitivity, and specificity [5].

Microbead-based arrays are an emerging technology used for early diagnosis, and in simultaneous detection, quantification and profiling of a range of targets of interest relevant to a particular disease. Dated back to 1920s, this technique began using particulate materials. Over the hundred years of continuous development, this technique is now used in a variety of applications, especially for biomarker analysis, such as proteins, genes, and DNA profiles. Results from some applications are quite promising as the detected biomarkers are able to characterize specific disease states for diagnosis or predication [6, 7].

A magnetic beads based micro-immunoassay platform with extremely sensitive quantitative property has been proposed [8]. The general principle can be summarized in Figure 6.1. The procedure is similar to other immunoassay methods as the magnetic beads, sample, detection antibody with fluorescent tag are mixed together, then the mixture droplet is placed on a slide for magnetic rotor manipulation, after that fluorescence microscopy is used to record results. The main feature of this detection method is to incorporate a periodic fluctuation into the observed fluorescence by rotating

the magnetic field, which aids in the identification and quantification of the specific signal. This reduces the impact of background fluorescence and enables increased sensitivity. This work has demonstrated that the system was able to manipulate small sample volume (10 μL) in an applied magnetic field, and the signal was captured as periodic change in observed fluorescence. After data processing, this strategy successfully achieved lower detection limit compared to commercial methodologies. Moreover, this format can be easily adaptable to the detection of many targets and incorporated as a detection method into a microdevice for the parallel detection and quantification of biomarker panels.

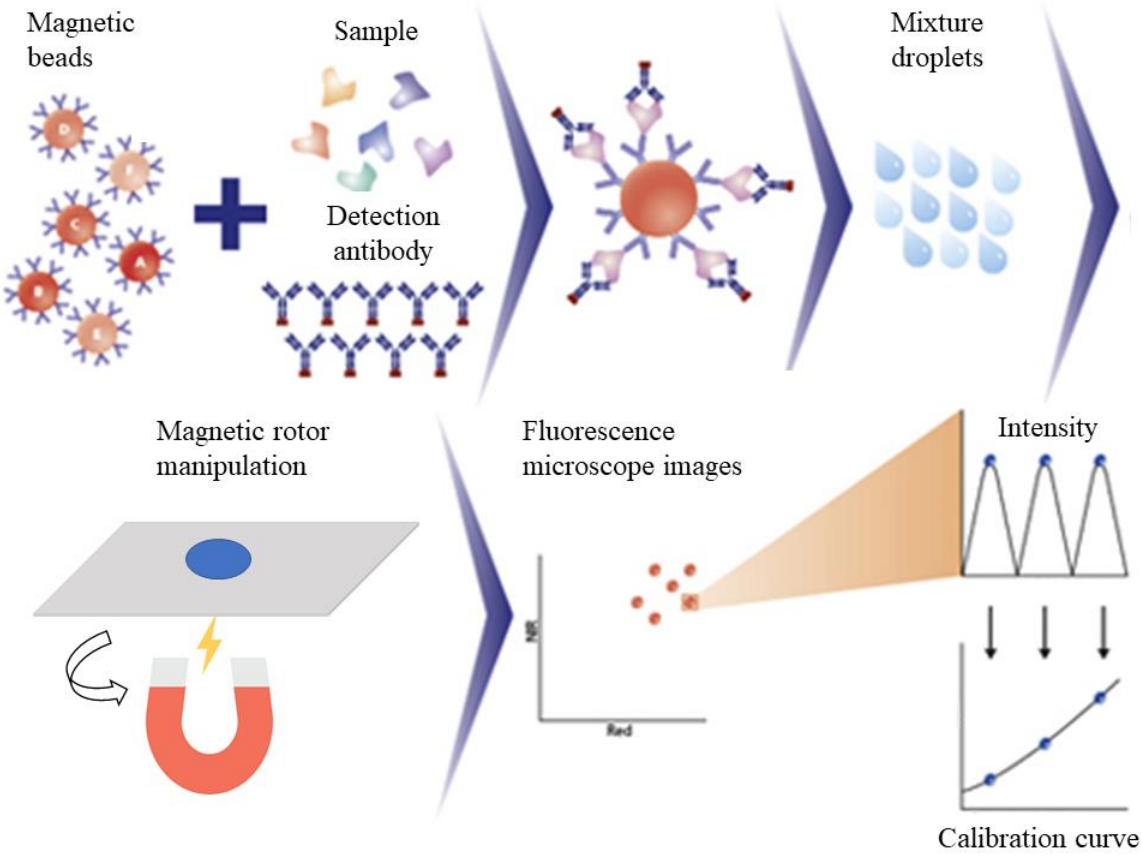


Figure 6.1 A schematic for general procedure of microbead immunoassay.

To further broaden the capability of this detection method, electrophoretic exclusion is used to allow for parallel separation and preconcentration of biomarker samples. Electrophoretic exclusion is a counterflow gradient focusing technique which exploits hydrodynamic flow and opposed electrophoretic velocity to exclude, enrich and separate analytes with different mobilities. Previous work has demonstrated that this technique was able to manipulate particles, dye molecules and various proteins [9-15]. Theoretical work indicated that this technique could achieve higher resolution comparable to conventional electrophoresis [16].

Myoglobin (Mb) and cardiac troponins (cTnI) are used in the present work as model study. They are both acute myocardial infarction (AMI) biomarkers recognized by the American College of Cardiology (ACC) and the American Heart Association (AHA) [17]. Mb is a relatively small protein (only 17.8 kDa), abundant in both cardiac and striated muscle, and currently used as a routine biomarker for AMI [18]. This is one of the earliest biomarkers to appear during the development of the disease [19]. No single marker currently has shown adequate diagnostic accuracy for AMI, but a combination of Mb and cTnI may achieve a high sensitivity and specificity as part of a biomarker panel [20-22]. The troponin protein complex consists of 3 subunits, and the I subunit (TnI) maintains the structural position of the troponin-tropomyosin complex. It is one of the most tissue-specific biomarkers related to cardiac damage and has been included as a diagnostic criterion for several cardiac-related pathologies [23].

In present work, the array-based electrophoretic exclusion microdevice was used for sample separation and preconcentration. Experiments using a single target were conducted to assess the ability of the device to enrich an individual species in central

reservoirs. Simulations for protein exclusion phenomenon were also investigated. Experiments were also performed using a mixture of Mb and cTnI to evaluate the proficiency of the device in performing separations along the primary separation channel. The possibility for achieving a point-of-care device has been investigated with a regular 9 V battery without bulky high voltage power supply applied. Furthermore, an intermediate design has been developed and tested, and the capacity of this device and the limitations were also assessed. Additionally, a new design has been proposed and is expected to achieve better performance.

## 6.2 Experimental

### 6.2.1 Reagents

Aspartic acid and hydrochloric acid were obtained from VWR (Radnor, PA). Sodium chloride, potassium chloride, disodium hydrogen phosphate, potassium dihydrogen phosphate, acetone and isopropanol were purchased from Sigma-Aldrich (St. Louis, MO). 10X phosphate buffer saline (PBS) was prepared by dissolving 80.0 g NaCl, 2.0 g KCl, 14.4 g $Na_2HPO_4$ and 2.4 g $KH_2PO_4$ in 1 liter of DI water. Myoglobin (Mb) and cardiac troponin I (cTnI) were purchased from Life Diagnostics (West Chester, PA). NHS-rhodamine and NHS-fluorescein were obtained from Thermo Scientific (Waltham, MA). For all solutions, ultrapure deionized water was used (Barnstead International, Inc., Dubuque, IA).

### 6.2.2 Labeling step

NHS-fluorescein and NHS-rhodamine were dissolved in DMSO to concentrations of 10 mg/mL. Protein samples were thawed and equally divided into ten centrifuge tubes

upon receiving, then kept frozen. One centrifuge tube (about 0.1 mg, 10 μL) was used for each preparation. For Mb, the content in the centrifuge tube was thawed first, and 3.0 μL of NHS-rhodamine was added into the tube directly according to the instruction (Thermo Scientific, Waltham, MA). The sample was incubated in the dark at room temperature for one hour to allow full reaction of the reagents. For cTnI, the content in the tube was transferred to a dialysis tube unit (Thermo Scientific, Waltham, MA) and placed in 1000 ml 1X PBS buffer overnight. The content in the dialysis tube was then transferred into a centrifuge tube, and 1.5 μL NHS-fluorescein was added into the tube according to the manual instruction and reacted in the same manner. After reaction, the crude reaction mixtures were added to dialysis tube units with a molecular weight cut-off of 3,500 Daltons. Samples were dialyzed against 100 mM PBS, pH 7.2 overnight. After dialysis, the final concentration of each sample was 0.33 mg/mL Mb and 0.2 mg/mL cTnI, respectively.

### 6.2.3 Microdevice fabrication

The microdevice was fabricated with the same procedure described in the previous chapters.

### 6.2.4 Microdevice operation

The protein sample was mixed with 5 mM aspartic acid buffer solution to a concentration of 0.05 mg/mL. The microdevice was filled with protein solution using the entrance ports and the device was then placed on the microscope stage, connected to the voltage divider and high voltage configuration applied. The voltage for each channel was confirmed through a digital multimeter (DM-4400A Sperry, Menomonee Falls, WI, USA). After 5 minutes, voltage was released.

### 6.2.5 Mobility measurement

The capillary electrophoresis instrument was from LabAlliance, model 500 (serial# 093/27228, model# 0200-9060) with a home-built software (package-PCI6023E.exe). The detection lamp was set to 250 nm for protein molecules and 207 nm for dye molecules. Total length of capillary was 47.0 cm, while the distance to detection was 35.0 cm, with 360 μm outer diameter, and 75 μm inner diameter. Two reservoirs were filled with 5 mM aspartic acid buffers and labeled as “cathode vial” and “anode vial”.

Upon use, the lamp was turned on at least 15 minutes ahead of time. The capillary was rinsed with NaOH first and then 5 mM aspartic acid buffer for 20 minutes each with around ~20 Pa pressure applied. A sample was injected with siphoning action by elevating the injection tube relative to the exit reservoir for 10 seconds. Afterwards, a high voltage power supply was set to 5 kV and turned on. 207 nm and 250 nm detection wavelengths were chosen for the dye molecule sample as a control to demonstrate signal only shows up with 207 nm, not 250 nm. Then two detection wavelengths were selected for the protein sample, which both 207 and 250 nm showed similar migration times. The software generated both spectroscopic signal and current signal (for reference). The high voltage power supply was turned off when a peak was detected or when necessary.

### 6.2.5 Data analysis/image processing

Data collection used an inverted microscope with fluorescence capabilities (IX70, Olympus) using a 100 W high-pressure Hg lamp as the light source. Light was passed through a band-pass filter and 5X microscope objective to the array. Light emitted from the sample was collected through a long-pass dichroic mirror and band-pass filter to a CCD

camera capable of image-capture (QICAM, Q imaging, Inc.). Color images focusing on central reservoir area were taken with an SLR camera (Nikon, Tokyo, Japan) from time 0 to about 15 seconds as RGB files. ImageJ (NIH, Bethesda, MD) was used for image analysis. For each file, red (R), green (G), blue (B) channels were split and the fluorescence intensity of each channel was compared in the central reservoir area to monitor protein exclusion. TSC SP5 confocal microscopy (Leica Camera AG, Wetzlar, Germany) was used for the portable device section. Argon 488 laser line was used to excite labeled cTnI (green), and 561 laser line was used for labeled Mb (red).

### 6.2.6 Theoretical modeling

The simulations were conducted based on the structure built (electrode aligned with channel entrance) in Chapter 4. Some of the parameters were adjusted to reflect the protein exclusion conditions, including the mobility $10^{-4}$ $cm^2/Vs$, electric field 10 V/cm, and concentration $10^{-6}$ mol/L. Diffusion coefficient was varied from $10^{-9}$ to $10^{-6}$ $cm^2/s$.

## 6.3 Results and Discussion

### 6.3.1 Exclusion of individual protein

The behavior of Mb under varying electric fields was investigated by filling the array device with aspartic acid buffer (pH 2.95) with NHS-rhodamine labeled Mb showing red fluorescence (Figure 6.2 A). As discussed in Chapter 3, when exclusion occurs the channel area is dark; when the voltage is released the sample flows back through the channel. In this work, results on central reservoir area presented more straightforward exclusion phenomena. Labeled Mb was concentrated within a reservoir immediately upstream of that channel as the noticeable arc of increased concentration

grew (Figure 6.2 A, left). This was confirmed with the intensity measurement within the central reservoir area (Figure 6.2 A, bottom left), as a higher electric field applied, the intensity of red channel increased (green and blue channel did not have significant intensity change, acting as background control). It also underwent a slight decrease when the electric field applied for a longer time, which indicated the lateral diffusion of the concentrated bolus. With a lower electric field, when the electrophoretic velocity was smaller than the hydrodynamic flow, there was no significant change with the channel area remained red (Figure 6.2 A, right). Similarly, the temporal intensity change of the central reservoir was investigated and the intensity of red channel also increased. This was mainly because the applied electric field, though was not sufficient enough to cause exclusion, still hindered the outflow that left the central reservoir. With the inflow (the flow entered the central reservoir) still kept consistent, the amount of the samples in the central reservoir during that time-frame increased, leading to a higher concentration and/or intensity.

From the results, it can also be concluded that the threshold electric field for exclusion of Mb in this device was between 50 V/cm and 100 V/cm. Given the average linear flow rate 0.02 cm/s (estimated from experiment and simulation in Chapter 4), the calculated mobility from experiment was 2.00-4.00x$10^{-4}$ $cm^2$/Vs. The mobility measured from benchtop CE was 2.00x$10^{-4}$ $cm^2$/Vs (Figure 6.2 C, right), which was consistent with the experimental results, also suggested that the calculated electric field for exclusion was around 100 V/cm. Compared to the literature value of Mb mobility, this number is about one order of magnitude larger. The existing literature values are all based on pH 7, however in this case, a more acidic pH environment is applied. With a lower pH, the

mobility tends to increase based on the experimental values from Davis and Cohn's work [24]. Moreover, with a lower pH, most of the proteins process net charges as the pH is away from their pIs, thus the greater the net charge and therefore the greater the mobility.

The behavior of cTnI under varying electric fields was also investigated. cTnI was labeled with NHS-fluorescein, showing green color with fluorescence microscopy. cTnI needs an even higher electric field to achieve exclusion since its mobility is even smaller (Figure 6.2 C, right) according to discussion in Chapter 3. Based on the current conditions (50 V/cm and 100 V/cm), it might be difficult to capture cTnI, as none of the experimental electric field strengths were sufficiently large to exclude cTnI with the averaged linear flow rate 0.02 cm/s. No significant exclusion phenomena took place in central reservoirs as the channel area did not change color (for Figure 6.2 B, left, the channel area was dark all the time, mainly due to the artifact when preparing the microchip). Moreover, the results from central reservoir intensity of green channel measurement matched with the visual results as the intensity in the region of interest enhanced (red and blue channel did not have significant intensity change, acting as background control). The grey area on the right side could be interpreted as breaking through of some impurities (Figure 6.2 B, left). This process was consistent with the electropherogram of cTnI showing several extra peaks after the main peak (Figure 6.2 C, right).

A)

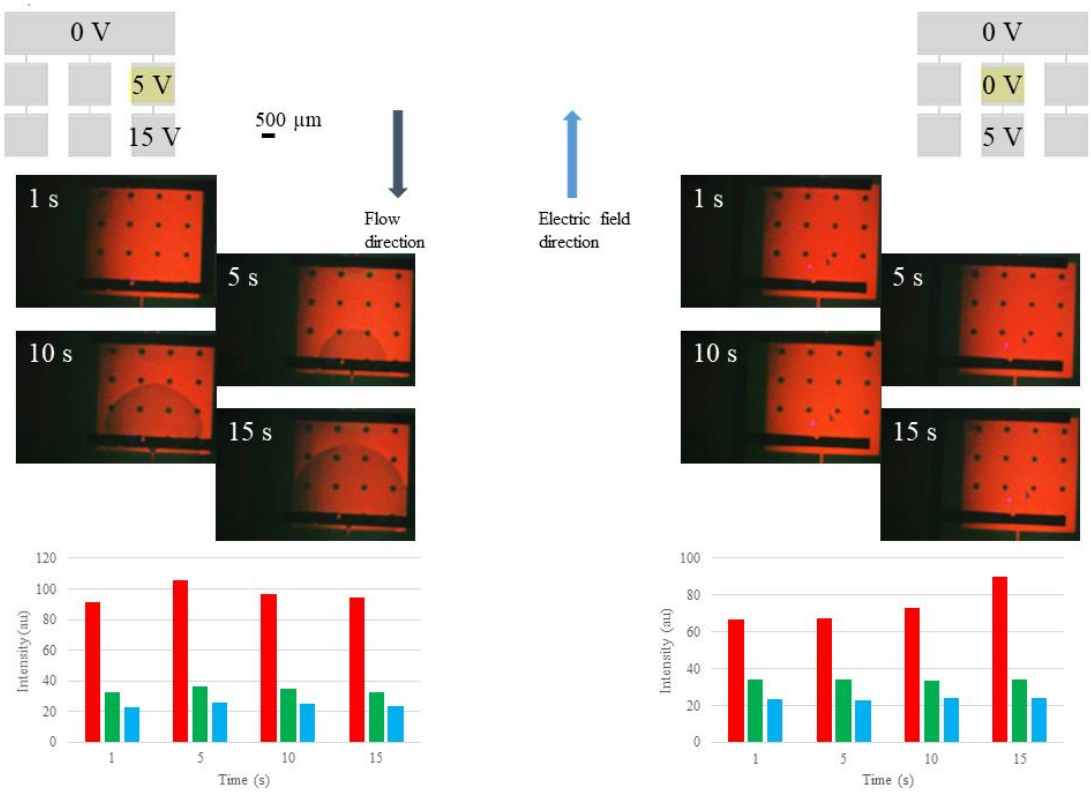


(see figure legend on Page 136)

B)

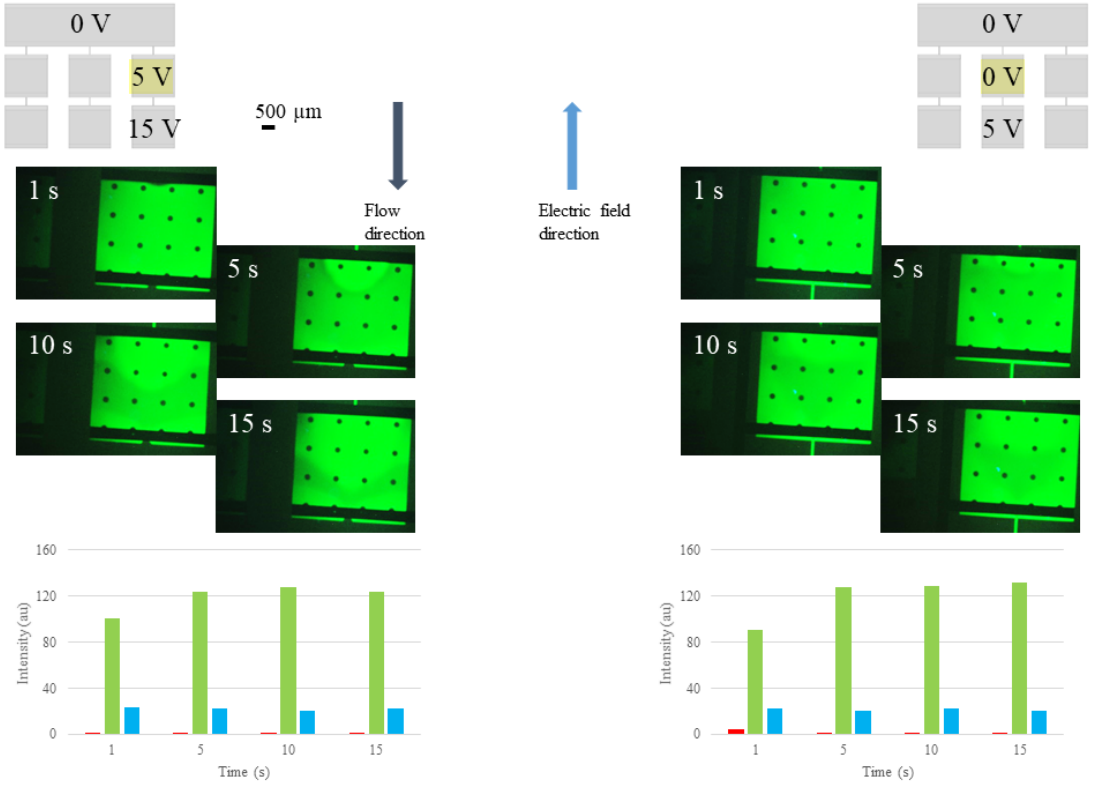


(see figure legend on Page 136)

C)

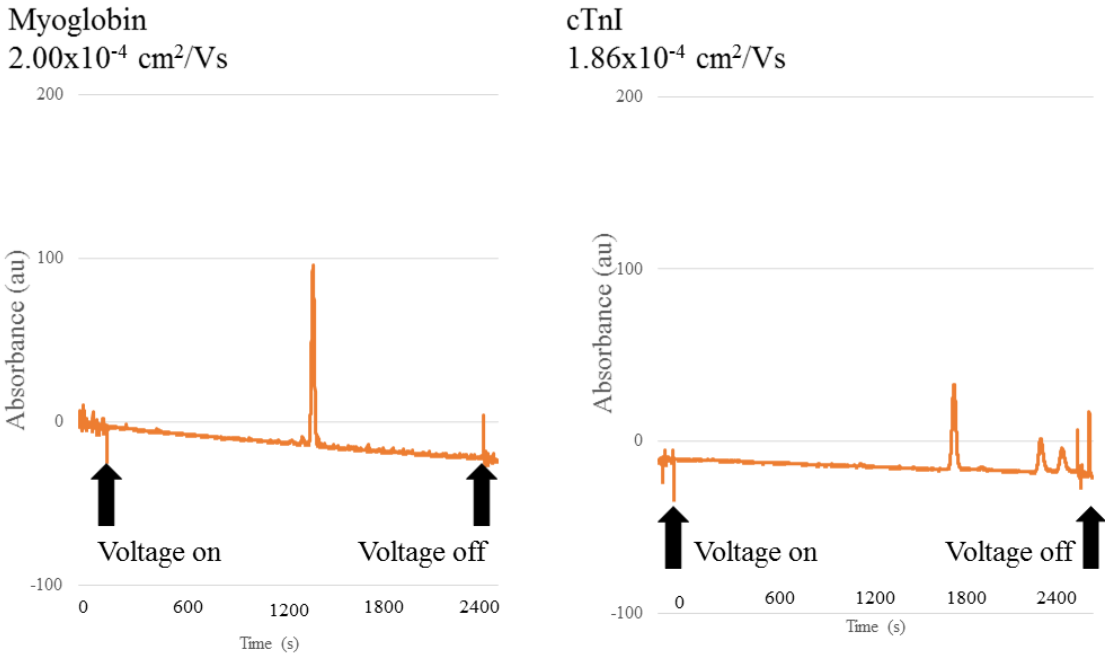


Figure 6.2 Individual protein test and mobility measurement. A) Behaviors of myoglobin were presented as well as intensity measurement in the central reservoir. With a higher electric field (100 V/cm), myoglobin was excluded into the upstream reservoir and a clear semi-circle was formed (left); while with a lower electric field (50 V/cm), no obvious exclusion phenomenon was observed (right). B) Behaviors of cTnI were presented as well as intensity measurement in the central reservoir. With a higher electric field (100 V/cm), no clear exclusion was taken place for cTnI (left); while with an even lower electric field, no significant observation was captured (right). C) Mobility was measurement with a commercial CE instrument and the mobility of Myoglobin was higher than that of cTnI, consistent with their molecular weights.

### 6.3.2 Simulations varying diffusion coefficient

From the figures presented, when exclusion took place, the intensity of the central reservoir varied and was heterogeneous. A growing concentrated arc was formed in the central reservoir (Figure 6.2 A, left). It was mainly due to the competing interaction between diffusion and electrophoretic velocity.

Simulations with different diffusion coefficients on the 3D model developed in Chapter 4 were presented below (Figure 6.3). When the diffusion coefficient was relatively low, there was almost no concentrated arc forming in the upstream reservoir. With the diffusion coefficient increased, a more significant concentrated arc was established. For a typical protein with size of 20 kDa, this diffusion coefficient is around $10^{-7}$ $cm^2/s$ [25], giving rise to a consistent results comparing experimental results with simulations.

However, the simulated results in the channel area did not fully match the experimental evidence. That was mainly due to the complex structure of protein. Protein was considered as a point charge in the simulation, however, the non-uniform surface charge density of protein particle in the actual experiment contributed to the inconsistence [26].

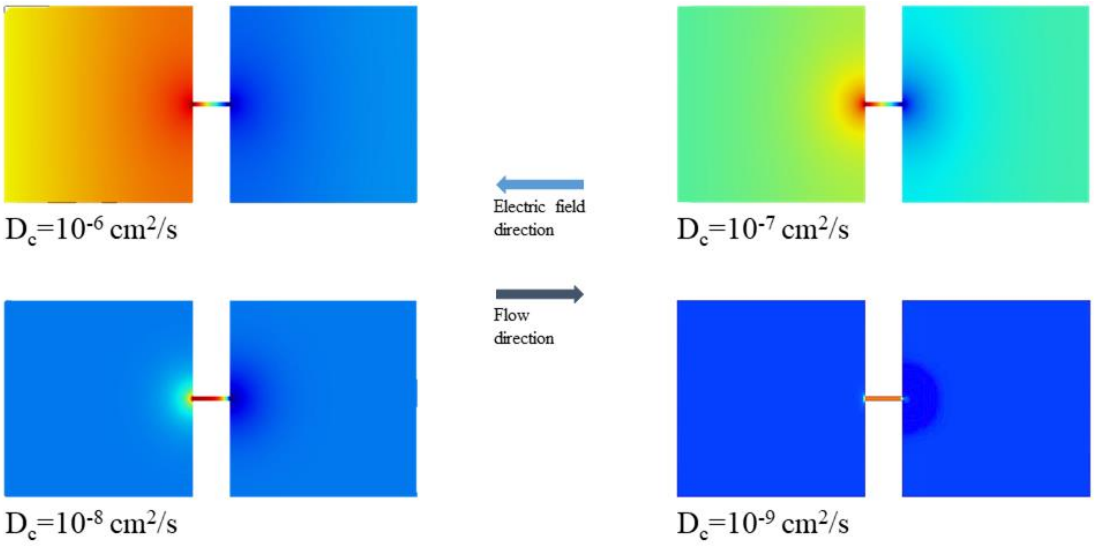


Figure 6.3 Simulations with different diffusion coefficients. With a higher diffusion coefficient, the concentrated arc in the upstream reservoir got larger.

### 6.3.3 Differentiation of a mixture of two proteins

Experiments were performed to demonstrate the capability of electrophoretic exclusion to separate labeled proteins Mb (red) from cTnI (green) within the array. A mixture of two proteins was loaded into the device, and central reservoirs were monitored simultaneously (Figure 6.4). The separation can be clearly visualized as Mb was excluded in the central reservoir starting off from the exit channel area and cTnI was not. With a higher electric field, the exclusion of Mb with a red arc originated from the exit channel as well as the penetration of cTnI with a green arc from the upstream entrance channel could still be observed, which were consistent with individual protein test (Figure 6.4 left); with a lower electric field, there was no significant response (results not shown).

The phenomena of Mb exclusion with cTnI penetration can be interpreted as schematics below (Figure 6.4, right). The structure with a larger square and a smaller rectangle represents reservoir and upstream channel, respectively. Based on the information from CE measurement, the mobility of cTnI is smaller than that of Mb. When the electric field is lower than threshold exclusion electric field of Mb, both Mb and cTnI can still enter the reservoir with different rates, so two semi-circular bands can be observed (Figure 6.4, top right). When the applied electric field is between the threshold electric field of Mb and cTnI, this is the desired situation, where Mb can be excluded while cTnI can still enter the reservoir (Figure 6.4, bottom right).

Proteins behave in predictable manners evidenced by the results discussed above. With consistent behaviors from both proteins, it is possible to forgo the labeling process and manipulate with more dilute solutions to push the limit of separation and enrichment.

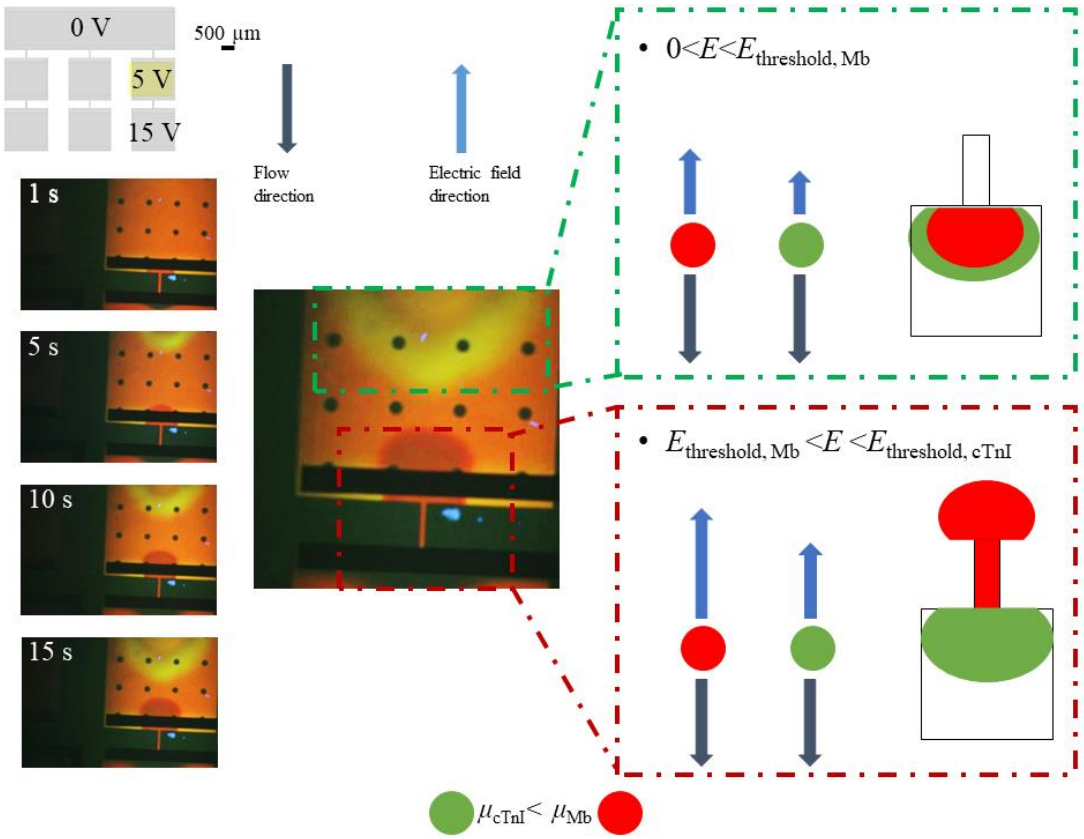


Figure 6.4 Results from a protein mixture and a possible explanation. A mixture of two proteins was loaded into device and the same voltage configuration was applied. Mb exclusion was observed as indicated by the red bolus from channel and grew into the reservoir. cTnl was not excluded at this condition. Moreover, some cTnI penetrated the reservoir through the upstream channel. Possible explanation for the phenomena of Mb exclusion with cTnI penetration was interpreted on the left.

### 6.3.4 Possibility to achieve a portable device

A portable setup was created and tested to show that these systems can be powered by a regular 9 V battery as a step towards future point-of-care diagnosis. Based on the information retrieved from section 6.3.1, the threshold electric field for Mb exclusion was between 50 V/cm to 100 V/cm, while the threshold electric field for cTnI exclusion was beyond 100 V/cm. With a 9 V battery, an electric field of 90 V/cm was generated, which was expected to exclude Mb but not cTnI.

The device uses a 9 V battery connected to a subunit through copper wires (Figure 6.5 A). The imaging area was the channel region between central reservoir 2 and exit reservoir 2 (red area highlighted). Confocal microscopy was used to record results under this condition (Figure 6.5 B). The results were consistent with Mb being excluded when the electric field applied leading to the red color gradually disappeared. The green color remaining in the imaging area is evidence supporting cTnI was not excluded. Further supporting evidence is found in the overlay images, as the color of the channel area was orange at the beginning and turned to green when the electric field was applied, indicating red species (Mb) was removed. Results from confocal microscopy can be used to further confirm the behavior of two proteins as they showed consistent results under fluorescence microscopy.

A)

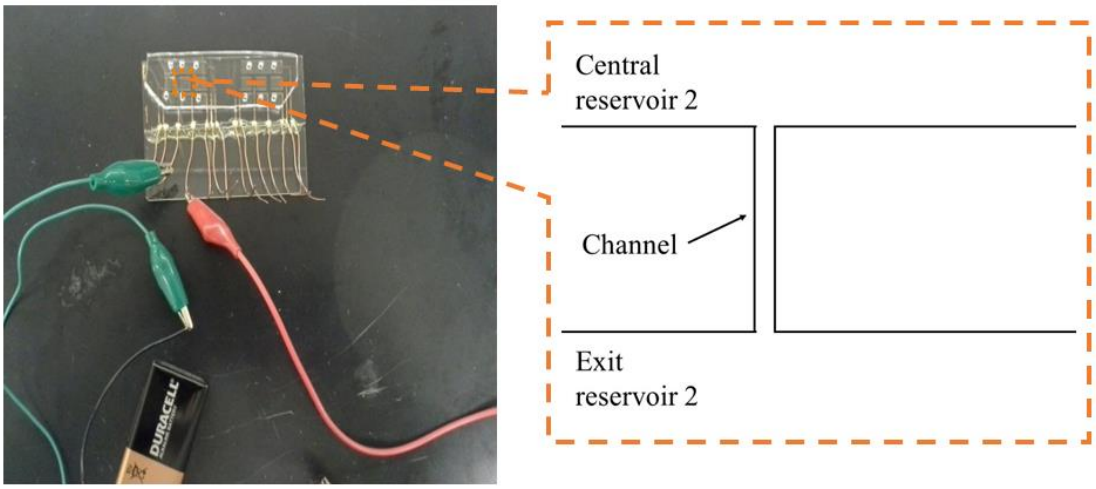


B)

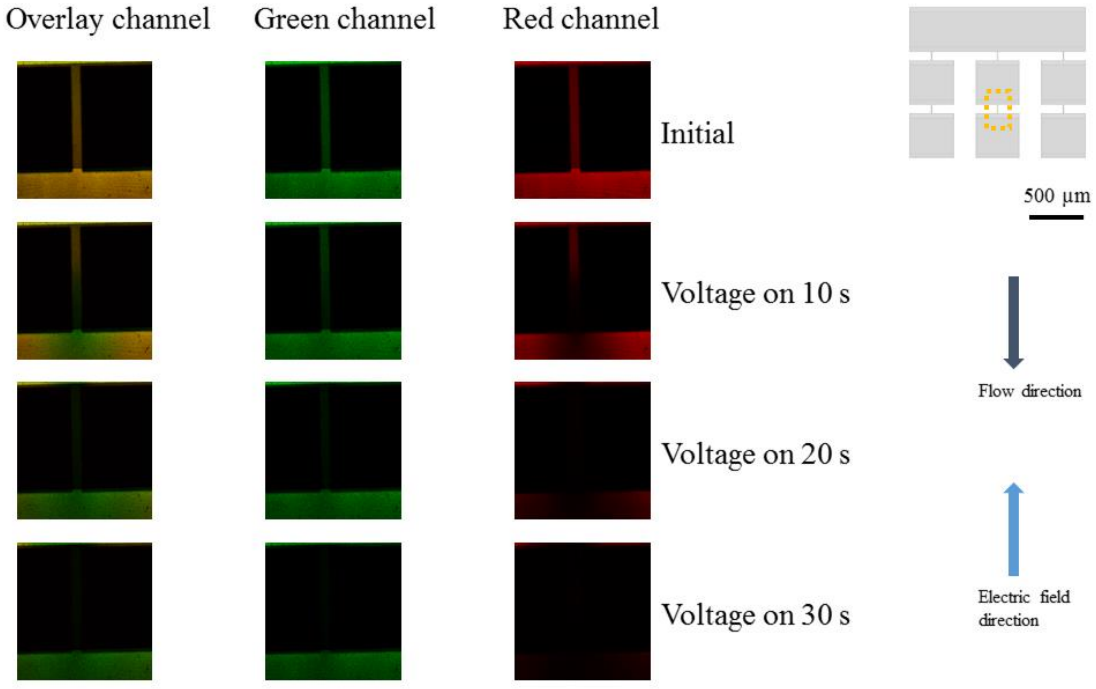


Figure 6.5 Device connection and results from confocal microscopy. A) A regular 9 V battery was connected to the device through copper wires to power the device. The imaging area was the channel between central reservoir 2 and exit reservoir 2 (red area highlighted in picture). B) Results were monitored with confocal microscopy. Green laser was used to excite and monitor cTnI, while red laser was used to excite Myoglobin. The

images on the left side are the overlay of two sets of data. When electric field was applied, Mb was excluded and cTnI did not show a significant difference.

### 6.3.5 Examination of an intermediate design for sensitive immunoassay

An intermediate device (Figure 6.6) for sample separation, concentration and quantification was proposed by Dr. Woolley, fabricated by the author, and tested together [27]. With this device, three AMI protein biomarkers were expected to achieve separation and quantification as a multiplex platform for potentially better diagnosis of AMI.

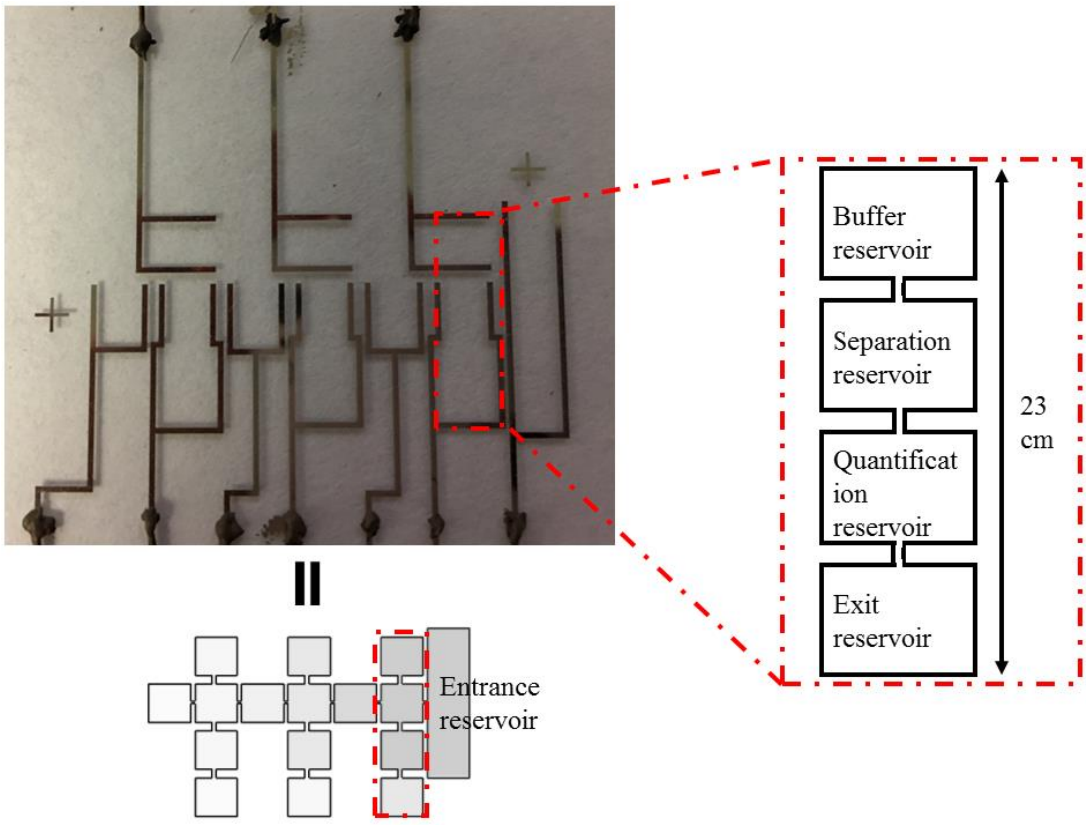


Figure 6.6 Microdevice for protein separation and quantitation by immunoassay. Photograph (top left) of the complete microfluidic device with one separation channel and three isolation channels, and a schematic of a single (right) isolation channel explaining terminology used in the device.

With this integrated device, a mixture of Mb and cTnI was used to evaluate the proficiency of the device towards performing separations along the primary separation

channel. The experimental results exhibited a similar trend as the Mb was excluded while the cTnI was not. These results demonstrated the ability of the device to isolate and concentrate analyte in one of the separation channel reservoirs prior to quantification.

Data consistent with the concentration of cTnI was observed in separation reservoir, as evidenced by the increase in fluorescence intensity. The concentrated samples were observed to enter the quantitation reservoir by removing the electric potential and adding buffer to the buffer reservoir. However, the flow into the reservoir was slow, and incomplete over the time course of the experiment. The magnetic chains in the quantitation reservoir could be observed with a higher magnification. However, not all material was effectively binding as there was still a high background fluorescence intensity. This was probably due to the protein denaturation or the interference from fluorescent dyes.

### 6.3.6 Proposing new designs for future applications

The current and the intermediate devices were able to achieve separation and preliminary quantification of proteins. However, the concentrations of protein biomarkers currently used in experiments were still magnitude higher than those used in actual clinical applications [18]. As discussed in section 6.3.2, with consistent behaviors from protein tests, it was possible to eliminate the labeling process and move forward to a lower concentration. Moreover, to further optimize the performance of this integrated system, valves are desired for better manipulation and control. Incorporation of physical valves can improve the overall performance within a microfluidic device [28]. Valves, especially with PDMS valves can be designed with soft lithography techniques [28-31],

and are easy to fabricate, maintain a low device fabrication cost, and may easily be scaled to fit the dimensions of system.

A design combined with electrophoretic exclusion (EE), insulated dielectrophoresis (iDEP) and immunoassay detection on an integrated platform is proposed below (Figure 6.7).

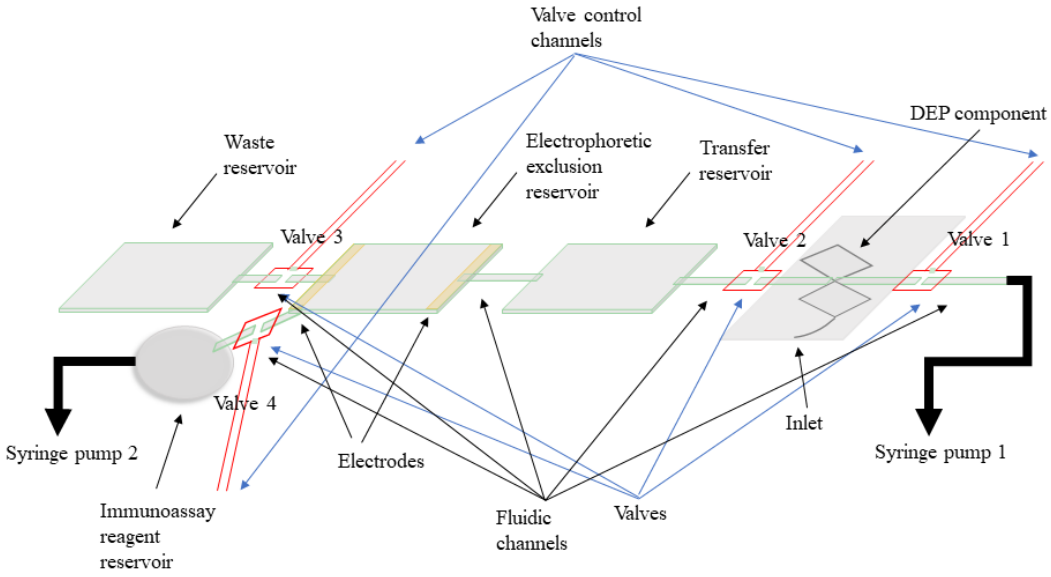


Figure 6.7 A proposed new design incorporating DEP component, EE component and immunoassay detection technique as an integrated platform for future clinical applications.

The general procedure is described below. Fluorescently labeled sample is first introduced from inlet of the DEP component, meanwhile all the valves are closed, and both the syringe pumps are not in use. Analytes in the sample are accumulated at different gates in the DEP component upon a proper electric field applied. After that, syringe pump 1 with working buffer starts to work at a reasonable flow rate. Valve 1, 2, and 3 are open thereafter, and each analyte is transferred to corresponding transfer reservoir. Meanwhile, electric fields are applied to the electrodes in the EE reservoir,

enriching target analytes in the EE reservoir, and flushing unwanted or interfering species to the waste reservoir. Then syringe pump 1 is closed, so are valve 1,2 and 3. Syringe pump 2 (with a higher flow rate) is turned on and valve 4 is open, bringing excess immunoassay reagents/magnetic beads from the immunoassay reservoir into the EE reservoir. Then close syringe pumps 2 and valve 4. Incubate for 1 hour. After incubation, open syringe pump 1 and valve 1, 2, and 3 again, flushing excess reagents into the waste reservoir. Meanwhile, holding a magnet underneath each EE reservoir to avoid magnetic beads-target analytes complex being flushed away. Finally, close all the valves and syringe pumps, detecting signal with microscopy.

In addition, it is advisable to incorporate a gas-removing setup (membrane or pump) to minimize the bubble formation. The interface between the syringe pump and the microdevice needs to be refined. Furthermore, ITO can be used as materials for transparent electrodes to ensure clearer capture of exclusion phenomenon and better understanding of this technique.

### 6.4 Concluding remarks

Electrophoretic exclusion is advanced, where protein biomarker enrichment and separation has been performed. Evidence from the central reservoirs show that electrophoretic exclusion of proteins on a microfluidic device behaves in a predictable manner. Due to the low flow rate in the system, the electric field applied to achieve separation and preconcentration is relatively low, which also facilitate the development of a portable device without using high voltage power supply. An intermediate design for multifunction (separation, preconcentration, quantification) is also designed and tested.

This intermediate design still has some drawbacks, leading to the proposal of a next-generation design, which will provide new insight for the future application of this device on more complex samples and/or more practical situations.

### 6.5 References


[1] Parsa, S. F., Vafajoo, A., Rostami, A., Salarian, R., Rabiee, M., Rabiee, N., Rabiee, G., Tahriri, M., Yadegari, A., Vashaee, D., Tayebi, L., Hamblin, M. R., *Anal Chim Acta* 2018, *1032*, 1-17.

[2] Humphries, S., *Journal of epidemiology and community health* 1991, *45*, 173.

[3] Ebert, M. P., Korc, M., Malfertheiner, P., Röcken, C., *Journal of proteome research* 2006, *5*, 19-25.

[4] Jacobs, I. J., Menon, U., *Molecular & Cellular Proteomics* 2004, *3*, 355-366.

[5] Ray, S., Reddy, P. J., Jain, R., Gollapalli, K., Moiyadi, A., Srivastava, S., *Proteomics* 2011, *11*, 2139-2161.

[6] Barber, R. C., *The Journal of the American Osteopathic Association* 2010, *110*, S10-15.

[7] Pepe, M. S., Etzioni, R., Feng, Z., Potter, J. D., Thompson, M. L., Thornquist, M., Winget, M., Yasui, Y., *Journal of the National Cancer Institute* 2001, *93*, 1054-1061.

[8] Woolley, C. F., Hayes, M. A., *Anal Methods* 2015, *7*, 8632-8639.

[9] Polson, N. A., Savin, D. P., Hayes, M. A., *Journal of Microcolumn Separations* 2000, *12*, 98-106.

[10] Pacheco, J. R., Chen, K. P., Hayes, M. A., *Electrophoresis* 2007, *28*, 1027-1035.

[11] Meighan, M. M., Keebaugh, M. W., Quihuis, A. M., Kenyon, S. M., Hayes, M. A., *Electrophoresis* 2009, *30*, 3786-3792.

[12] Meighan, M. M., Vasquez, J., Dziubcynski, L., Hews, S., Hayes, M. A., *Analytical chemistry* 2011, *83*, 368-373.

[13] Kenyon, S. M., Weiss, N. G., Hayes, M. A., *Electrophoresis* 2012, *33*, 1227-1235.

[14] Keebaugh, M. W., Mahanti, P., Hayes, M. A., *Electrophoresis* 2012, *33*, 1924-1930.

[15] Zhu, F., Hayes, M. A., *Electrophoresis* 2019, *40*, 304-314.

[16] Kenyon, S. M., Keebaugh, M. W., Hayes, M. A., *Electrophoresis* 2014, *35*, 2551-2559.

[17] Vasan, R. S., *Circulation* 2006, *113*, 2335-2362.

[18] Macdonald, S. P., Nagree, Y., Fatovich, D. M., Phillips, M., Brown, S. G., *Emerg Med J* 2013, *30*, 149-154.

[19] Sallach, S. M., Nowak, R., Hudson, M. P., Tokarski, G., Khoury, N., Tomlanovich, M. C., Jacobsen, G., de Lemos, J. A., McCord, J., *Am J Cardiol* 2004, *94*, 864-867.

[20] Ishii, J., Wang, J. H., Naruse, H., Taga, S., Kinoshita, M., Kurokawa, H., Iwase, M., Kondo, T., Nomura, M., Nagamura, Y., Watanabe, Y., *Clinical Chemistry* 1997, *43*, 1372-1378.

[21] Setsuta, K., Seino, Y., Mizuno, K., *Int J Cardiol* 2014, *176*, 1323-1325.

[22] Huang, C. H., Tsai, M. S., Chien, K. L., Hsu, C. Y., Chang, W. T., Wang, T. D., Chen, S. C., Ma, M. H., Chen, W. J., *Clin Chim Acta* 2014, *435*, 7-13.

[23] Katrukha, I. A., *Biochemistry (Mosc)* 2013, *78*, 1447-1465.

[24] Davis, B. D., Cohn, E. J., *Journal of the American Chemical Society* 1939, *61*, 2092-2098.

[25] Liu, M. K., Li, P., Giddings, J. C., *Protein Science* 1993, *2*, 1520-1531.

[26] Matyushov, D. V., *Molecular Physics* 2014, *112*, 2029-2039.

[27] Woolley, C. F., *School of Molecular Sciences*, Arizona State University, Tempe, AZ 2015, pp. 184-206.

[28] Araci, I. E., Quake, S. R., *Lab Chip* 2012, *12*, 2803-2806.

[29] Unger, M. A., Chou, H. P., Thorsen, T., Scherer, A., Quake, S. R., *Science* 2000, *288*, 113-116.

[30] Studer, V., Hang, G., Pandolfi, A., Ortiz, M., French Anderson, W., Quake, S. R., *Journal of Applied Physics* 2004, *95*, 393-398.

[31] Weaver, J. A., Melin, J., Stark, D., Quake, S. R., Horowitz, M. A., *Nature Physics* 2010, *6*, 218-223.

# CHAPTER 7

# CONCLUDING REMARKS

## 7.1 Developmental aspects of electrophoretic exclusion

Electrophoretic exclusion is emerging as a punctuated microgradient technique for separation and preconcentration with enhanced resolution and performance. An array-based design has enabled parallel spatial separation of analytes. The electrophoretic exclusion studies presented here on the developmental aspects of the device has helped evolve the understanding of the interfacial zone and built the foundation for designing novel and more efficient interfaces.

Initial work described the general basis of electrophoretic exclusion of dye molecules on an array-based microfluidic design (Chapter 3). Planar microchip experiments demonstrated the ability to exclude dye molecules at specific locations. These results indicated that the technique was useful for addressing analytes with varying properties.

Additionally, the electrode placement along asymmetric interface was investigated to understand the impact of seemingly subtle changes to the entrance flow and electric field configurations (Chapter 4). Experimental data and simulation results showed strong qualitative agreement. The complexity of the electric and flow fields about this interface and the agreement between models and testing suggests the theoretical assessment capabilities can be used to construct next-generation designs that enable integration into parallel configurations for multiplexed separations.

New design perspectives include but are not limited to the refinement of channel geometry, electrode shapes/position, and surface properties. In order to evaluate the performance of possible new designs in an effective and efficient way, concentration profile along the centerline can be assessed. The optimized next-generation design is expected to generate a higher concentration enhancement in the interfacial zone, meanwhile achieve large exclusion efficiency in the channel area. Moreover, the concentrated bolus needs to be conserved or confined into a small region/volume to reduce the lateral diffusion, which can be potentially achieved with the application of droplet microfluidics. One direction that can be tested first is to flatten hydrodynamic flow velocity profile and/or curve the electrophoretic velocity profile, which can be realized by different geometries and electrode designs with 3D printing possibility, and combination of slip and non-slip surface etc.

### 7.2 Practical applications of electrophoretic exclusion

In addition to developmental investigations, applications with practical samples continue to push the limit of the current device.

The coupling of electrophoretic exclusion to TEM was developed to prepare diluted small volume protein samples for electron microscopy imaging, which broadened the capability of electrophoretic exclusion (Chapter 5). It also suggested that the technique was capable of handling more diluted species and facilitating further structural determination or other clinical applications.

Good separation and preconcentration properties from the current device also enabled the applications with two protein biomarkers (Chapter 6). Consistent behaviors

of these two samples were observed from experiments. An intermediate design aimed to incorporating this separation/preconcentration feature prior to sensitive microbeads immunoassay detection showed some preliminary progress. Further refinement of the system, including incorporation of physical valves and gas-free setup, holds the potential for the development of an optimized system for multiplexed quantification.

### 7.3 Future directions

The array-based design of electrophoretic exclusion enabled separation and preconcentration in parallel and/or in series with potentially high resolution at the interfacial zone. This feature is not achievable with conventional linear single channel separation interfaces.

Current studies have demonstrated its wide applications in biological studies, from hyphened strategies with downstream detection techniques to practical samples. The further optimized devices will potentially enable coupling with more downstream techniques, not limited to transmission electron microscopy, but also a variety of other techniques, such as matrix assisted laser desorption/ionization (MALDI) and surface enhanced laser spectroscopy (SERS). The work will also facilitate the advancement of proteomics. Even though LC-MS has been a routine technique in the field, it is nearing the fundamental limitations and significant improvements are unlikely to be realized in the current stage. While electrophoretic exclusion will serve as an alternative approach with high effectiveness and efficiency in top-down proteomics for intact protein separation and preconcentration prior to detection, and potentially achieve better performance compared with conventional chromatographic methods. In addition, the

array-based design enables spatial separation into corresponding reservoirs and multiplexed detection of multiple targets simultaneously. These works are expected to promote the future development of clinical trials for point-of-care diagnosis for rapid identification and quantification with reduced time, decreased sample amount, increased capability, as well as enhanced sensitivity and specificity.

REFERENCES

## CHAPTER 1


[1] Kohlrausch, F., *Annalen der Physik* 1897, *298*, 209-239.

[2] Tiselius, A., *Transactions of the Faraday Society* 1937, *33*, 524-531.

[3] NobelPrize.org, Nobel Media AB 2019, p. https://www.nobelprize.org/prizes/chemistry/1948/summary/.

[4] Tiselius, A., Flodin, P., *In Advances in Protein Chemistry* 1953, *8*, 461-486.

[5] Hjertén, S., *Chromatographic reviews* 1967, *9*, 122-219.

[6] Virtanen, R., *Acta Polytechnica Scandinavica-Chemical Technology Series* 1974, *123*, 1-67.

[7] Jorgenson, J. W., Lukacs, K. D., *Journal of Chromatography A* 1981, *218*, 209-216.

[8] Jorgenson, J. W., Lukacs, K. D., *Clinical chemistry* 1981, *27*, 1551-1553.

[9] Jorgenson, J. W., Lukacs, K. D., *Science* 1983, *222*, 266-274.

[10] Jorgenson, J. W., Lukacs, K. D., *Journal of High Resolution Chromatography* 1985, *8*, 407-411.

[11] Rajput, H. H., Deokate, U. A., Nawale, R. B., *World J. Pharm. Pharm. Sci* 2016, *5*, 450-465.

[12] Breadmore, M. C., *Electrophoresis* 2007, *28*, 254-281.

[13] Breadmore, M. C., Thabano, J. R., Dawod, M., Kazarian, A. A., Quirino, J. P., Guijt, R. M., *Electrophoresis* 2009, *30*, 230-248.

[14] Breadmore, M. C., Dawod, M., Quirino, J. P., *Electrophoresis* 2011, *32*, 127-148.

[15] Breadmore, M. C., *J Chromatogr A* 2012, *1221*, 42-55.

[16] Breadmore, M. C., Shallan, A. I., Rabanes, H. R., Gstoettenmayr, D., Abdul Keyon, A. S., Gaspar, A., Dawod, M., Quirino, J. P., *Electrophoresis* 2013, *34*, 29-54.

[17] Breadmore, M. C., Tubaon, R. M., Shallan, A. I., Phung, S. C., Abdul Keyon, A. S., Gstoettenmayr, D., Prapatpong, P., Alhusban, A. A., Ranjbar, L., See, H. H., Dawod, M., Quirino, J. P., *Electrophoresis* 2015, *36*, 36-61.

[18] Breadmore, M. C., Wuethrich, A., Li, F., Phung, S. C., Kalsoom, U., Cabot, J. M., Tehranirokh, M., Shallan, A. I., Abdul Keyon, A. S., See, H. H., Dawod, M., Quirino, J. P.,

*Electrophoresis* 2017, *38*, 33-59.

[19] Giddings, J. C., Dahlgren, K., *Separation Science* 1971, *6*, 345-356.

[20] Ista, L. K., Lopez, G. P., Ivory, C. F., Ortiz, M. J., Schifani, T. A., Schwappach, C. D., Sibbett, S. S., *Lab on a chip* 2003, *3*, 266-272.

[21] Wang, Q., Tolley, H. D., LeFebre, D. A., Lee, M. L., *Analytical and bioanalytical chemistry* 2002, *373*, 125-135.

[22] Righetti, P. G., Chillemi, F., *Journal of Chromatography A* 1978, *157*, 243-251.

[23] Shackman, J. G., Ross, D., *Electrophoresis* 2007, *28*, 556-571.

[24] O'FARRELL, P. H., *Science* 1985, *227*, 1586-1589.

[25] Greenlee, R. D., Ivory, C. F., *Biotechnology progress* 1998, *14*, 300-309.

[26] Ren, C. L., Li, D., *J Colloid Interface Sci* 2006, *294*, 482-491.

[27] Barz, D. P. J., *Microfluidics and Nanofluidics* 2008, *7*, 249-265.

[28] Humble, P. H., Kelly, R. T., Woolley, A. T., Tolley, H. D., Lee, M. L., *Analytical chemistry* 2004, *76*, 5641-5648.

[29] Sun, X., Farnsworth, P. B., Woolley, A. T., Tolley, H. D., Warnick, K. F., Lee, M. L., *Analytical chemistry* 2008, *80*, 451-460.

[30] Sun, X., Farnsworth, P. B., Tolley, H. D., Warnick, K. F., Woolley, A. T., Lee, M. L., *Journal of chromatography. A* 2009, *1216*, 159-164.

[31] Hoebel, S. J., Balss, K. M., Jones, B. J., Malliaris, C. D., Munson, M. S., Vreeland, W. N., Ross, D., *Analytical chemistry* 2006, *78*, 7186-7190.

[32] Shackman, J. G., Munson, M. S., Ross, D., *Analytical and bioanalytical chemistry* 2007, *387*, 155-158.

[33] Shackman, J. G., Munson, M. S., Ross, D., *Analytical chemistry* 2007, *79*, 565-571.

[34] Burke, J. M., Ivory, C. F., *Electrophoresis* 2008, *29*, 1013-1025.

[35] Strychalski, E. A., Henry, A. C., Ross, D., *Analytical chemistry* 2009, *81*, 10201-10207.

[36] Strychalski, E. A., Henry, A. C., Ross, D., *Analytical chemistry* 2011, *83*, 6316-6322.

[37] Smejkal, P., Bottenus, D., Breadmore, M. C., Guijt, R. M., Ivory, C. F., Foret, F., Macka, M., *Electrophoresis* 2013, *34*, 1493-1509.

[38] Ross, D., Munson, M. S., *Electrophoresis* 2014, *35*, 770-776.

[39] Sikorsky, A. A., Fourkas, J. T., Ross, D., *Analytical chemistry* 2014, *86*, 3625-3632.

[40] Polson, N. A., Savin, D. P., Hayes, M. A., *Journal of Microcolumn Separations* 2000, *12*, 98-106.

[41] Pacheco, J. R., Chen, K. P., Hayes, M. A., *Electrophoresis* 2007, *28*, 1027-1035.

[42] Meighan, M. M., Keebaugh, M. W., Quihuis, A. M., Kenyon, S. M., Hayes, M. A., *Electrophoresis* 2009, *30*, 3786-3792.

[43] Meighan, M. M., Vasquez, J., Dziubcynski, L., Hews, S., Hayes, M. A., *Analytical chemistry* 2011, *83*, 368-373.

[44] Kenyon, S. M., Keebaugh, M. W., Hayes, M. A., *Electrophoresis* 2014, *35*, 2551-2559.

[45] Halldorsson, S., Lucumi, E., Gomez-Sjoberg, R., Fleming, R. M. T., *Biosens Bioelectron* 2015, *63*, 218-231.

[46] Lim, C. T., Zhang, Y., *Biosens Bioelectron* 2007, *22*, 1197-1204.

[47] Tabeling, P., *Introduction to microfluidics*, Oxford University Press on Demand 2005.

[48] Humphries, S., *Journal of epidemiology and community health* 1991, *45*, 173.

[49] Naylor, S., 2003, 525-529.

[50] Vogenberg, F. R., Barash, C. I., Pursel, M., *Pharmacy and Therapeutics* 2010, *35*, 560.

[51] Diamandis, E. P., *Mol Cell Proteomics* 2004, *3*, 367-378.

[52] Sonker, M., Sahore, V., Woolley, A. T., *Anal Chim Acta* 2017, *986*, 1-11.

[53] Rusling, J. F., Kumar, C. V., Gutkind, J. S., Patel, V., *Analyst* 2010, *135*, 2496-2511.

[54] Wu, L., Qu, X., *Chem Soc Rev* 2015, *44*, 2963-2997.

[55] Rifai, N., Gillette, M. A., Carr, S. A., *Nat Biotechnol* 2006, *24*, 971-983.

[56] Hanash, S. M., Pitteri, S. J., Faca, V. M., *Nature* 2008, *452*, 571-579.

[57] Nahavandi, S., Tang, S. Y., Baratchi, S., Soffe, R., Nahavandi, S., Kalantar-zadeh, K., Mitchell, A., Khoshmanesh, K., *Small* 2014, *10*, 4810-4826.

[58] Chandramouli, K., Qian, P. Y., *Hum Genomics Proteomics* 2009, *2009*.

**CHAPTER 2**

[1] Strohmeier, O., Keller, M., Schwemmer, F., Zehnle, S., Mark, D., von Stetten, F., Zengerle, R., Paust, N., *Chemical Society reviews* 2015, *44*, 6187-6229.

[2] Breadmore, M. C., *Electrophoresis* 2007, *28*, 254-281.

[3] Breadmore, M. C., Thabano, J. R., Dawod, M., Kazarian, A. A., Quirino, J. P., Guijt, R. M., *Electrophoresis* 2009, *30*, 230-248.

[4] Breadmore, M. C., Dawod, M., Quirino, J. P., *Electrophoresis* 2011, *32*, 127-148.

[5] Breadmore, M. C., Shallan, A. I., Rabanes, H. R., Gstoettenmayr, D., Abdul Keyon, A. S., Gaspar, A., Dawod, M., Quirino, J. P., *Electrophoresis* 2013, *34*, 29-54.

[6] Breadmore, M. C., Tubaon, R. M., Shallan, A. I., Phung, S. C., Abdul Keyon, A. S., Gstoettenmayr, D., Prapatpong, P., Alhusban, A. A., Ranjbar, L., See, H. H., Dawod, M., Quirino, J. P., *Electrophoresis* 2015, *36*, 36-61.

[7] Zeng, J., Deng, Y., Vedantam, P., Tzeng, T.-R., Xuan, X., *Journal of Magnetism and Magnetic Materials* 2013, *346*, 118-123.

[8] Han, X., Feng, Y., Cao, Q., Li, L., *Microfluidics and Nanofluidics* 2014, *18*, 1209-1220.

[9] Laurell, T., Petersson, F., Nilsson, A., *Chemical Society reviews* 2007, *36*, 492-506.

[10] Destgeer, G., Lee, K. H., Jung, J. H., Alazzam, A., Sung, H. J., *Lab Chip* 2013, *13*, 4210-4216.

[11] Li, P., Mao, Z., Peng, Z., Zhou, L., Chen, Y., Huang, P. H., Huang, T. J., *Proceedings of the National Academy of Sciences* 2015, *112*, 4970-4975.

[12] Kim, S. B., Yoon, S. Y., Sung, H. J., Kim, S. S., *Analytical chemistry* 2008, *80*, 2628-2630.

[13] Jung, J. H., Lee, K. H., Lee, K. S., Ha, B. H., Oh, Y. S., Sung, H. J., *Microfluidics and Nanofluidics* 2013, *16*, 635-644.

[14] Gongora, J. S. T., Fratalocchi, A., *Optics and Lasers in Engineering* 2016, *76*, 40-44.

[15] Song, J. Z., Chen, H. F., Tian, S. J., Sun, Z. P., *Journal of Chromtagraphy B: Biomedical Sciences and Applications* 1998, *708*, 277-283.

[16] Yang, H., Chien, R. L., *Journal of chromatography. A* 2001, *924*, 155-163.

[17] Jung, B., Bharadwaj, R., Santiago, J. G., *Electrophoresis* 2003, *24*, 3476-3483.

[18] Bharadwaj, R., Santiago, J. G., *Journal of Fluid Mechanics* 2005, *543*, 57.

[19] Jung, B., Bharadwaj, R., Santiago, J. G., *Analytical chemistry* 2006, 2319-2327.

[20] Mala, Z., Gebauer, P., Bocek, P., *Electrophoresis* 2011, *32*, 116-126.

[21] Chen, Y., Lü, W., Chen, X., Teng, M., *Central European Journal of Chemistry* 2012, *10*, 611-638.

[22] Slampova, A., Mala, Z., Pantuckova, P., Gebauer, P., Bocek, P., *Electrophoresis* 2013, *34*, 3-18.

[23] Lian, D. S., Zhao, S. J., Li, J., Li, B. L., *Analytical and bioanalytical chemistry* 2014, *406*, 6129-6150.

[24] Mala, Z., Slampova, A., Krivankova, L., Gebauer, P., Bocek, P., *Electrophoresis* 2015, *36*, 15-35.

[25] Thormann, W., *Separation Science and Technology* 2006, *19*, 455-467.

[26] Gebauer, P., Mala, Z., Bocek, P., *Electrophoresis* 2011, *32*, 83-89.

[27] Rogacs, A., Qu, Y., Santiago, J. G., *Analytical chemistry* 2012, *84*, 5858-5863.

[28] Wen, Y., Li, J., Ma, J., Chen, L., *Electrophoresis* 2012, *33*, 2933-2952.

[29] Mala, Z., Gebauer, P., Bocek, P., *Electrophoresis* 2013, *34*, 19-28.

[30] Smejkal, P., Bottenus, D., Breadmore, M. C., Guijt, R. M., Ivory, C. F., Foret, F., Macka, M., *Electrophoresis* 2013, *34*, 1493-1509.

[31] Strychalski, E. A., Konek, C., Butts, E. L., Vallone, P. M., Henry, A. C., Ross, D., *Electrophoresis* 2013, *34*, 2522-2530.

[32] Rogacs, A., Marshall, L. A., Santiago, J. G., *Journal of chromatography. A* 2014, *1335*, 105-120.

[33] Mala, Z., Gebauer, P., Bocek, P., *Electrophoresis* 2015, *36*, 2-14.

[34] Petersson, F., Aberg, L., Sward-Nilsson, A. M., Laurell, T., *Analytical chemistry* 2007, *79*, 5117-5123.

[35] Becker, M., Mansouri, A., Beilein, C., Janasek, D., *Electrophoresis* 2009, *30*, 4206-4212.

[36] Turgeon, R. T., Bowser, M. T., *Analytical and bioanalytical chemistry* 2009, *394*, 187-198.

[37] Wildgruber, R., Weber, G., Wise, P., Grimm, D., Bauer, J., *Proteomics* 2014, *14*, 629-636.

[38] Benz, C., Boomhoff, M., Appun, J., Schneider, C., Belder, D., *Angewandte Chemie* 2015, *54*, 2766-2770.

[39] Koegler, W. S., Ivory, C. F., *Biotechnology progress* 1996, *12*, 822-836.

[40] Greenlee, R. D., Ivory, C. F., *Biotechnology progress* 1998, *14*, 300-309.

[41] Wang, Q., Tolley, H. D., LeFebre, D. A., Lee, M. L., *Analytical and bioanalytical chemistry* 2002, *373*, 125-135.

[42] Kelly, R. T., Woolley, A. T., *Journal of Separation Science* 2005, *28*, 1985-1993.

[43] Shackman, J. G., Ross, D., *Electrophoresis* 2007, *28*, 556-571.

[44] Ivory, C. F., *Electrophoresis* 2007, *28*, 15-25.

[45] Meighan, M. M., Staton, S. J., Hayes, M. A., *Electrophoresis* 2009, *30*, 852-865.

[46] Vyas, C. A., Flanigan, P. M., Shackman, J. G., *Bioanalysis* 2010, *2*, 815-827.

[47] Cheng, H., Han, C., Xu, Z., Liu, J., Wang, Y., *Food Analytical Methods* 2014, *7*, 2153-2162.

[48] Giri, B., Dutta, D., *Analytica chimica acta* 2014, *810*, 32-38.

[49] Sueyoshi, K., Kitagawa, F., Otsuka, K., *Analytical Sciences* 2013, *29*, 133-138.

[50] Won, S. Y., Chandra, P., Hee, T. S., Shim, Y. B., *Biosensors & bioelectronics* 2013, *39*, 204-209.

[51] Bottenus, D., Jubery, T. Z., Dutta, P., Ivory, C. F., *Electrophoresis* 2011, *32*, 550-562.

[52] Bottenus, D., Jubery, T. Z., Ouyang, Y., Dong, W.-J., Dutta, P., Ivory, C. F., *Lab on a Chip* 2011, *11*, 890.

[53] Jacroux, T., Bottenus, D., Rieck, B., Ivory, C. F., Dong, W. J., *Electrophoresis* 2014, *35*, 2029-2038.

[54] Shintaku, H., Nishikii, H., Marshall, L. A., Kotera, H., Santiago, J. G., *Analytical chemistry* 2014, *86*, 1953-1957.

[55] Kuriyama, K., Shintaku, H., Santiago, J. G., *Electrophoresis* 2015, *36*, 1658-1662.

[56] Shintaku, H., Palko, J. W., Sanders, G. M., Santiago, J. G., *Angewandte Chemie* 2014, *53*, 13813-13816.

[57] Han, C. M., Katilius, E., Santiago, J. G., *Lab Chip* 2014, *14*, 2958-2967.

[58] Marshall, L. A., Rogacs, A., Meinhart, C. D., Santiago, J. G., *Journal of chromatography. A* 2014, *1331*, 139-142.

[59] Bahga, S. S., Chambers, R. D., Santiago, J. G., *Analytical chemistry* 2011, *83*, 6154-6162.

[60] Bahga, S. S., Santiago, J. G., *Electrophoresis* 2012, *33*, 1048-1059.

[61] Qu, Y., Marshall, L. A., Santiago, J. G., *Analytical chemistry* 2014, *86*, 7264-7268.

[62] Prest, J. E., Baldock, S. J., Fielden, P. R., Goddard, N. J., Goodacre, R., O'Connor, R., Treves Brown, B. J., *Journal of chromatography. B, Analytical technologies in the biomedical and life sciences* 2012, *903*, 53-59.

[63] Xu, Z., Murata, K., Arai, A., Hirokawa, T., *Biomicrofluidics* 2010, *4*, 14108.

[64] Wu, R., Yeung, W. S., Fung, Y. S., *Electrophoresis* 2011, *32*, 3406-3414.

[65] Rosenfeld, T., Bercovici, M., *Lab Chip* 2014, *14*, 4465-4474.

[66] Moghadam, B. Y., Connelly, K. T., Posner, J. D., *Analytical chemistry* 2014, *86*, 5829-5837.

[67] Smejkal, P., Breadmore, M. C., Guijt, R. M., Foret, F., Bek, F., Macka, M., *Electrophoresis* 2012, *33*, 3166-3172.

[68] Smejkal, P., Breadmore, M. C., Guijt, R. M., Grym, J., Foret, F., Bek, F., Macka, M., *Analytica chimica acta* 2012, *755*, 115-120.

[69] Smejkal, P., Breadmore, M. C., Guijt, R. M., Foret, F., Bek, F., Macka, M., *Analytica chimica acta* 2013, *803*, 135-142.

[70] Inglis, D. W., Goldys, E. M., Calander, N. P., *Angewandte Chemie* 2011, *50*, 7546-7550.

[71] Hsu, W. L., Inglis, D. W., Jeong, H., Dunstan, D. E., Davidson, M. R., Goldys, E. M., Harvie, D. J., *Langmuir : the ACS journal of surfaces and colloids* 2014, *30*, 5337-5348.

[72] Hsu, W. L., Harvie, D. J., Davidson, M. R., Jeong, H., Goldys, E. M., Inglis, D. W., *Lab Chip* 2014, *14*, 3539-3549.

[73] Koegler, W. S., Ivory, C. F., *Journal of Chromatography A* 1996, *726*, 229-236.

[74] Burke, J. M., Ivory, C. F., *Electrophoresis* 2008, *29*, 1013-1025.

[75] Tracy, N. I., Huang, Z., Ivory, C. F., *Biotechnology progress* 2008, *23*, 444-451.

[76] Tracy, N. I., Ivory, C. F., *Electrophoresis* 2008, *29*, 2820-2827.

[77] Humble, P. H., Kelly, R. T., Woolley, A. T., Tolley, H. D., Lee, M. L., *Analytical chemistry* 2004, *76*, 5641-5648.

[78] Liu, J., Sun, X., Farnsworth, P. B., Lee, M. L., *Analytical chemistry* 2006, *78*, 4654-4662.

[79] Sun, X., Farnsworth, P. B., Woolley, A. T., Tolley, H. D., Warnick, K. F., Lee, M. L., *Analytical chemistry* 2008, *80*, 451-460.

[80] Sun, X., Farnsworth, P. B., Tolley, H. D., Warnick, K. F., Woolley, A. T., Lee, M. L., *Journal of chromatography. A* 2009, *1216*, 159-164.

[81] Sun, X., Li, D., Woolley, A. T., Farnsworth, P. B., Tolley, H. D., Warnick, K. F., Lee, M. L., *Journal of chromatography. A* 2009, *1216*, 6532-6538.

[82] Trickett, C. A., Henderson, R. D., Guijt, R. M., Breadmore, M. C., *Electrophoresis* 2012, *33*, 3254-3258.

[83] Shameli, S. M., Glawdel, T., Ren, C. L., *Electrophoresis* 2015, *36*, 668-674.

[84] Burke, J. M., Ivory, C. F., *Electrophoresis* 2010, *31*, 893-901.

[85] Burke, J. M., Smith, C. D., Ivory, C. F., *Electrophoresis* 2010, *31*, 902-909.

[86] Strychalski, E. A., Henry, A. C., Ross, D., *Analytical chemistry* 2009, *81*, 10201-10207.

[87] Sikorsky, A. A., Fourkas, J. T., Ross, D., *Analytical chemistry* 2014, *86*, 3625-3632.

[88] Meighan, M. M., Keebaugh, M. W., Quihuis, A. M., Kenyon, S. M., Hayes, M. A., *Electrophoresis* 2009, *30*, 3786-3792.

[89] Meighan, M. M., Vasquez, J., Dziubcynski, L., Hews, S., Hayes, M. A., *Analytical chemistry* 2011, *83*, 368-373.

[90] Kenyon, S. M., Weiss, N. G., Hayes, M. A., *Electrophoresis* 2012, *33*, 1227-1235.

[91] Kenyon, S. M., Keebaugh, M. W., Hayes, M. A., *Electrophoresis* 2014, *35*, 2551-2559.

[92] Zhu, F., Hayes, M. A., *Electrophoresis* 2019, *40*, 304-314.

[93] Balss, K. M., Vreeland, W. N., Phinney, K. W., Ross, D., *Analytical chemistry* 2004, *76*, 7243-7249.

[94] Balss, K. M., Vreeland, W. N., Howell, P. B., Henry, A. C., Ross, D., *Journal of the American Chemical Society* 2004, *126*, 1936-1937.

[95] Munson, M. S., Meacham, J. M., Locascio, L. E., Ross, D., *Analytical chemistry* 2008, *80*, 172-178.

[96] Kim, S. M., Sommer, G. J., Burns, M. A., Hasselbrink, E. F., *Analytical chemistry* 2006, *78*, 8028-8035.

[97] Sommer, G. J., Kim, S. M., Littrell, R. J., Hasselbrink, E. F., *Lab Chip* 2007, *7*, 898-907.

[98] Schwarzkopf, F., Scholl, T., Ohla, S., Belder, D., *Electrophoresis* 2014, *35*, 1880-1886.

[99] Matsui, T., Franzke, J., Manz, A., Janasek, D., *Electrophoresis* 2007, *28*, 4606-4611.

[100] Ge, Z., Wang, W., Yang, C., *Lab Chip* 2011, *11*, 1396-1402.

[101] Zhang, H. D., Zhou, J., Xu, Z. R., Song, J., Dai, J., Fang, J., Fang, Z. L., *Lab Chip* 2007, *7*, 1162-1170.

[102] Akbari, M., Bahrami, M., Sinton, D., *Microfluidics and Nanofluidics* 2011, *12*, 221-228.

[103] Gao, M., Gui, L., Liu, J., *Journal of Heat Transfer* 2013, *135*, 091402.

[104] Shameli, S. M., Glawdel, T., Liu, Z., Ren, C. L., *Analytical chemistry* 2012, *84*, 2968-2973.

[105] Shameli, S. M., Glawdel, T., Fernand, V. E., Ren, C. L., *Electrophoresis* 2012, *33*, 2703-2710.

[106] Holtzel, A., Tallarek, U., *Journal of separation science* 2007, *30*, 1398-1419.

[107] Kuo, T. C., Cannon, D. M., Shannon, M. A., Bohn, P. W., Sweedler, J. V., *Sensors and Actuators A: Physcial* 2003, *102*, 223-233.

[108] Kuo, T. C., Cannon, D. M., Chen, Y., Tulock, J. J., Shannon, M. A., Sweedler, J. V., Bohn, P. W., *Analytical chemistry* 2003, *75*, 1861-1867.

[109] Kim, S. J., Ko, S. H., Kang, K. H., Han, J., *Nature nanotechnology* 2010, *5*, 297-301.

[110] Kwak, R., Kim, S. J., Han, J., *Analytical chemistry* 2011, *83*, 7348-7355.

[111] Jeon, H., Lee, H., Kang, K. H., Lim, G., *Scientific reports* 2013, *3*, 3483.

[112] MacDonald, B. D., Gong, M. M., Zhang, P., Sinton, D., *Lab Chip* 2014, *14*, 681-685.

[113] Ko, S. H., Song, Y. A., Kim, S. J., Kim, M., Han, J., Kang, K. H., *Lab Chip* 2012, *12*, 4472-4482.

[114] Kim, M., Jia, M., Kim, T., *The Analyst* 2013, *138*, 1370-1378.

[115] Jia, M., Kim, T., *Analytical chemistry* 2014, *86*, 10365-10372.

[116] Scarff, B., Escobedo, C., Sinton, D., *Lab Chip* 2011, *11*, 1102-1109.

[117] Yang, R. J., Pu, H. H., Wang, H. L., *Biomicrofluidics* 2015, *9*, 014122.

[118] Yuan, X., Renaud, L., Audry, M. C., Kleimann, P., *Analytical chemistry* 2015, *87*, 8695-8701.

[119] Dhopeshwarkar, R., Hlushkou, D., Nguyen, M., Tallarek, U., Crooks, R. M., *Journal of the American Chemical Society* 2008, *130*, 10480-10481.

[120] Hlushkou, D., Perdue, R. K., Dhopeshwarkar, R., Crooks, R. M., Tallarek, U., *Lab Chip* 2009, *9*, 1903-1913.

[121] Laws, D. R., Hlushkou, D., Perdue, R. K., Tallarek, U., Crooks, R. M., *Analytical chemistry* 2009, *81*, 8923-8929.

[122] Anand, R. K., Sheridan, E., Hlushkou, D., Tallarek, U., Crooks, R. M., *Lab Chip* 2011, *11*, 518-527.

[123] Perdue, R. K., Laws, D. R., Hlushkou, D., Tallarek, U., Crooks, R. M., *Analytical chemistry* 2009, *81*, 10149-10155.

[124] Sheridan, E., Hlushkou, D., Knust, K. N., Tallarek, U., Crooks, R. M., *Analytical chemistry* 2012, *84*, 7393-7399.

[125] Sheridan, E., Knust, K. N., Crooks, R. M., *The Analyst* 2011, *136*, 4134-4137.

[126] Anand, R. K., Sheridan, E., Knust, K. N., Crooks, R. M., *Analytical chemistry* 2011, *83*, 2351-2358.

[127] Knust, K. N., Sheridan, E., Anand, R. K., Crooks, R. M., *Lab Chip* 2012, *12*, 4107-4114.

[128] Song, H., Wang, Y., Garson, C., Pant, K., *Analytical methods : advancing methods and applications* 2015, *7*, 1273-1279.

**CHAPTER 3**

[1] Breadmore, M. C., *Electrophoresis* 2007, *28*, 254-281.

[2] Breadmore, M. C., Thabano, J. R., Dawod, M., Kazarian, A. A., Quirino, J. P., Guijt, R. M., *Electrophoresis* 2009, *30*, 230-248.

[3] Breadmore, M. C., Dawod, M., Quirino, J. P., *Electrophoresis* 2011, *32*, 127-148.

[4] Breadmore, M. C., Shallan, A. I., Rabanes, H. R., Gstoettenmayr, D., Abdul Keyon, A.

S., Gaspar, A., Dawod, M., Quirino, J. P., *Electrophoresis* 2013, *34*, 29-54.

[5] Breadmore, M. C., Tubaon, R. M., Shallan, A. I., Phung, S. C., Abdul Keyon, A. S., Gstoettenmayr, D., Prapatpong, P., Alhusban, A. A., Ranjbar, L., See, H. H., Dawod, M., Quirino, J. P., *Electrophoresis* 2015, *36*, 36-61.

[6] Breadmore, M. C., Wuethrich, A., Li, F., Phung, S. C., Kalsoom, U., Cabot, J. M., Tehranirokh, M., Shallan, A. I., Abdul Keyon, A. S., See, H. H., Dawod, M., Quirino, J. P., *Electrophoresis* 2017, *38*, 33-59.

[7] O'FARRELL, P. H., *Science* 1985, *227*, 1586-1589.

[8] Giddings, J. C., Dahlgren, K., *Separation Science* 1971, *6*, 345-356.

[9] Culbertson, C. T., Jorgenson, J. W., *Analytical chemistry* 1994, *66*, 955-962.

[10] Koegler, W. S., Ivory, C. F., *Biotechnology progress* 1996, *12*, 822-836.

[11] Koegler, W. S., Ivory, C. F., *Journal of Chromatography A* 1996, *726*, 229-236.

[12] Greenlee, R. D., Ivory, C. F., *Biotechnology progress* 1998, *14*, 300-309.

[13] Huang, Z., Ivory, C. F., *Analytical chemistry* 1999, *71*, 1628-1632.

[14] Humble, P. H., Kelly, R. T., Woolley, A. T., Tolley, H. D., Lee, M. L., *Analytical chemistry* 2004, *76*, 5641-5648.

[15] Kelly, R. T., Woolley, A. T., *Journal of Separation Science* 2005, *28*, 1985-1993.

[16] Burke, J. M., Ivory, C. F., *Electrophoresis* 2008, *29*, 1013-1025.

[17] Tracy, N. I., Huang, Z., Ivory, C. F., *Biotechnology progress* 2008, *23*, 444-451.

[18] Tracy, N. I., Ivory, C. F., *Electrophoresis* 2008, *29*, 2820-2827.

[19] Sun, X., Farnsworth, P. B., Woolley, A. T., Tolley, H. D., Warnick, K. F., Lee, M. L., *Analytical chemistry* 2008, *80*, 451-460.

[20] Sun, X., Farnsworth, P. B., Tolley, H. D., Warnick, K. F., Woolley, A. T., Lee, M. L., *Journal of chromatography. A* 2009, *1216*, 159-164.

[21] Hoebel, S. J., Balss, K. M., Jones, B. J., Malliaris, C. D., Munson, M. S., Vreeland, W. N., Ross, D., *Analytical chemistry* 2006, *78*, 7186-7190.

[22] Shackman, J. G., Munson, M. S., Ross, D., *Analytical and bioanalytical chemistry* 2007, *387*, 155-158.

[23] Shackman, J. G., Munson, M. S., Ross, D., *Analytical chemistry* 2007, *79*, 565-571.

[24] Strychalski, E. A., Henry, A. C., Ross, D., *Analytical chemistry* 2009, *81*, 10201-10207.

[25] Ross, D., Romantseva, E. F., *Analytical chemistry* 2009, *81*, 7326-7335.

[26] Strychalski, E. A., Henry, A. C., Ross, D., *Analytical chemistry* 2011, *83*, 6316-6322.

[27] Sikorsky, A. A., Fourkas, J. T., Ross, D., *Analytical chemistry* 2014, *86*, 3625-3632.

[28] Ross, D., Munson, M. S., *Electrophoresis* 2014, *35*, 770-776.

[29] Polson, N. A., Savin, D. P., Hayes, M. A., *Journal of Microcolumn Separations* 2000, *12*, 98-106.

[30] Pacheco, J. R., Chen, K. P., Hayes, M. A., *Electrophoresis* 2007, *28*, 1027-1035.

[31] Meighan, M. M., Keebaugh, M. W., Quihuis, A. M., Kenyon, S. M., Hayes, M. A., *Electrophoresis* 2009, *30*, 3786-3792.

[32] Meighan, M. M., Vasquez, J., Dziubcynski, L., Hews, S., Hayes, M. A., *Analytical chemistry* 2011, *83*, 368-373.

[33] Kenyon, S. M., Weiss, N. G., Hayes, M. A., *Electrophoresis* 2012, *33*, 1227-1235.

[34] Ng, J. M., Gitlin, I., Stroock, A. D., Whitesides, G. M., *Electrophoresis* 2002, *23*, 3461-3473.

**CHAPTER 4**

[1] Issaq, H. J., *Electrophoresis* 2001, *22*, 3629-3638.

[2] Smejkal, P., Bottenus, D., Breadmore, M. C., Guijt, R. M., Ivory, C. F., Foret, F., Macka, M., *Electrophoresis* 2013, *34*, 1493-1509.

[3] Gebauer, P., Mala, Z., Bocek, P., *Electrophoresis* 2011, *32*, 83-89.

[4] Mala, Z., Gebauer, P., Bocek, P., *Electrophoresis* 2013, *34*, 19-28.

[5] Mala, Z., Gebauer, P., Bocek, P., *Electrophoresis* 2015, *36*, 2-14.

[6] Lian, D. S., Zhao, S. J., Li, J., Li, B. L., *Analytical and bioanalytical chemistry* 2014, *406*, 6129-6150.

[7] Quirino, J. P., Kim, J. B., Terabe, S., *Journal of Chromatography A* 2002, *965*, 357-373.

[8] Shackman, J. G., Ross, D., *Electrophoresis* 2007, *28*, 556-571.

[9] Koegler, W. S., Ivory, C. F., *Biotechnology progress* 1996, *12*, 822-836.

[10] Koegler, W. S., Ivory, C. F., *Journal of Chromatography A* 1996, *726*, 229-236.

[11] Huang, Z., Ivory, C. F., *Analytical chemistry* 1999, *71*, 1628-1632.

[12] Tracy, N. I., Huang, Z., Ivory, C. F., *Biotechnology progress* 2008, *23*, 444-451.

[13] Tracy, N. I., Ivory, C. F., *Electrophoresis* 2008, *29*, 2820-2827.

[14] Humble, P. H., Kelly, R. T., Woolley, A. T., Tolley, H. D., Lee, M. L., *Analytical chemistry* 2004, *76*, 5641-5648.

[15] Liu, J., Sun, X., Farnsworth, P. B., Lee, M. L., *Analytical chemistry* 2006, *78*, 4654-4662.

[16] Sun, X., Farnsworth, P. B., Tolley, H. D., Warnick, K. F., Woolley, A. T., Lee, M. L., *Journal of chromatography. A* 2009, *1216*, 159-164.

[17] Sun, X., Farnsworth, P. B., Woolley, A. T., Tolley, H. D., Warnick, K. F., Lee, M. L., *Analytical chemistry* 2008, *80*, 451-460.

[18] Burke, J. M., Ivory, C. F., *Electrophoresis* 2008, *29*, 1013-1025.

[19] Strychalski, E. A., Henry, A. C., Ross, D., *Anal Chem* 2011, *83*, 6316-6322.

[20] Shackman, J. G., Munson, M. S., Ross, D., *Analytical chemistry* 2007, *79*, 565-571.

[21] Ross, D., Munson, M. S., *Electrophoresis* 2014, *35*, 770-776.

[22] Sikorsky, A. A., Fourkas, J. T., Ross, D., *Analytical chemistry* 2014, *86*, 3625-3632.

[23] Strychalski, E. A., Henry, A. C., Ross, D., *Analytical chemistry* 2009, *81*, 10201-10207.

[24] Hoebel, S. J., Balss, K. M., Jones, B. J., Malliaris, C. D., Munson, M. S., Vreeland, W. N., Ross, D., *Analytical chemistry* 2006, *78*, 7186-7190.

[25] Shackman, J. G., Munson, M. S., Ross, D., *Analytical and bioanalytical chemistry* 2007, *387*, 155-158.

[26] Polson, N. A., Savin, D. P., Hayes, M. A., *Journal of Microcolumn Separations* 2000, *12*, 98-106.

[27] Pacheco, J. R., Chen, K. P., Hayes, M. A., *Electrophoresis* 2007, *28*, 1027-1035.

[28] Meighan, M. M., Keebaugh, M. W., Quihuis, A. M., Kenyon, S. M., Hayes, M. A., *Electrophoresis* 2009, *30*, 3786-3792.

[29] Meighan, M. M., Vasquez, J., Dziubcynski, L., Hews, S., Hayes, M. A., *Analytical chemistry* 2011, *83*, 368-373.

[30] Keebaugh, M. W., Mahanti, P., Hayes, M. A., *Electrophoresis* 2012, *33*, 1924-1930.

[31] Kenyon, S. M., Weiss, N. G., Hayes, M. A., *Electrophoresis* 2012, *33*, 1227-1235.

[32] Kenyon, S. M., Keebaugh, M. W., Hayes, M. A., *Electrophoresis* 2014, *35*, 2551-2559.

[33] Kler, P. A., López, E. J., Dalcín, L. D., Guarnieri, F. A., Storti, M. A., *Computer Methods in Applied Mechanics and Engineering* 2009, *198*, 2360-2367.

[34] Saville, D. A., Palusinski, O. A., *AIChE Journal* 1986, *32*, 207-214.

[35] Bahga, S. S., Bercovici, M., Santiago, J. G., *Electrophoresis* 2012, *33*, 3036-3051.

[36] Ermakov, S. V., Stephen C. Jacobson, and J. Michael Ramsey. , *Analytical chemistry* 1998, *70*, 4494-4504.

[37] Ermakov, S. V., Jacobson, S. C., Ramsey, J. M., *In Proc. Conf. Modeling Simulation Microsyst* 1999, 534-537.

[38] Bianchi, F., R. Ferrigno, and H. H. Girault., *Analytical chemistry* 2000, *72*, 1987-1993.

[39] Barz, D. P. J., Ehrhard, P., *Pamm* 2005, *5*, 535-536.

[40] Chatterjee, A., *Journal of Micromechanics and Microengineering* 2003, *13*.

[41] Cardona, A., Nigro, N., Sonzogni, V., Storti, M., *Mecanica Computacional* 2006, *25*, 2573-2583.

[42] Kler, P., Guarnieri, F., Berli, C., *Mecanica Computacional* 2008, *27*, 3367-3380.

[43] Kler, P. A., Berli, C. L. A., Guarnieri, F. A., *Microfluidics and Nanofluidics* 2010, *10*, 187-198.

[44] Mansouri, A., Scheuerman, C., Bhattacharjee, S., Kwok, D. Y., Kostiuk, L. W., *J Colloid Interface Sci* 2005, *292*, 567-580.

[45] Stone, H. A., Stroock, A. D., Ajdari, A., *Annual Review of Fluid Mechanics* 2004, *36*, 381-411.

[46] Li, D., *Electrokinetics in microfluidics*, Elsevier 2004.

[47] Squires, T. M., Quake, S. R., *Reviews of modern physics* 2005, *77*, 977.

[48] Tabeling, P., *Introduction to microfluidics*, Oxford University Press on Demand 2005.

[49] Hwang, Y., Candler, R. N., *Lab on a chip* 2017.

**CHAPTER 5**

[1] Arnold, S. A., Muller, S. A., Schmidli, C., Syntychaki, A., Rima, L., Chami, M., Stahlberg, H., Goldie, K. N., Braun, T., *Proteomics* 2018, *18*, e1700176.

[2] Quentin, D., Raunser, S., *J Mol Med (Berl)* 2018, *96*, 483-493.

[3] Krishnan, V. V., Rupp, B., 2012.

[4] Murata, K., Wolf, M., *Biochim Biophys Acta Gen Subj* 2018, *1862*, 324-334.

[5] Thompson, R. F., Walker, M., Siebert, C. A., Muench, S. P., Ranson, N. A., *Methods* 2016, *100*, 3-15.

[6] Dubochet, J., Adrian, M., Chang, J. J., Homo, J. C., Lepault, J., McDowall, A. W., Schultz, P., *Q Rev Biophys* 1988, *21*, 129-228.

[7] Barber, R. C., *The Journal of the American Osteopathic Association* 2010, *110*, S10-15.

[8] Querfurth, H. W., Laferla, F. M., *N Engl J Med* 2010, *362*, 329-344.

[9] Hajipour, M. J., Santoso, M. R., Rezaee, F., Aghaverdi, H., Mahmoudi, M., Perry, G., *Trends Biotechnol* 2017, *35*, 937-953.

[10] Georganopoulou, D. G., Chang, L., Nam, J. M., Thaxton, C. S., Mufson, E. J., Klein, W. L., Mirkin, C. A., *Proc Natl Acad Sci U S A* 2005, *102*, 2273-2276.

[11] Schagger, H., Cramer, W. A., Vonjagow, G., *Analytical biochemistry* 1994, *217*, 220-230.

[12] Polson, N. A., Savin, D. P., Hayes, M. A., *Journal of Microcolumn Separations* 2000, *12*, 98-106.

[13] Pacheco, J. R., Chen, K. P., Hayes, M. A., *Electrophoresis* 2007, *28*, 1027-1035.

[14] Meighan, M. M., Staton, S. J., Hayes, M. A., *Electrophoresis* 2009, *30*, 852-865.

[15] Meighan, M. M., Keebaugh, M. W., Quihuis, A. M., Kenyon, S. M., Hayes, M. A., *Electrophoresis* 2009, *30*, 3786-3792.

[16] Kenyon, S. M., Meighan, M. M., Hayes, M. A., *Electrophoresis* 2011, *32*, 482-493.

[17] Meighan, M. M., Vasquez, J., Dziubcynski, L., Hews, S., Hayes, M. A., *Analytical chemistry* 2011, *83*, 368-373.

[18] Kenyon, S. M., Weiss, N. G., Hayes, M. A., *Electrophoresis* 2012, *33*, 1227-1235.

[19] Keebaugh, M. W., Mahanti, P., Hayes, M. A., *Electrophoresis* 2012, *33*, 1924-1930.

[20] Kenyon, S. M., Keebaugh, M. W., Hayes, M. A., *Electrophoresis* 2014, *35*, 2551-2559.

[21] Keebaugh, M. W., Hayes, M. A., *Electrophoresis* 2016.

[22] Zhu, F., Hayes, M. A., *Electrophoresis* 2019, *40*, 304-314.

[23] Tabeling, P., *Introduction to microfluidics*, Oxford University Press on Demand 2005.

[24] Giss, D., Kemmerling, S., Dandey, V., Stahlberg, H., Braun, T., *Analytical chemistry* 2014, *86*, 4680-4687.

[25] Mukhitov, N., Spear, J. M., Stagg, S. M., Roper, M. G., *Analytical chemistry* 2016, *88*, 629-634.

[26] Arnold, S. A., Albiez, S., Bieri, A., Syntychaki, A., Adaixo, R., McLeod, R. A., Goldie, K. N., Stahlberg, H., Braun, T., *J Struct Biol* 2017, *197*, 220-226.

[27] Feng, X., Fu, Z., Kaledhonkar, S., Jia, Y., Shah, B., Jin, A., Liu, Z., Sun, M., Chen, B., Grassucci, R. A., Ren, Y., Jiang, H., Frank, J., Lin, Q., *Structure* 2017, *25*, 663-670 e663.

[28] Ashtiani, D., Venugopal, H., Belousoff, M., Spicer, B., Mak, J., Neild, A., de Marco, A., *J Struct Biol* 2018, *203*, 94-101.

[29] Russo, C. J., Passmore, L. A., *Science* 2014, *346*, 1377-1380.

[30] Arnold, S. A., Albiez, S., Opara, N., Chami, M., Schmidli, C., Bieri, A., Padeste, C., Stahlberg, H., Braun, T., *ACS Nano* 2016, *10*, 4981-4988.

**CHAPTER 6**

[1] Parsa, S. F., Vafajoo, A., Rostami, A., Salarian, R., Rabiee, M., Rabiee, N., Rabiee, G., Tahriri, M., Yadegari, A., Vashaee, D., Tayebi, L., Hamblin, M. R., *Anal Chim Acta* 2018, *1032*, 1-17.

[2] Humphries, S., *Journal of epidemiology and community health* 1991, *45*, 173.

[3] Ebert, M. P., Korc, M., Malfertheiner, P., Röcken, C., *Journal of proteome research* 2006, *5*, 19-25.

[4] Jacobs, I. J., Menon, U., *Molecular & Cellular Proteomics* 2004, *3*, 355-366.

[5] Ray, S., Reddy, P. J., Jain, R., Gollapalli, K., Moiyadi, A., Srivastava, S., *Proteomics* 2011, *11*, 2139-2161.

[6] Barber, R. C., *The Journal of the American Osteopathic Association* 2010, *110*, S10-15.

[7] Pepe, M. S., Etzioni, R., Feng, Z., Potter, J. D., Thompson, M. L., Thornquist, M.,

Winget, M., Yasui, Y., *Journal of the National Cancer Institute* 2001, *93*, 1054-1061.

[8] Woolley, C. F., Hayes, M. A., *Anal Methods* 2015, *7*, 8632-8639.

[9] Polson, N. A., Savin, D. P., Hayes, M. A., *Journal of Microcolumn Separations* 2000, *12*, 98-106.

[10] Pacheco, J. R., Chen, K. P., Hayes, M. A., *Electrophoresis* 2007, *28*, 1027-1035.

[11] Meighan, M. M., Keebaugh, M. W., Quihuis, A. M., Kenyon, S. M., Hayes, M. A., *Electrophoresis* 2009, *30*, 3786-3792.

[12] Meighan, M. M., Vasquez, J., Dziubcynski, L., Hews, S., Hayes, M. A., *Analytical chemistry* 2011, *83*, 368-373.

[13] Kenyon, S. M., Weiss, N. G., Hayes, M. A., *Electrophoresis* 2012, *33*, 1227-1235.

[14] Keebaugh, M. W., Mahanti, P., Hayes, M. A., *Electrophoresis* 2012, *33*, 1924-1930.

[15] Zhu, F., Hayes, M. A., *Electrophoresis* 2019, *40*, 304-314.

[16] Kenyon, S. M., Keebaugh, M. W., Hayes, M. A., *Electrophoresis* 2014, *35*, 2551-2559.

[17] Vasan, R. S., *Circulation* 2006, *113*, 2335-2362.

[18] Macdonald, S. P., Nagree, Y., Fatovich, D. M., Phillips, M., Brown, S. G., *Emerg Med J* 2013, *30*, 149-154.

[19] Sallach, S. M., Nowak, R., Hudson, M. P., Tokarski, G., Khoury, N., Tomlanovich, M. C., Jacobsen, G., de Lemos, J. A., McCord, J., *Am J Cardiol* 2004, *94*, 864-867.

[20] Ishii, J., Wang, J. H., Naruse, H., Taga, S., Kinoshita, M., Kurokawa, H., Iwase, M., Kondo, T., Nomura, M., Nagamura, Y., Watanabe, Y., *Clinical Chemistry* 1997, *43*, 1372-1378.

[21] Setsuta, K., Seino, Y., Mizuno, K., *Int J Cardiol* 2014, *176*, 1323-1325.

[22] Huang, C. H., Tsai, M. S., Chien, K. L., Hsu, C. Y., Chang, W. T., Wang, T. D., Chen, S. C., Ma, M. H., Chen, W. J., *Clin Chim Acta* 2014, *435*, 7-13.

[23] Katrukha, I. A., *Biochemistry (Mosc)* 2013, *78*, 1447-1465.

[24] Davis, B. D., Cohn, E. J., *Journal of the American Chemical Society* 1939, *61*, 2092-2098.

[25] Liu, M. K., Li, P., Giddings, J. C., *Protein Science* 1993, *2*, 1520-1531.

[26] Matyushov, D. V., *Molecular Physics* 2014, *112*, 2029-2039.

[27] Woolley, C. F., *School of Molecular Sciences*, Arizona State University, Tempe, AZ 2015, pp. 184-206.

[28] Araci, I. E., Quake, S. R., *Lab Chip* 2012, *12*, 2803-2806.

[29] Unger, M. A., Chou, H. P., Thorsen, T., Scherer, A., Quake, S. R., *Science* 2000, *288*, 113-116.

[30] Studer, V., Hang, G., Pandolfi, A., Ortiz, M., French Anderson, W., Quake, S. R., *Journal of Applied Physics* 2004, *95*, 393-398.

[31] Weaver, J. A., Melin, J., Stark, D., Quake, S. R., Horowitz, M. A., *Nature Physics* 2010, *6*, 218-223.

# APPENDIX A

## PUBLISHED PORTIONS

Chapters 2 and 4 were published previously in the journals referenced below.

Zhu, F., Hayes, M. A., *Separations* 2016, *3*, 12.

Zhu, F., Hayes, M. A., *Electrophoresis* 2019, *40*, 304-314.

Chapter 5 was submitted to the journal as referenced below.

Zhu, F., Nannenga, B., Hayes, M. A., *Analyst*, submitted.

Published portions or portions in preparation for publication were included with the permission of all coauthors.